bioRxiv preprint doi: https://doi.org/10.1101/2020.06.02.129825; this version posted June 9, 2021. The copyright holder for this preprint (which was not certified by peer review) is the author/funder, who has granted bioRxiv a license to display the preprint in perpetuity. It is made available under aCC-BY 4.0 International license.

An Hourglass Circuit Motif Transforms a Motor Program via Subcellularly Localized Muscle Calcium Signaling and Contraction

Steven R. Sando[1], Nikhil Bhatla[1,2,3], Eugene L. Q. Lee[1,3], H. Robert Horvitz[1,*]

[1]Howard Hughes Medical Institute, Department of Biology, McGovern Institute for Brain Research, Massachusetts Institute of Technology, Cambridge, MA, 02139, USA

[2]Miller Institute, Helen Wills Neuroscience Institute, Department of Molecular and Cellular Biology, University of California, Berkeley, Berkeley, 94720, USA

[3]Department of Brain and Cognitive Sciences, Massachusetts Institute of Technology, Cambridge, MA, 02139, USA

*Correspondence: horvitz@mit.edu

Draft 6/9/2021

bioRxiv preprint doi: https://doi.org/10.1101/2020.06.02.129825; this version posted June 9, 2021. The copyright holder for this preprint (which was not certified by peer review) is the author/funder, who has granted bioRxiv a license to display the preprint in perpetuity. It is made available under aCC-BY 4.0 International license.

Abstract

Neural control of muscle function is fundamental to animal behavior. Many muscles can generate multiple distinct behaviors. Nonetheless, individual muscle cells are generally regarded as the smallest units of motor control. We report that muscle cells can alter behavior by contracting subcellularly. We previously discovered that noxious tastes reverse the net flow of particles through the *C. elegans* pharynx, a neuromuscular pump, resulting in spitting. We now show that spitting results from the subcellular contraction of the anterior region of the pm3 muscle cell. Subcellularly localized calcium increases accompany this contraction. Spitting is controlled by an “hourglass” circuit motif: parallel neural pathways converge onto a single motor neuron that differentially controls multiple muscles and the critical subcellular muscle compartment. We conclude that subcellular muscle units enable modulatory motor control and propose that subcellular muscle contraction is a fundamental mechanism by which neurons can reshape behavior.

bioRxiv preprint doi: https://doi.org/10.1101/2020.06.02.129825; this version posted June 9, 2021. The copyright holder for this preprint (which was not certified by peer review) is the author/funder, who has granted bioRxiv a license to display the preprint in perpetuity. It is made available under aCC-BY 4.0 International license.

Introduction

How animal nervous systems differentially control muscle contractions to generate the variety of flexible, context-appropriate behaviors necessary for survival and reproduction is a fundamental problem in neuroscience. In many cases, distinct behaviors must be performed using the same muscle or set of muscles. For example, the muscles of the human jaw and tongue control both feeding and speech, while the *Drosophila* wing muscles produce both flight and song (O'Sullivan *et al.*, 2018). Such modulation of muscle function can be achieved via neuronally-mediated alteration of the amplitudes and relative timing of muscle motions (Briggman and Kristan, 2008; Marder and Calabrese, 1996).

We are analyzing the neuromuscular control of behavior using the *C. elegans* feeding organ, the pharynx, as a model neuromuscular system. The pharynx (Figure 1A) is a neuromuscular pump that contracts rhythmically ("pumps") to generate the suction that ingests bacterial food (Avery and You, 2012). The pharynx contains 14 classes of neurons (20 neurons in total), 8 classes of muscles (20 muscle cells in total), 4 glands, and 16 structural cells, and the connectome of these cells has been completely described (Albertson and Thomson, 1976; Cook *et al.*, 2020).

bioRxiv preprint doi: https://doi.org/10.1101/2020.06.02.129825; this version posted June 9, 2021. The copyright holder for this preprint (which was not certified by peer review) is the author/funder, who has granted bioRxiv a license to display the preprint in perpetuity. It is made available under aCC-BY 4.0 International license.

Behavioral functions are known for 9 of the 14 pharyngeal neuron classes (15 of the 20 total neurons). The two M2 neurons, single M4, and two MC neurons promote pumping and/or ingestion (Avery and Horvitz, 1987, 1989; Trojanowski *et al.*, 2014); the two M3 and single I5 neurons regulate the timing of muscle relaxation (Avery, 1993); the two I2 neurons inhibit pumping (Bhatla and Horvitz, 2015); the two I1 neurons promote or inhibit pumping dependent on context (Dent *et al.*, 2000; Trojanowski *et al.*, 2014; Bhatla *et al.*, 2015); the two NSM neurons regulate locomotion and feeding in response to food or food-related odors (Sawin *et al.*, 2000; Li *et al.*, 2012; Flavell *et al.*, 2013; Rhoades *et al.*, 2019); and, as described in more detail below, the single M1 neuron controls spitting behavior (Bhatla *et al.*, 2015).

We previously found that short-wavelength violet or ultraviolet (UV) light inhibits *C. elegans* feeding behavior and that this modulation likely is mediated by light-generated reactive oxygen species (ROS) and thus reflects a response to noxious taste stimuli (Bhatla and Horvitz, 2015). Consistent with this hypothesis, the same set of genes and neurons necessary for light-induced feeding inhibition is required for the inhibition of feeding by the ROS hydrogen peroxide (H_2O_2) (Bhatla and Horvitz, 2015). Because we and others have found that light and ROS act similarly to elicit behavioral responses (Hill and Schaefer, 2009; Kim *et al.*, 2013b; Kim and Johnson, 2014; Guntur

bioRxiv preprint doi: https://doi.org/10.1101/2020.06.02.129825; this version posted June 9, 2021. The copyright holder for this preprint (which was not certified by peer review) is the author/funder, who has granted bioRxiv a license to display the preprint in perpetuity. It is made available under aCC-BY 4.0 International license.

et al., 2015; Du *et al.*, 2016; Arenas *et al.*, 2017; Birkholz and Beane, 2017; Guntur *et al.*, 2017), and because of the high precision with which light can be controlled as an experimental stimulus, we are using light as a tool to analyze how the neuromusculature of the pharynx produces behavioral responses to noxious stimuli.

We found that upon exposure to short-wavelength light, pharyngeal pumping rapidly stops (“acute inhibition”) and then transiently resumes (“burst pumping”; e.g., see Figure 1B). After the removal of light, the pumping rate is depressed and slowly recovers (“recovery”) to the 4-5 Hz of normal feeding over about a minute (Bhatla and Horvitz, 2015). Our previous studies implicated four classes of pharyngeal neurons in the pumping response to light (Bhatla and Horvitz, 2015; Bhatla *et al.*, 2015). Light inhibits pumping by altering the activity of the I1, I2, and MC neurons. Subsequently, the M1 motor neuron promotes the burst pumping phase, during which the net flow of particles through the anterior pharynx is reversed, producing a spitting behavior that ejects ingested material from the pharynx.

We now report that light transforms feeding pumps into spitting pumps -- i.e. reverses the direction in which particles are driven by pharyngeal pumping -- by inducing sustained contractions of subcellular regions of individual muscle cells, the three pm3 pharyngeal muscle cells. Subcellularly localized calcium signals occur in

bioRxiv preprint doi: https://doi.org/10.1101/2020.06.02.129825; this version posted June 9, 2021. The copyright holder for this preprint (which was not certified by peer review) is the author/funder, who has granted bioRxiv a license to display the preprint in perpetuity. It is made available under aCC-BY 4.0 International license.

those regions of the pm3 muscles undergoing contraction. Both spitting and the associated localized muscle calcium response are controlled by the M1 neuron. M1 sits at the waist of an "hourglass" circuit motif, in which multiple upstream sensory neurons converge onto M1, which in turn makes divergent outputs onto multiple muscle classes that control distinct subcomponents of the spitting reflex. Weak activation of M1 via a subset of upstream neurons can evoke a subset of M1's motor outputs, producing an attenuated variant of spitting and showing how graded neuronal activation can produce context-appropriate variations of a core behavior. Together, our results provide an example of how muscle function can be modulated at a subcellular level to produce flexible, contextual behavior and identify subcellularly localized calcium as a mechanistic basis of such modulation.

Results

Worms Spit as a Consequence of the Sustained Contraction of Anterior Pharyngeal Muscles

We previously defined burst pumping as the transient increase in pumping rate that follows acute light-induced pumping inhibition (Figure 1B) (Bhatla and Horvitz, 2015). Because 365 nm (UV) light evokes burst pumping most robustly (Bhatla and Horvitz,

bioRxiv preprint doi: https://doi.org/10.1101/2020.06.02.129825; this version posted June 9, 2021. The copyright holder for this preprint (which was not certified by peer review) is the author/funder, who has granted bioRxiv a license to display the preprint in perpetuity. It is made available under aCC-BY 4.0 International license.

2015), we used this wavelength in the experiments described below. We further characterized the burst pumping phase and observed that there are three alterations to pharyngeal function that occur during burst pumping: (a) as described previously (Bhatla and Horvitz, 2015; Bhatla *et al.*, 2015), pumping rate increases; (b) the valve at the anterior end of the pharynx that closes to capture food during feeding instead remains open, causing pharyngeal pumps to conclude with the spitting of pharyngeal contents; and (c) a filter that otherwise restricts particle influx opens, facilitating the rinsing of the pharyngeal lumen (Figure 1A).

In this work, we first confirmed that pumping rate increases during burst pumping, as reported previously (Bhatla and Horvitz, 2015). We scored pumping in the burst pumping phase in real time by eye, using the assay validated by Bhatla and Horvitz (2015) and based on the rate of contraction of the grinder ("grinder pumps"), a readily-observed cuticular structure in the terminal bulb (Figure 1A and 1B).

We next confirmed and extended the previous observation that worms spit during the burst pumping phase (Bhatla *et al.*, 2015). We distinguished feeding and spitting pumps by recording high-speed videos of worms feeding on a mixture of *E. coli* bacterial food and comparably-sized 1 μm polystyrene beads (Fang-Yen *et al.*, 2009; Bhatla *et al.*, 2015). We designated pumps that trapped ingested material in the anterior

bioRxiv preprint doi: https://doi.org/10.1101/2020.06.02.129825; this version posted June 9, 2021. The copyright holder for this preprint (which was not certified by peer review) is the author/funder, who has granted bioRxiv a license to display the preprint in perpetuity. It is made available under aCC-BY 4.0 International license.

pharynx as feeding pumps (Video 1) and pumps that failed to trap material as spitting pumps (Video 2; Figure 1C). We previously found that violet light (436 nm) induces spitting (Bhatla *et al.*, 2015) and have replicated this result using UV light (365 nm) (Figure 1C-1E). Consistent with the hypothesis that the pumping response to light reflects a response to light-generated ROS, the odor of H_2O_2 also induced spitting (Figure 1—figure supplement 1A). While light reversed the net anterior-to-posterior flow of beads that occurs during feeding through the anterior pharynx, light did not reverse this anterior-to-posterior movement of beads in more posterior pharyngeal regions, i.e., the anterior bulb, isthmus, and posterior bulb (Figure 1A).

We identified the biomechanical mechanism by which net particle flow is reversed to produce spitting. In feeding, contraction of the pharyngeal muscles opens the lumen of the pharynx, generating suction and drawing food and fluid inwards. Two cuticular structures project from pharyngeal muscle into the lumen of the anterior pharynx and buccal cavity: the metastomal flaps and the pharyngeal valve (Figure 1A) (Albertson and Thomson, 1976). The metastomal flaps were previously shown to limit the size and flow of particles that enter the pharyngeal lumen from the buccal cavity (Fang-Yen *et al.*, 2009). For this reason, we will refer to the metastomal flaps as the "metastomal filter." The pharyngeal valve is located immediately posterior to the filter

bioRxiv preprint doi: https://doi.org/10.1101/2020.06.02.129825; this version posted June 9, 2021. The copyright holder for this preprint (which was not certified by peer review) is the author/funder, who has granted bioRxiv a license to display the preprint in perpetuity. It is made available under aCC-BY 4.0 International license.

and prevents the escape of ingested particles from the pharyngeal lumen to the buccal cavity: prior to the onset of pharyngeal muscle relaxation, the pharyngeal valve closes, sealing the anterior end of the lumen to retain bacteria while fluid is released via channels that border the lumen (Fang-Yen *et al.*, 2009). Given the importance of the pharyngeal valve in feeding, we hypothesized that spitting involves a modulation of the motions of this structure. We recorded videos of animals feeding and spitting under a coverslip such that the anterior pharyngeal muscles and lumen were clearly visualized. As reported previously (Fang-Yen *et al.*, 2009), feeding pumps involved the closure of the pharyngeal valve, thus trapping food (Figure 1F; Video 3). By contrast, spitting pumps were characterized by a strikingly different motion: rather than relaxing and closing at each pump's conclusion, the anterior tip of the pharynx remained contracted -- i.e., open -- throughout the pumping cycle (Figure 1F; Video 4). This sustained contraction prevented the pharyngeal valve from closing and capturing food at the end of the pump, such that closure of the lumen expelled the pharyngeal contents. These open-valve pumping motions occurred specifically during the burst pumping phase, confirming that they are specific to spitting (Figure 1—figure supplement 1B and 1C).

In addition to increasing the rate of muscle contraction and preventing the closure of the pharyngeal valve, light altered a third aspect of pharyngeal pumping

bioRxiv preprint doi: https://doi.org/10.1101/2020.06.02.129825; this version posted June 9, 2021. The copyright holder for this preprint (which was not certified by peer review) is the author/funder, who has granted bioRxiv a license to display the preprint in perpetuity. It is made available under aCC-BY 4.0 International license.

during the burst pumping phase: the metastomal filter, which is partially closed during feeding (Fang-Yen *et al.*, 2009), instead appeared to be open during spitting. We inferred the configuration of the flaps of the metastomal filter based on the movement of beads through the buccal cavity – whereas during feeding pumps beads accumulated in the buccal cavity and filtered only gradually into the pharynx (Figure 1C and 1G; Video 1), during spitting pumps beads appeared to flow unrestricted from the buccal cavity into the pharynx (Video 2), indicating that the metastomal filter likely opens during spitting. We speculate that, in combination with the opening of the pharyngeal valve, this opening of the metastomal filter produces a rinsing effect, in which greatly increased quantities of material are drawn into and then expelled from the pharynx. Such a mechanism might act to rinse out harmful material before it is ingested (see Discussion).

Although incoming beads were typically impeded by the metastomal filter, we noticed that beads flushed freely into the pharynx during about 25% of feeding pumps; presumably during at least some of these pumps the metastomal filter was partially or fully opened (Figure 1G, Video 5). Because the amount of material ingested and retained during these pumps far exceeded the amount ingested and retained during most feeding pumps (Figure 1—figure supplement 1D), we designated such pumps as

bioRxiv preprint doi: https://doi.org/10.1101/2020.06.02.129825; this version posted June 9, 2021. The copyright holder for this preprint (which was not certified by peer review) is the author/funder, who has granted bioRxiv a license to display the preprint in perpetuity. It is made available under aCC-BY 4.0 International license.

"gulps" and propose that "gulping" might be regulated to modulate rates of food ingestion.

In summary, we found that the spitting reflex was characterized by three changes to pharyngeal behavior: (a) the pumping rate increased; (b) the pharyngeal valve remained open instead of closing, producing spitting; and (c) the metastomal filter opened, increasing the number of particles rinsed in and out with each pump. These changes transformed the pharyngeal motor program from one that promotes feeding into one that promotes spitting from and rinsing of the procorpus (Figure 1A and 1H).

Subcellularly Localized Muscle Contractions and Calcium Increases Open the Pharyngeal Valve to Produce Spitting

We next asked which muscles control the light-induced spitting reflex. The anterior pharynx contains three pharyngeal muscle classes: pm1, pm2, and pm3 (Figure 2A). pm1 is a single hexanucleate cell, while the pm2 and pm3 classes consist of three binucleate cells each (Albertson and Thomson, 1976). The pm1 and pm2 muscles, small cells of unknown function, form a ring around the anterior opening of the pharynx. The metastomal filter protrudes from this ring into the buccal cavity (Figure 2A) such

bioRxiv preprint doi: https://doi.org/10.1101/2020.06.02.129825; this version posted June 9, 2021. The copyright holder for this preprint (which was not certified by peer review) is the author/funder, who has granted bioRxiv a license to display the preprint in perpetuity. It is made available under aCC-BY 4.0 International license.

that contraction of the radially arranged myofilaments of the pm1 and/or pm2 muscles would be expected to pull the filter open and thus expand the aperture of the anterior pharynx (Figure 2A). It is also conceivable that contraction of the pm2s could close the flaps in the absence of contraction by pm1 (Figure 2A). The pm3 muscles make up the remainder of the musculature of the procorpus, and one leaf of the pharyngeal valve protrudes from the anterior end of each of the pm3 muscle cells. Because the filter and valve are held open in spitting, we hypothesized that spitting involves the sustained contraction of some or all of pm1, the pm2s, and/or the anterior end of the pm3s.

We sought to determine the roles of these muscles in spitting. We laser-killed the pm1 and pm2 muscles singly and in combination to determine what, if any, function they have in spitting; because the pm3s are required for the structural integrity of the pharynx (Leon Avery, personal communication), pharyngeal function cannot be studied after pm3 ablation. Laser ablation of pm1, the pm2s, or both classes together did not eliminate burst pumping or spitting (Figure 2B-2E; Videos 7-9), implying that the pm3s can hold open the pharyngeal valve and thus produce spitting in the absence of pm1 and the pm2s. Given that the pm3s are the only muscles in the vicinity of the valve once pm1 and the pm2s have been ablated, we conclude that the contraction of a subcellular region of the pm3 muscles must be sufficient to open the valve, i.e. the anterior regions

bioRxiv preprint doi: https://doi.org/10.1101/2020.06.02.129825; this version posted June 9, 2021. The copyright holder for this preprint (which was not certified by peer review) is the author/funder, who has granted bioRxiv a license to display the preprint in perpetuity. It is made available under aCC-BY 4.0 International license.

of the pm3s of these animals underwent sustained contraction and held open the valve while the rest of the pm3s rhythmically contracted and relaxed.

While the pm1 and pm2 muscles were not necessary for spitting (i.e., the sustained opening of the pharyngeal valve), their ablation altered several aspects of pharyngeal function. First, pm2-ablated animals were partially defective in opening the metastomal filter -- the filter often appeared to be closed during spitting (Video 6, Figure 2F). This abnormality might reflect a functional requirement for the pm2s in opening the flaps (as suggested by the anatomy) or an ablation-induced abnormality that reduced the mobility of the filter. Second, consistent with an earlier observation by others (L. Avery and C. Fang-Yen, personal communication), ablation of pm1 eliminated the metastomal filter (data not shown). For this reason, we were unable to determine whether pm1 is also involved in opening the filter. However, because pm2-ablated animals were not completely defective in opening the filter (Figure 2F) and because pm1 is the only other muscle positioned to perform this function, we think it likely that pm1 contributes to filter opening.

Consistent with a role for the metastomal filter in regulating particle influx, we observed that pm1- and pm1/2-ablated animals often ingested more beads into the

bioRxiv preprint doi: https://doi.org/10.1101/2020.06.02.129825; this version posted June 9, 2021. The copyright holder for this preprint (which was not certified by peer review) is the author/funder, who has granted bioRxiv a license to display the preprint in perpetuity. It is made available under aCC-BY 4.0 International license.

procorpus than did mock-ablated animals (the “stuffed pharynx” phenotype; Avery and Horvitz, 1987; Figure 2—figure supplement 1A and 1B). Some of these pm1- or pm1/2-ablated animals with full pharynges ejected beads less efficiently (5 of 9 animals; Video 7), requiring more pumps to spit out material than mock-ablated animals. The reduced spitting efficiency of these pm1-ablated animals might be a consequence of their enhanced ingestion of beads in the anterior pharynx -- we also observed similarly impaired spitting in one of two mock-ablated animals that had spontaneously ingested greater than normal quantities of beads. However, because we cannot separate the effects of pm1 ablation on the metastomal flaps and particle intake from its effects on spitting behavior, we cannot exclude the possibility that pm1 functions in part to increase the efficiency of spitting. It is also possible that contractions of pm1 and/or pm2, despite being unnecessary for spitting given the results of our ablation studies, might be sufficient in non-ablated animals to open the pharyngeal valve even in the absence of pm3 contraction. With these *caveats*, our ablation experiments establish that, whatever role pm1 and the pm2s might play in other contexts, they are not required for light-induced spitting (i.e., opening of the pharyngeal valve).

We were surprised to observe a functional uncoupling of subdomains -- the anterior end and the rest of the cell -- within each of the pm3 muscle cells. We next

bioRxiv preprint doi: https://doi.org/10.1101/2020.06.02.129825; this version posted June 9, 2021. The copyright holder for this preprint (which was not certified by peer review) is the author/funder, who has granted bioRxiv a license to display the preprint in perpetuity. It is made available under aCC-BY 4.0 International license.

239 sought the physiological mechanism that produces the sustained subcellular pm3
240 muscle contractions. Given the central role of intracellular calcium in initiating muscle
241 contraction (Kuo and Ehrlich, 2015), we examined intracellular calcium levels by
242 expressing the calcium reporter GCaMP3 (Tian *et al.*, 2009) in pharyngeal muscle and
243 imaging light-induced fluorescence calcium changes in the pharynges of immobilized
244 animals (Kim *et al.*, 2013a). These imaging conditions differed from those we used to
245 analyze spitting in the free-moving assay; for imaging, animals were immobilized and
246 this immobilization suppressed spontaneous pumping. Nonetheless, light often
247 stimulated burst pumping by immobilized animals (Figure 2—figure supplement 1C and
248 1D and see Materials and Methods below), and these light-stimulated burst pumps were
249 dependent on the M1 neuron (Figure 2— figure supplement 1D), which is necessary for
250 spitting (Bhatla *et al.*, 2015), and resulted in the expulsion of previously ingested mineral
251 oil, as is the case for spitting by free-moving animals (Video 10). Taken together, these
252 results indicate that the light-induced pumps of immobilized animals are spits.

253 We first used the *gpa-16* promoter (Jansen *et al.*, 1999) to broadly drive the
254 expression of GCaMP3 in pharyngeal muscle. We characterized the expression pattern
255 of this transgene using confocal microscopy and observed bright fluorescence in the
256 pm2 and pm3 muscles and also in the mc1 marginal cells (Figure 2—figure supplement

bioRxiv preprint doi: https://doi.org/10.1101/2020.06.02.129825; this version posted June 9, 2021. The copyright holder for this preprint (which was not certified by peer review) is the author/funder, who has granted bioRxiv a license to display the preprint in perpetuity. It is made available under aCC-BY 4.0 International license.

2A). We also observed occasional dim fluorescence in pm1 (3 of 10 animals). After stimulating animals with light, we often detected pumps as calcium increases across the procorpus and the anterior and terminal bulbs, indicating that functional GCaMP was present in these regions (Video 11, Figure 2G-2H). Interestingly, calcium signals at the tip of the pharynx began before and persisted after calcium signals in posterior regions (Figure 2H-2J). Additionally, during many trials (12 of 20) this anterior region responded with a sustained rise in calcium even when the rest of the pharynx did not respond (Figure 2I). These calcium responses to light were imaged at an acquisition rate of 2 Hz, so we lacked the temporal resolution to distinguish whether each localized calcium signal was a single sustained increase or a rapid series of short-duration calcium pulses. The location and temporal dynamics of the sustained calcium signals in the anterior pharynx coincided precisely with those of the sustained contraction of the muscle region surrounding the anterior pharyngeal valve that underwent sustained contraction (i.e., became uncoupled from the 4-5 Hz rate of pumping) during spitting behavior. Consistent with previous reports (Kerr *et al.*, 2000; Shimozono *et al.*, 2004), we did not observe spatially restricted calcium signals in the anterior pharynx during feeding pumps stimulated with serotonin, indicating that these localized calcium transients are specific to spitting (Video 12, Figure 2—figure supplement 1E).These

bioRxiv preprint doi: https://doi.org/10.1101/2020.06.02.129825; this version posted June 9, 2021. The copyright holder for this preprint (which was not certified by peer review) is the author/funder, who has granted bioRxiv a license to display the preprint in perpetuity. It is made available under aCC-BY 4.0 International license.

observations strongly suggest that these localized calcium increases act physiologically to drive the subcellular contraction of the anterior ends of the pm3s.

To determine if the calcium transients we observed were restricted cell-specifically to the pm1 and/or pm2 muscles or whether they reflected subcellularly-localized activity in the pm3s and/or mc1s, we used two different promoters that each drive expression specifically in the pm3s and/or mc1s but not in pm1 or the pm2s.

The *myo-2p* promoter drives expression in the pm3s and in no other cell in the anterior pharynx (Okkema *et al.*, 1993; Okkema and Fire, 1994). We obtained animals that express GCaMP3 under this promoter (Kozlova *et al.*, 2019) and used confocal microscopy to confirm that these *myo-2p::GCaMP3* animals expressed GCaMP in the pm3s but not in pm1 or the pm2s (Figure 2—figure supplement 2B). After stimulation with light, 16 of the 19 *myo-2p::GCaMP* animals examined responded with subcellular calcium responses at the anterior tips of the pm3s (Video 13); 11 of these 16 animals also showed a subsequent calcium increase in the posterior *myo*-2-expressing regions of the pharynx (Figure 2K-2L). We did not observe localized fluorescence signals when we imaged animals expressing a *myo-2p::GFP* transgene (Miedel *et al.*, 2012) that drives expression of GFP in pharyngeal muscle (Figure 2—figure supplement 1F),

bioRxiv preprint doi: https://doi.org/10.1101/2020.06.02.129825; this version posted June 9, 2021. The copyright holder for this preprint (which was not certified by peer review) is the author/funder, who has granted bioRxiv a license to display the preprint in perpetuity. It is made available under aCC-BY 4.0 International license.

indicating that the localized GCaMP3 fluorescence increases we observed were not a motion artefact or other calcium-independent effect. These observations demonstrate that light induces subcellularly localized calcium increases in the anterior ends of the pm3s. Unlike other strains tested in this study, immobilized animals carrying the *myo-2p::GCaMP3* transgene did not pump when stimulated with light (Figure 2—figure supplement 1D; see Material and Methods below). The *myo-2* promoter used in this transgene drives transgene expression more strongly than the other pharyngeal muscle promoters used in this study (i.e., *gpa-16p* and *C32F10.8p*), and the failure of animals expressing *myo-2p::GCaMP3* to pump while immobilized might be a consequence of GCaMP-mediated intracellular calcium-buffering (a known artefact of GCaMP overexpression -- e.g., as noted by Singh *et al.*, 2018) or another abnormality induced by transgene overexpression.

To confirm the conclusion that light induces subcellularly localized increases in the anterior ends of the pm3s, we used a second promoter to express GCaMP in the pm3s but not in pm1 or the pm2s, C*32F10.8p.* We identified C*32F10.8p* using confocal microscopy to screen GFP fluorescent transcriptional reporters of genes reported to be expressed in the muscles of the anterior pharynx; C*32F10.8p::GFP* (McKay *et al.*, 2003; Hunt-Newbury *et al.*, 2007) was expressed in both the pm3s and mc1s but not in pm1 or

bioRxiv preprint doi: https://doi.org/10.1101/2020.06.02.129825; this version posted June 9, 2021. The copyright holder for this preprint (which was not certified by peer review) is the author/funder, who has granted bioRxiv a license to display the preprint in perpetuity. It is made available under aCC-BY 4.0 International license.

the pm2s (Figure 2—figure supplement 2C). We used the *C32F10.8* promoter to drive expression of GCaMP3 and confirmed using confocal microscopy that this expression was specific to the pm3s and mc1s (Figure 2—figure supplement 2D). Because of the occasional loss of extrachromosomal transgene arrays during cell division, *C. elegans* extrachromosomal arrays are expressed mosaically and the specific subset of cells that inherit the array varies from animal to animal (Stinchcomb *et al.*, 1985). We selected and imaged mosaic *C32F10.8p::GCaMP3* transgene-positive animals with bright transgene expression in the anterior pharynx and observed localized fluorescence increases in response to light in the anterior pharynges of these animals (Figure 2—figure supplement 1G), showing that a GCaMP response to light occurs subcellularly in the anterior ends of the pm3s and/or mc1s. To clarify whether the pm3s, mc1s or both respond to light, we identified transgene-bearing mosaic animals that sparsely but brightly expressed GCaMP3 in one or several cells in the procorpus, examined those animals using our calcium-imaging assay, and then determined their transgene expression pattern using confocal microscopy. By combining pm3- and mc1-identifying landmarks in our calcium imaging videos with 3D reconstructions of GCaMP3 expression, we were able to obtain videos from which we could confidently determine the identities of specific cells that responded to light. Of the 39 videos we recorded, 12

bioRxiv preprint doi: https://doi.org/10.1101/2020.06.02.129825; this version posted June 9, 2021. The copyright holder for this preprint (which was not certified by peer review) is the author/funder, who has granted bioRxiv a license to display the preprint in perpetuity. It is made available under aCC-BY 4.0 International license.

showed cells we unambiguously identified as pm3, and 10 of these 12 videos (~83%) showed subcellular responses in the anterior end of that pm3 (Figure 2M-2N; Video 14). Of the seven videos in which we could unambiguously identify the anterior end of an mc1 marginal cell, only one showed a calcium increase. The response of the set of 10 cells unambiguously identified as pm3s (Figure 2M-2N) was similar to the response of the set of 10 unidentified cells we imaged in animals selected based on general procorpus expression (i.e., the set described in Figure 2—figure supplement 1G). These observations demonstrate that the pm3s responded to light with robust subcellularly localized calcium increases. The mc1s might also exhibit a response that is less frequent, less intense, and/or at least partially outside of the dynamic range of GCaMP3.

In conclusion, our imaging of strains carrying three different reporters -- *gpa-16p::GCaMP3, myo-2p::GCaMP3*, and *C32F10.8p::GCaMP3* -- establish that a subcellular compartment of the anterior tip of the pm3s undergoes a sustained calcium increase in response to light. Taken together, our results indicate that the pm1, pm2, and pm3 muscles play specialized roles in controlling pharyngeal particle flow during spitting: the pm2 and likely the pm1 muscles actively open the metastomal filter, increasing the aperture size of the anterior lumen and thus facilitating particle influx,

bioRxiv preprint doi: https://doi.org/10.1101/2020.06.02.129825; this version posted June 9, 2021. The copyright holder for this preprint (which was not certified by peer review) is the author/funder, who has granted bioRxiv a license to display the preprint in perpetuity. It is made available under aCC-BY 4.0 International license.

while a subcellular anterior compartment of the pm3s opens the pharyngeal valve via subcellular calcium signaling, preventing the retention of ingested material and thus producing spitting.

Pharyngeally-Expressed Gustatory Receptor Orthologs *lite-1* and *gur-3* Play Major and Minor Roles, Respectively, in the Light-Induced Spitting Reflex

Previously-described *C. elegans* locomotory and pharyngeal feeding responses to light depend on the gustatory receptor orthologs *lite-1* and/or *gur-3*, which are expressed in a number of pharyngeal and extra-pharyngeal neurons (Edwards *et al.*, 2008; Liu *et al.*, 2010; Bhatla and Horvitz, 2015). We asked if gustatory receptor orthologs similarly control the light-induced spitting reflex. The burst pumping rates of animals carrying null alleles of *gur-3* (Bhatla and Horvitz, 2015) or its paralogs *egl-47/gur-1, gur-4,* and *gur-5* were similar to that of wild-type animals (Figure 3—figure supplement 1A-1E). *lite-1* null mutants (Edwards *et al.*, 2008) could not be tested directly, because they exhibit substantial defects in light-induced pumping inhibition (Bhatla and Horvitz, 2015), thus obscuring burst pumping behavior (Figure 3—figure supplement 1F and 1G).

bioRxiv preprint doi: https://doi.org/10.1101/2020.06.02.129825; this version posted June 9, 2021. The copyright holder for this preprint (which was not certified by peer review) is the author/funder, who has granted bioRxiv a license to display the preprint in perpetuity. It is made available under aCC-BY 4.0 International license.

To examine the role of *lite-1* in burst pumping, we tested *lite-1* mutants in an *eat-2* mutant background. *eat-2* mutants are severely defective in feeding pumping (Raizen *et al.*, 1995) but not in burst pumping (Figure 3—figure supplement 1H). Thus, the burst pumping rate rises above the slow *eat-2* feeding pumping rate and can be scored even in animals defective in light-induced inhibition of feeding. We found that in *eat-2* mutants *lite-1* but not *gur-3* was required for wild-type burst pumping, a defect that was partially rescued by expression of a wild-type copy of *lite-1* (Figure 3—figure supplement 1H-1L). Thus, light-induced stimulation of pumping requires *lite-1* but not *gur-3.*

These experiments established a role for *lite-1* in controlling burst pumping -- i.e., light-induced contractions of the grinder. To determine directly whether *lite-1* and/or *gur-3* are required for spitting -- i.e., the opening of the pharyngeal valve -- we used the polystyrene bead-feeding assay to measure light-induced spitting (i.e., the failure to capture beads at the conclusion of a pump) by *lite-1* and *gur-3* single mutants and *lite-1 gur-3* double mutants. Both *gur-3* and *lite-1* mutants spit less than controls, and *lite-1* mutants also displayed a dramatic reduction in peak spitting rate compared to wild-type animals (Figure 3A-3C and 3G). Strikingly, *lite-1 gur-3* double mutants did not spit in response to light (Figure 3D). *lite-1* and *gur-3* mutants were also defective in opening the metastomal filter (Figure 3H). Rescue transgenes expressing wild-type copies of

bioRxiv preprint doi: https://doi.org/10.1101/2020.06.02.129825; this version posted June 9, 2021. The copyright holder for this preprint (which was not certified by peer review) is the author/funder, who has granted bioRxiv a license to display the preprint in perpetuity. It is made available under aCC-BY 4.0 International license.

either *lite-1* (Bhatla and Horvitz, 2015) or *gur-3* (this study) restored both light-induced spitting and filter-opening in *lite-1 gur-3* double mutants (Figure 3F-3H). Together, these results indicate that both *lite-1* and *gur-3* function in light-induced spitting and opening of the filter, with *lite-1* likely playing a greater role.

Next we assayed the pharyngeal muscle calcium response to light in *lite-1* and *gur-3* mutants using the pan-pharyngeal *gpa-16p::GCaMP3* reporter. *gur-3* mutants resembled wild-type animals (Figure 3I, 3J, and 3M), while *lite-1* mutants were almost completely defective in the pharyngeal muscle calcium response to light, except for a very weak, fast response (Figure 3I, 3K, 3M, and 3N). This fast response depended on *gur-3*, as the response of *lite-1 gur-3* double mutants was completely defective (Figure 3I, 3L, and 3N). Thus, consistent with our behavioral observations, *lite-1* and *gur-3* function together in light-induced calcium increases in pharyngeal muscle, with *lite-1* playing the major role and *gur-3* playing a minor role.

Taken together, these results indicate that *lite-1* and *gur-3* both contribute to light-induced spitting. *lite-1* is necessary for the full response -- an increase in pumping rate (burst pumping), opening of the pharyngeal valve (i.e., spitting), opening of the metastomal filter, and a robust increase in pharyngeal muscle calcium -- while *gur-3* is

bioRxiv preprint doi: https://doi.org/10.1101/2020.06.02.129825; this version posted June 9, 2021. The copyright holder for this preprint (which was not certified by peer review) is the author/funder, who has granted bioRxiv a license to display the preprint in perpetuity. It is made available under aCC-BY 4.0 International license.

sufficient in the absence of *lite-1* to produce an attenuated response -- partial opening of the valve and filter and weak activation of pharyngeal muscle.

The M1 Pharyngeal Neuron Innervates the Pharyngeal Valve and Controls Light-Induced Spitting

The M1 pharyngeal neuron is the only major source of innervation of the pm1, pm2, and pm3 muscles at the anterior tip of the pharynx (Albertson and Thomson, 1976), and these M1 synapses are located in the region of the metastomal filter, the pharyngeal valve at the anterior corpus, the subcellular muscle contractions and the subcellular calcium increases we observed during spitting (Figure 4A). We previously found that M1 is required for spitting induced by violet light (Bhatla *et al.*, 2015). We tested whether M1 is also required for spitting induced by UV light, which, as noted above, we used throughout this study to induce spitting. We laser-killed M1 and also generated an M1 genetic-ablation strain in which the mammalian caspase ICE (Cerretti *et al.*, 1992; Thornberry *et al.*, 1992; Zheng *et al.*, 1999) is expressed under the M1-specific *lury-1* promoter (Ohno *et al.*, 2017). Unlike mock-ablated or transgene-negative control animals, animals lacking M1 because of laser or genetic ablation were completely

bioRxiv preprint doi: https://doi.org/10.1101/2020.06.02.129825; this version posted June 9, 2021. The copyright holder for this preprint (which was not certified by peer review) is the author/funder, who has granted bioRxiv a license to display the preprint in perpetuity. It is made available under aCC-BY 4.0 International license.

414 defective in UV light-induced burst pumping and spitting (Figure 4B-4E and Figure 4—
415 figure supplement 1A-C). Genetic ablation of M1 also eliminated burst pumping in *eat-2*
416 mutants (Figure 4—figure supplement 1D). Finally, laser ablation of M1 in animals
417 carrying the broadly-expressed *gpa-16p::GCaMP3* reporter also eliminated the light-
418 induced calcium signals in anterior pharyngeal muscles (Figure 4F-4G), consistent with
419 their being induced by M1. A *caveat* concerning this interpretation is that ablation of M1
420 might also have affected the development or function of other pharyngeal components,
421 but we note that when we previously laser-killed each pharyngeal neuron class
422 individually and tested the response of these ablated animals to light, only ablation of
423 M1 caused a reduction in burst pumping (Bhatla *et al.*, 2015). We could not directly
424 determine whether ablation of M1 altered the function of the metastomal filter in wild-
425 type animals, because M1-ablated animals did not spit and rarely pumped in the
426 presence of light (but see below). To determine if M1 activity is acutely required for
427 spitting, we generated animals expressing the HisCl1 histamine-gated chloride channel
428 (Pokala *et al.*, 2014) in M1 using an extrachromosomal array that drives *HisCl1* gene
429 expression by the *glr-2* promoter (Brockie *et al.*, 2001), which overlaps with the M1-
430 specific *lury-1* promoter only in M1, and hyperpolarized M1 with exogenous histamine.
431 Consistent with an acute function for M1 in spitting, exogenous histamine significantly

bioRxiv preprint doi: https://doi.org/10.1101/2020.06.02.129825; this version posted June 9, 2021. The copyright holder for this preprint (which was not certified by peer review) is the author/funder, who has granted bioRxiv a license to display the preprint in perpetuity. It is made available under aCC-BY 4.0 International license.

delayed light-induced spitting in animals with array-expressing M1s, but not animals with array-negative M1s (Figure 4H-4L). We conclude that the M1 neuron is required for UV light-induced burst pumping, spitting, and muscle calcium physiology.

We observed that the pumping rate of M1-ablated animals recovered significantly more quickly than did controls after stimulation with light and that these pumps, in contrast to typical pumps in which the procorpus and grinder contract together, were characterized by contractions of the grinder but not the procorpus (Figure 4—figure supplement 1E-1H). These observations suggest that in addition to controlling pumping and spitting in the burst pumping phase, M1 also inhibits the grinder during the recovery phase.

Given that light-induced spitting requires M1, we asked whether M1 is acutely activated by light. We generated transgenic animals expressing the calcium reporter GCaMP6s (Chen *et al.*, 2013) in M1 under the control of the *glr-2* promoter (Brockie *et al.*, 2001) and measured light-induced calcium changes. As indicated by robust GCaMP6s fluorescence increases, light increased M1 somatic calcium levels, consistent with an acute function for M1 in spitting (Figure 4M-4O, Video 15).

bioRxiv preprint doi: https://doi.org/10.1101/2020.06.02.129825; this version posted June 9, 2021. The copyright holder for this preprint (which was not certified by peer review) is the author/funder, who has granted bioRxiv a license to display the preprint in perpetuity. It is made available under aCC-BY 4.0 International license.

We next asked if *lite-1* and *gur-3* control M1's calcium response to light. *lite-1* is expressed in M1 (Bhatla and Horvitz, 2015; Taylor *et al.*, 2019). The *gur-3* expression pattern was first determined using extrachromosomal arrays expressing GFP under the *gur-3* promoter (Bhatla and Horvitz, 2015) and subsequently examined using single-cell transcriptomic analysis of the *C. elegans* nervous system (Taylor *et al.*, 2019). Although neither method detected *gur-3* expression in M1, when we integrated the previously-generated extrachromosomal arrays into the genome we noted that, in addition to being expressed in the I2 and I4 neurons as reported previously (Bhatla and Horvitz, 2015), the stably integrated *gur-3*$_{promoter}$*::GFP* transgene was also expressed in M1 and another pharyngeal neuron, MI (Figure 3—figure supplement 1M and 1N), consistent with possible functions for both *lite-1* and *gur-3* in M1. As was the case with pharyngeal muscle calcium increases, both *lite-1* and *gur-3* were required for light-induced calcium increases in the M1 soma (Figure 4P-4U), with *lite-1's* playing the major role in the overall response (Figure 4T) and *gur-3's* playing a minor role necessary only in the acute response (Figure 4U), suggesting that the differential requirement for *lite-1* and *gur-3* in spitting occurs at or upstream of M1's activation.

We then asked if M1 might be activated directly by light, as suggested by its expression of *lite-1* and *gur-3*, or whether it instead is activated indirectly by input from

bioRxiv preprint doi: https://doi.org/10.1101/2020.06.02.129825; this version posted June 9, 2021. The copyright holder for this preprint (which was not certified by peer review) is the author/funder, who has granted bioRxiv a license to display the preprint in perpetuity. It is made available under aCC-BY 4.0 International license.

other light-sensitive neurons via synaptic, humoral (i.e., dense core vesicle), or gap junction inputs. Synaptic and humoral dense-core vesicle signaling respectively require *unc-13*, which encodes the *C. elegans* homolog of UNC13A (Maruyama and Brenner, 1991; Richmond *et al.*, 1999, 2001), and *unc-31,* which encodes the *C. elegans* homolog of CADPS/CAPS (Berwin *et al.*, 1998), so we examined light-induced M1 calcium responses in these mutants. In both *unc-13(s69)* reduction-of-function mutants (Richmond *et al.*, 1999) -- null mutations are lethal (Kohn *et al.*, 2000) -- and *unc-31(u280)* presumptive null mutants (Speese *et al.*, 2007), M1's calcium response was reduced in magnitude but still significant (Figure 4—figure supplement 1I-1L). These results suggest that M1 likely can function as a cellular photoreceptor but do not preclude the possibility that M1's activation occurs through residual *unc-13* function, gap junctions, or a pathway in which *unc-13* and *unc-31* function redundantly.

To determine whether acute activation of M1 is sufficient to produce spitting, we expressed channelrhodopsin 2 (ChR2) (Nagel *et al.*, 2003; Boyden *et al.*, 2005) in M1. Because the light used to activate ChR2 also activates the endogenous pharyngeal response to light, we performed these experiments using *lite-1 gur-3* mutant animals. While no *lite-1 gur-3* mutant animals grown in the absence of the essential ChR2 cofactor all-*trans* retinal (ATR) showed spitting behavior in response to stimulation with

bioRxiv preprint doi: https://doi.org/10.1101/2020.06.02.129825; this version posted June 9, 2021. The copyright holder for this preprint (which was not certified by peer review) is the author/funder, who has granted bioRxiv a license to display the preprint in perpetuity. It is made available under aCC-BY 4.0 International license.

470 nm blue light, 25% of animals grown with ATR did so when illuminated (Figure 4V and 4W). Thus, optogenetic activation of M1 can produce spitting behavior, although not as efficiently as UV light does in the wild-type background.

Next, we asked what neurotransmitter or neurotransmitters M1 uses to activate pharyngeal muscle. M1 expresses the cholinergic marker genes *unc-17* and *cha-1* (Franks *et al.*, 2009; Taylor *et al.*, 2019), and consistent with a cholinergic function for M1 we found that animals with loss-of-function mutations in genes required for signaling by acetylcholine (ACh) (*unc-17, cha-1*) but not by other neurotransmitters (*unc-25, eat-4, cat-2, tdc-1, tph-1,* and *ser-4; mod-1 ser-1 ser-7)* were severely defective in burst pumping, as were *ric-1* mutants, which are defective in nicotinic ACh receptor maturation (Halevi *et al.*, 2002) (Figure 4—figure supplement 1M-1V).

We assayed the burst pumping behavior of 36 strains, each carrying a mutation in one of 36 of the 37 known *C. elegans* ACh receptors or receptor subunits (null mutation in the 37th receptor subunit, *acr-9*, results in lethality) (The *C. elegans* Deletion Mutant Consortium, 2012). While several strains showed modest defects, none was strikingly defective, suggesting that multiple acetylcholine receptors function redundantly downstream of M1 (Figure 4—figure supplement 2A-2P').

bioRxiv preprint doi: https://doi.org/10.1101/2020.06.02.129825; this version posted June 9, 2021. The copyright holder for this preprint (which was not certified by peer review) is the author/funder, who has granted bioRxiv a license to display the preprint in perpetuity. It is made available under aCC-BY 4.0 International license.

Together these observations confirmed and extended our previous finding that M1 is necessary for spitting, additionally showing that M1 controls spatially-restricted muscle calcium signals, that it is acutely activated by light, and that its activation can suffice for spitting.

The *gur-3*-Expressing I2 and I4 Neurons Can Weakly Activate M1 to Open the Metastomal Filter and Pharyngeal Valve Without Increasing Pumping Rate

The M1 neuron's expression of *lite-1* and *gur-3* suggests that M1 is a likely site of action of *lite-1* and *gur-3* in the spitting response to light. However, *unc-13* and *unc-31* mutants were significantly reduced in M1 activation (Figure 4—figure supplement 1I-1L), consistent with the possibility that other *lite-1* and/or *gur-3* neurons provide stimulatory inputs to M1.

To identify light-sensing neurons that function upstream of M1, we first focused on pharyngeal neurons known to express *gur-3*. The pharyngeal I2 neurons express *gur-3* and control light-induced pumping inhibition (Bhatla and Horvitz, 2015). Since the I2s form electrical and chemical synapses with M1 (Albertson and Thomson, 1976), we tested the hypothesis that they provide functional inputs to M1 for the induction of

bioRxiv preprint doi: https://doi.org/10.1101/2020.06.02.129825; this version posted June 9, 2021. The copyright holder for this preprint (which was not certified by peer review) is the author/funder, who has granted bioRxiv a license to display the preprint in perpetuity. It is made available under aCC-BY 4.0 International license.

spitting by expressing a wild-type copy of *gur-3* under an I2-specific promoter (Bhatla and Horvitz, 2015) in *lite-1 gur-3* double mutants. I2-specific rescue of *gur-3* restored robust light-induced spitting, opening of the metastomal filter, and weak M1 calcium increases to *lite-1 gur-3* double mutants, indicating that light can activate M1 via *gur-3* function in the I2 neurons (Figure 5A-5E).

Laser ablation of M1 suppressed this *gur-3*-dependent spitting and opening of the metastomal filter (Figure 5F-5H), showing that the I2 neurons act via (or possibly in parallel to) M1 to induce spits and open the filter.

Since the I2 neurons can strongly stimulate spitting, we next asked if they could increase pumping rates in slow-pumping *eat-2* mutants. Light did not increase the pumping rate of *eat-2*; *lite-1 gur-3;* $I2_{promoter}$*::gur-3(+)* animals (Figure 5I). Thus, while the I2 neurons can activate M1 and thereby open the pharyngeal valve and metastomal filter, they are unable to activate M1 sufficiently strongly to drive pumping rate increases. This finding is consistent with our calcium imaging results indicating the I2 neurons can activate M1 only weakly (Figure 5D-5E) and with our observation that *lite-1,* but not *gur-3,* is required for burst pumping (Figure 3—figure supplement 1H-1L).

bioRxiv preprint doi: https://doi.org/10.1101/2020.06.02.129825; this version posted June 9, 2021. The copyright holder for this preprint (which was not certified by peer review) is the author/funder, who has granted bioRxiv a license to display the preprint in perpetuity. It is made available under aCC-BY 4.0 International license.

We also observed that *lite-1 gur-3*; *I2$_{promoter}$::gur-3(+)* animals inhibited pumping only weakly, if at all (Figure 5B and 5F). This finding was initially surprising, because prior work showed that the I2s inhibit pumping in response to light (Bhatla and Horvitz, 2015). Interestingly, after we ablated M1 in these animals, we observed robust light-induced pumping inhibition (Figure 5G, and 5J). This finding suggests that the I2 neurons' stimulatory effect on M1 outweighs their inhibitory effect on pharyngeal muscle. Initially, it seemed paradoxical that the I2s would function in this manner. However, when we compared the rate of feeding pumps (i.e., pumps that capture food) in M1- and mock-ablated *lite-1 gur-3; I2$_{promoter}$::gur-3* animals, it became clear that the I2s' activation of M1 serves to reduce the overall feeding rate, because activating M1 eliminates feeding pumps by turning them into spits (Figure 5K). Thus, rather than simply acting as nonspecific inhibitors of the rates of both feeding and spitting pumps, the I2s reduce food intake via two mechanisms: direct inhibition of feeding by hyperpolarizing pharyngeal muscles (Bhatla and Horvitz, 2015; Bhatla *et al.*, 2015) and indirect transformation of feeding pumps into spits by activating M1 (Figure 5L).

We used an I2-specific genetic-ablation transgene (Bhatla and Horvitz, 2015) to kill the I2 neurons in wild-type and *lite-1* genetic backgrounds. Spitting persisted after ablation of the I2 neurons in both cases (Figure 6A and 6B), confirming that the I2

bioRxiv preprint doi: https://doi.org/10.1101/2020.06.02.129825; this version posted June 9, 2021. The copyright holder for this preprint (which was not certified by peer review) is the author/funder, who has granted bioRxiv a license to display the preprint in perpetuity. It is made available under aCC-BY 4.0 International license.

552 neurons are not necessary for spitting. Thus, *gur-3*-expressing neurons other than the
553 I2 neurons can promote spitting.

554 *gur-3* is also expressed in the pharyngeal I4 neuron (Figure 6C), which has no
555 known function. I4 is activated by light (Bhatla and Horvitz, 2015) and synapses onto
556 M1 (Albertson and Thomson, 1976). To determine if I4 contributes to M1's *gur-3*-
557 dependent activation by light, we laser-killed the I2s and I4 of *lite-1* mutants singly and
558 in combination and assayed spitting behavior. No ablation condition completely
559 eliminated spitting (Figure 6D-6H), but I4 ablation significantly reduced the spitting of
560 *lite-1* I2-ablated animals (Figure 6E, 6G, and 6H), suggesting that I4 promotes spitting in
561 *lite-1* I2-ablated animals. We did not observe significant differences in spitting or
562 pumping inhibition between *lite-1* I4-ablated and mock-ablated animals (Figure 6D, 6F,
563 6H, and 6I), so our conclusion that I4 promotes spitting is limited to the context of *lite-1*
564 animals lacking I2 neurons. More generally, the presence of I2s creates two issues that
565 affect the interpretation of all neuronal ablations in *lite-1* animals. First, when the I2
566 neurons are present they inhibit pumping, and this I2-dependent inhibition compresses
567 the dynamic range of the assay by ~50% (Figure 6I). This compression thus has the
568 potential to mask the contributions of non-I2 neurons to spitting and makes it difficult to
569 accurately assay the effect of a given ablation on spitting. Second, when the I2s are

bioRxiv preprint doi: https://doi.org/10.1101/2020.06.02.129825; this version posted June 9, 2021. The copyright holder for this preprint (which was not certified by peer review) is the author/funder, who has granted bioRxiv a license to display the preprint in perpetuity. It is made available under aCC-BY 4.0 International license.

present in a *lite-1* background this assay cannot distinguish between an increase in inhibition and a decrease in spitting. These limitations are specific to *lite-1* animals, because *lite-1* animals are so defective in pumping inhibition that the burst pumping phase is not clearly visible. For these reasons, we cannot interpret any ablation performed in the context of functional I2s in a *lite-1* background.

We detected small light-induced M1 calcium increases in mock-, I2-, and I4-ablated *lite-1* animals but not in I2/I4 double-ablated *lite-1* animals (Figure 6—figure supplement 1A-1C), and I2-, I4-, and I2/I4-ablated animals seemed to open the metastomal filter slightly less often than did mock-ablated controls (Figure 6—figure supplement 1D), but these differences were not statistically significant. We noticed that the pumping inhibition of *lite-1* I4-ablated animals (Figure 6F) was much stronger than that of *lite-1 gur-3;* $I2_{promoter}$*::gur-3(+)* animals (Figure 5D and 5H), suggesting that *gur-3* might function in neurons other than the I2s and I4 to regulate the balance between promotion and inhibition of pumping. Finally, these results are also consistent with *gur-3*'s functioning in another upstream neuron that acts via I4, rather than in I4 itself. In short, our ablation data suggest but do not prove that I4 can promote spitting.

To verify that the spitting we observed in these experiments was M1-dependent, we killed M1 in combination with the I2 and I4 neurons of *lite-1* mutants. As expected,

bioRxiv preprint doi: https://doi.org/10.1101/2020.06.02.129825; this version posted June 9, 2021. The copyright holder for this preprint (which was not certified by peer review) is the author/funder, who has granted bioRxiv a license to display the preprint in perpetuity. It is made available under aCC-BY 4.0 International license.

ablation of M1 eliminated spitting in all conditions (Figure 6J-6O). Consistent with our observation that I2 inhibits pumping in M1-ablated animals (Figure 5G), we found that M1- and M1/I4-ablated animals inhibited pumping in response to light, while triple-ablated animals lacking M1, I2, and I4 were defective in pumping inhibition (Figure 6K, 6M-6O). Some M1/I2-ablated animals inhibited pumping in response to light, suggesting that the I4 neuron might inhibit pumping in a manner similar to the I2 neurons, but this effect was not statistically significant (Figure 6L and 6O).

Because ablating the I2 and I4 neurons together failed to completely eliminate spitting, *gur-3* likely functions in one or more additional neurons. In addition to being expressed in M1 and MI, *gur-3* is also expressed in the extra-pharyngeal AVD neurons. These cells or others might be additional sites of residual *gur-3* function. In short, the I2 and I4 neurons and perhaps others likely function in parallel to promote *gur-3*-, M1-dependent spitting.

Discussion

To understand how the nervous system adapts the output of a single set of muscles to a changing environment, we analyzed the spitting reflex of the *C. elegans* pharynx. This

bioRxiv preprint doi: https://doi.org/10.1101/2020.06.02.129825; this version posted June 9, 2021. The copyright holder for this preprint (which was not certified by peer review) is the author/funder, who has granted bioRxiv a license to display the preprint in perpetuity. It is made available under aCC-BY 4.0 International license.

reflex comprises three parallel behavioral components: an increase in pumping rate, the opening of the pharyngeal valve at the anterior end of the procorpus, and the opening of the metastomal filter. Opening the pharyngeal valve permits the expulsion of ingested material (i.e., spitting), while opening the metastomal filter allows the worm to flush in and out large amounts of fluid and particles not previously in the pharynx, apparently rinsing its mouth in response to a bad taste (Figure 7A). The pm2 and likely the pm1 pharyngeal muscles open the metastomal filter, while a subcellular compartment of the pm3 muscles opens the pharyngeal valve, transforming feeding motions into spitting motions. The pm3s make up the bulk of the anterior pharynx, which pumps rhythmically during spitting. Opening of the pharyngeal valve by the pm3s requires that a subcellular compartment at the anterior end of each pm3 undergoes a sustained uncoupling from the rest of the cell and remains contracted. Strikingly, the bulk of each pm3 muscle cell continues to pump, ejecting ingested material. The subcellular contraction of the pm3s is accompanied by subcellularly localized increases in intracellular calcium at the site of the pharyngeal valve. Spitting behavior, opening of the metastomal filter, and muscle calcium physiology are controlled by the M1 neuron, which directly innervates the pharyngeal muscles that control the filter and valve. The gustatory-receptor orthologs *lite-1* and *gur-3* function together in the control of light-induced spitting: *lite-1* plays the

bioRxiv preprint doi: https://doi.org/10.1101/2020.06.02.129825; this version posted June 9, 2021. The copyright holder for this preprint (which was not certified by peer review) is the author/funder, who has granted bioRxiv a license to display the preprint in perpetuity. It is made available under aCC-BY 4.0 International license.

major role and suffices for nearly wild-type responses to light, while *gur-3* plays a smaller role and is sufficient to partially open the valve and filter but not to increase pumping rate. *gur-3* functions in the I2 pharyngeal neurons and likely also in the I4 neuron to evoke this attenuated spitting response via M1.

Subcellular muscle units driven by neuronally regulated subcellularly localized calcium signaling modulate motor behavior

We identified a likely physiological driver for the subcellular muscle contraction of the pm3s: subcellularly localized calcium transients in the anterior end of the pm3s, in the specific muscle region that undergoes sustained contraction during spitting and from which the pharyngeal valve protrudes. We propose that these calcium transients are the drivers of the subcellular muscle contraction of the pm3s.

Subcellularly localized calcium signaling in muscle has been observed in other systems. Subcellular muscle calcium transients known as “calcium sparks” result from calcium influx via individual ryanodine receptors (Cheng *et al.*, 1993). These localized calcium increases can trigger calcium-induced calcium release from the sarcoplasmic reticulum, resulting in a wave of calcium release that drives excitation-contraction coupling (Cheng *et al.*, 1993; Kuo and Ehrlich, 2015). Calcium sparks also allow local

bioRxiv preprint doi: https://doi.org/10.1101/2020.06.02.129825; this version posted June 9, 2021. The copyright holder for this preprint (which was not certified by peer review) is the author/funder, who has granted bioRxiv a license to display the preprint in perpetuity. It is made available under aCC-BY 4.0 International license.

increases in intracellular calcium to drive nearby signaling events without elevating global calcium levels (Nelson *et al.*, 1995; Navedo *et al.*, 2005; Nieves-Cintrón *et al.*, 2008).

Despite these examples of subcellularly localized muscle calcium function in physiological settings, how subcellular muscle calcium signaling contributes to behavior is poorly understood. The *C. elegans* pm5 pharyngeal muscle cells function to swallow food from the anterior pharynx to the terminal bulb via a peristaltic wave of subcellular contraction (Avery and Horvitz, 1987), and subcellular calcium signals in the pm5s likely underlie swallowing behavior (Shimozono *et al.*, 2004; Kozlova *et al.*, 2019). These transients have been reported to resemble calcium waves in cardiac muscle (Kozlova *et al.*, 2019), a phenomenon driven by the propagation of calcium-induced calcium release from internal stores (Cheng *et al.*, 1993). Subcellular signals have also been observed in murine enteric muscles, which can contract peristaltically, but the functional significance of these signals is unknown (Yamazawa and Iino, 2002). Our results identify a distinct and novel role for subcellular muscle contraction and calcium signaling: sustained, neuronally induced contraction of a stable, dedicated subcompartment of muscle, thus modulating function and transforming one behavioral output into another. While calcium sparks and *C. elegans* peristalsis behavior occur on

bioRxiv preprint doi: https://doi.org/10.1101/2020.06.02.129825; this version posted June 9, 2021. The copyright holder for this preprint (which was not certified by peer review) is the author/funder, who has granted bioRxiv a license to display the preprint in perpetuity. It is made available under aCC-BY 4.0 International license.

a timescale of tens of milliseconds, the contractions and calcium signals that we observed can last at least 10 seconds (with the *caveat* that our imaging assay lacks the temporal resolution to distinguish a sustained calcium influx from a series of rapid, short-lived calcium pulses). This timescale is more similar to that of calcium sparklets produced by L-type voltage-gated calcium channels (Navedo *et al.*, 2005).

We identify the M1 motor neuron, which innervates the anterior region of the pm3 muscles, as the driver of localized pm3 contraction and propose two alternative models for how M1 might produce the spatial and temporal contraction pattern that occurs during spitting. In the first model, the neuromuscular junctions (NMJs) of M1 at the anterior ends of the pm3s drive the entirety of the spitting response -- the pm3 subcellular calcium increases and sustained subcellular contraction as well as the rhythmic and global contractions -- i.e., pumps -- of pharyngeal muscle in general. For M1 to evoke sustained contraction of only the anterior ends of the pm3s while also stimulating pumps globally, the contracting region must be functionally distinct from the remainder of pm3. For example, the anterior region of pm3 might express a set of ion channels distinct from that expressed in the posterior region or might be modulated by a locally-acting M1-driven signaling cascade that inhibits the relaxation of the anterior subcompartment. In the second model, M1 promotes subcellular contraction and global

bioRxiv preprint doi: https://doi.org/10.1101/2020.06.02.129825; this version posted June 9, 2021. The copyright holder for this preprint (which was not certified by peer review) is the author/funder, who has granted bioRxiv a license to display the preprint in perpetuity. It is made available under aCC-BY 4.0 International license.

pumping via distinct sets of NMJs. In this case, the NMJs of M1 at the anterior end of pm3 would open the pharyngeal valve directly, while M1 indirectly stimulates global pumping by exciting one or more other neurons that form NMJs with more posterior regions of the pm3s or with other more posterior pharyngeal muscles. That the muscles of the pharynx are interconnected by gap junctions could allow the stimulation of one muscle to trigger a global contraction of other muscles. Eight pharyngeal neuron classes (I1, I2, I3, I5, M4, M5, MI, NSM), each of which forms NMJs with multiple pharyngeal muscle classes, receive synaptic input from M1 (Cook *et al.*, 2020), and at least two of these classes (I1 and M4) can promote pumping (Trojanowski *et al.*, 2014) and thus are plausible candidates to drive pan-pharyngeal M1-dependent contractions in response to light. This second model does not require that the anterior tip of pm3 be functionally specialized beyond receiving NMJs from M1, because the threshold for local contraction could be lower than that for depolarizing the entire muscle.

More generally, we suggest that subcellular muscle contraction via subcellular calcium signaling is a mechanism by which the nervous system can modulate muscle function to alter motor outputs and generate distinct behaviors. We suggest that *C. elegans* spitting behavior offers a system for the analysis of the molecular bases of subcellular calcium signaling in muscle using a highly genetically tractable organism.

bioRxiv preprint doi: https://doi.org/10.1101/2020.06.02.129825; this version posted June 9, 2021. The copyright holder for this preprint (which was not certified by peer review) is the author/funder, who has granted bioRxiv a license to display the preprint in perpetuity. It is made available under aCC-BY 4.0 International license.

Independent control of the pharyngeal valve and metastomal filter generates four distinct pumping behaviors

We observed that, in addition to opening the pharyngeal valve, spitting worms open the metastomal filter and this opening depends in part on the pm2 muscles. This finding suggests that in addition to passively filtering incoming material as reported previously (Fang-Yen *et al.*, 2009), the metastomal filter can also be actively opened to allow unrestricted entry of material into the pharynx. In the context of spitting pumps, opening the filter results in new material being flushed in and out, while closing the filter results in egestion without significant admission of new particles. We speculate that, in combination with the opening of the pharyngeal valve, this opening of the metastomal filter produces a rinsing effect, in which greatly increased quantities of material are drawn into and then expelled from the pharynx. Such a mechanism might act to eliminate toxic material before it is ingested as the animal -- in response to an aversive stimulus -- moves away from the source of such noxious chemicals into a less toxic neighborhood.

We observed that the filter sometimes also appears to open during feeding, producing “gulps” with greatly increased intake. Thus, the independent control of the

bioRxiv preprint doi: https://doi.org/10.1101/2020.06.02.129825; this version posted June 9, 2021. The copyright holder for this preprint (which was not certified by peer review) is the author/funder, who has granted bioRxiv a license to display the preprint in perpetuity. It is made available under aCC-BY 4.0 International license.

metastomal filter and pharyngeal valve produces four distinct pumping behavior variants -- feeding, gulping, spitting with rinsing, and spitting without rinsing. Given that M1 is the major source of innervation of the pm1 and pm2 muscles, from which the metastomal filter protrudes (Albertson and Thomson, 1976), we think it likely that M1 can function in the production of gulps by opening the metastomal filter without producing an accompanying contraction in the regions of pm3 that open the pharyngeal valve. Such a behavior might allow enhanced consumption of certain preferred food or, because it draws large amounts of material into the mouth, might allow the worm to more efficiently sample the environment while foraging. The possibility that a single neuron might control opposite behaviors (i.e., spitting and gulping) via the differential activation of multiple downstream muscles and subcellular muscle compartments is intriguing.

The M1 neuron drives spitting from the waist of an hourglass circuit motif

Our circuit studies show that the M1 motor neuron is a key regulator of spitting. We speculate that in addition to controlling the muscles that produce spitting, M1 functions as a central integrator of noxious taste information in the pharyngeal nervous system. Several lines of evidence support this hypothesis. First, a recent analysis of the pharyngeal connectome found that M1 exhibits a prominent and highly connected

bioRxiv preprint doi: https://doi.org/10.1101/2020.06.02.129825; this version posted June 9, 2021. The copyright holder for this preprint (which was not certified by peer review) is the author/funder, who has granted bioRxiv a license to display the preprint in perpetuity. It is made available under aCC-BY 4.0 International license.

position in the pharyngeal network (Cook *et al.*, 2020), suggesting that M1 plays an important role in pharyngeal network function. Second, M1 is particularly well-positioned to integrate noxious taste stimuli, as electron microscopy-based reconstructions of the pharyngeal nervous system indicate that M1 receives direct synaptic inputs from each of the other five *lite-1*- and/or *gur-3*-expressing pharyngeal neurons (i.e., the paired I2 and single I4, M4, M5, and MI neurons) (Albertson and Thomson, 1976; Bhatla and Horvitz, 2015). Consistent with this reported connectivity, we found that two of these neuron classes, the I2s and I4, contribute to M1's activation by light. Third, it is likely that M1 is itself light- and ROS-sensitive, as it expresses both *lite-1* (Bhatla and Horvitz, 2015) and *gur-3* (this study) and we show here that it can respond robustly to light even when synaptic and humoral inputs are substantially reduced or eliminated, respectively. For these reasons, we propose that M1 sits at the narrow waist of an "hourglass" circuit motif (Figure 7B). In this motif, multiple upstream parallel pathways converge on M1, which in turn makes divergent outputs onto the multiple downstream muscle groups classes that control the discrete motor outputs of the spitting reflex. Such an hourglass structure was recently described in a theoretical analysis of the larger *C. elegans* non-pharyngeal nervous system (Sabrin *et al.*, 2020). We propose that the neuromuscular

bioRxiv preprint doi: https://doi.org/10.1101/2020.06.02.129825; this version posted June 9, 2021. The copyright holder for this preprint (which was not certified by peer review) is the author/funder, who has granted bioRxiv a license to display the preprint in perpetuity. It is made available under aCC-BY 4.0 International license.

circuit we describe here constitutes a miniature variation of such an hourglass circuit organization.

The magnitude of M1 activation by the I2 and I4 neurons evokes a distinct subset of hourglass motor outputs

We explored circuitry upstream of the M1 neuron and identified the I2 and I4 neurons as likely sites of *gur-3* function in light-induced spitting. The I2s are activated by and inhibit pumping in response to light, and I4 was previously shown to be activated by light (Bhatla and Horvitz, 2015), but no function for I4 had previously been reported. Because I4 expresses *gur-3* and controls responses to light, we speculate that I4 is also a cellular receptor for light and ROS. Interestingly, although the pharyngeal connectome and our data suggest that M1 acts as a bottleneck through which signals must pass to evoke spitting, the I2/I4 circuit can selectively produce a subset of M1-dependent behaviors by weakly activating M1. Weak *gur-3*-dependent stimulation of M1 is sufficient to open the pharyngeal valve and metastomal filter, but not to increase pumping rates. Because UV light robustly activates the I2s (Bhatla and Horvitz, 2015), the fact that the I2s activate M1 only weakly suggests that their input to M1 is similarly weak. The weakness of this connection might be a design feature of the pharyngeal nervous system, allowing strong

bioRxiv preprint doi: https://doi.org/10.1101/2020.06.02.129825; this version posted June 9, 2021. The copyright holder for this preprint (which was not certified by peer review) is the author/funder, who has granted bioRxiv a license to display the preprint in perpetuity. It is made available under aCC-BY 4.0 International license.

activation of the I2 neurons to be converted into weak activation of the M1 neuron, thereby producing an attenuated variation of spitting. We speculate that I4 might function in a similar way, and that the I2s and I4 serve as modules to trigger attenuated spitting, while input from other cells and/or endogenous *lite-1* function in M1 produce spitting in a more robust manner, enabling the pharyngeal nervous system to generate graded variations of the spitting reflex and thus fine-tune its output to the environment. One problem that must be solved by an hourglass circuit structure with one or a few cells in the bottleneck is how to differentially evoke downstream outputs when all upstream inputs must be compressed together at the hourglass waist. We suggest that the M1 spitting circuit illustrates a simple solution to this problem: graded activation of M1 in the hourglass waist activates progressively larger subsets of downstream outputs. Outputs of such a circuit can thus be tuned by adjusting the magnitude of upstream inputs, allowing upstream neurons to input additively if their connections to the bottleneck are equally weighted or to evoke a subset of downstream outputs if they only weakly activate the bottleneck (as is the case with the I2 neurons).

Previous studies showed that the I2s inhibit pumping and that M1 is required for spitting (Bhatla and Horvitz, 2015; Bhatla *et al.*, 2015). We found that in addition the I2s can promote pumps (spitting pumps) and that M1 can inhibit pumping (it does so in the

bioRxiv preprint doi: https://doi.org/10.1101/2020.06.02.129825; this version posted June 9, 2021. The copyright holder for this preprint (which was not certified by peer review) is the author/funder, who has granted bioRxiv a license to display the preprint in perpetuity. It is made available under aCC-BY 4.0 International license.

recovery phase). Thus, each of these neuron classes can function in superficially opposite ways in different contexts. Although it might seem counterproductive for a given neuron to both promote and inhibit pumping, both spitting and the inhibition of pumping have the common effect of reducing food intake, since spitting pumps eject previously ingested food. We suggest that these differentially timed inhibitory and excitatory neural inputs to pharyngeal muscle allow the pharynx to generate a sequence of actions, first inhibiting pumping and/or stimulating spitting to eject noxious material, then increasing pumping rate and rinsing in the burst pumping phase if noxious stimulation continues, and finally inhibiting all pumping, including spitting, as the animal flees the site of the noxious encounter. Additionally, because spitting with an opened metastomal filter results in rinsing new material into the pharynx, it might be maladaptive if spitting persists when the animal is in a large region of noxious material; in this case, circuits promoting inhibition on a longer timescale than spitting would serve to limit additional exposure to noxious material.

In conclusion, we propose that subcellular muscle contraction induced by subcellular calcium signaling is a fundamental mechanism by which nervous systems can reshape motor behavior and suggest that hourglass motifs might function broadly in

bioRxiv preprint doi: https://doi.org/10.1101/2020.06.02.129825; this version posted June 9, 2021. The copyright holder for this preprint (which was not certified by peer review) is the author/funder, who has granted bioRxiv a license to display the preprint in perpetuity. It is made available under aCC-BY 4.0 International license.

neuronal circuit organization for the production of complex adaptive behavior in response to changing environments.

Acknowledgments

We thank N. An, R. Droste, S. Flavell, N. Ji, E. Jorgensen, R. Komuniecki, J. Meisel, S. Mitani, M. Treinin, Addgene, and the *Caenorhabditis* Genetics Center, which is funded by NIH Office of Research Infrastructure Programs (P40 OD010440), for strains and reagents; and K. Boulias, V. Dwivedi, K. Burkhart, D. Ghosh, H. Johnsen, T. Littleton, J. Meisel, C. Pender, P. Reddien, J. Saul, and Horvitz laboratory members for discussions and advice.

Competing interests: The authors declare that no competing interests exist.

bioRxiv preprint doi: https://doi.org/10.1101/2020.06.02.129825; this version posted June 9, 2021. The copyright holder for this preprint (which was not certified by peer review) is the author/funder, who has granted bioRxiv a license to display the preprint in perpetuity. It is made available under aCC-BY 4.0 International license.

813 **Materials and methods**

Key Resources Table				
Reagent type (species) or resource	**Designation**	**Source or reference**	**Identifiers**	**Additional information**
strain, strain background (*Caenorhabditis elegans*)	N2 (wild type)	Horvitz lab collection		Laboratory reference strain
strain, strain background (*C. elegans*)	CB1072	Horvitz lab collection		*unc-29(e1072)*
strain, strain background (*C. elegans*)	MT26279	this study		*lin-15(n765ts); nIs507 [inx-4$_{promoter}$::GFP; lin-15(+)]* 8x outcrossed to MT8189
strain, strain background (*C. elegans*)	MT8189	Horvitz lab collection		*lin-15(n765ts)*
strain, strain background (*C. elegans*)	MT23338	this study		*nIs686 [gpa-16$_{promoter}$::gcamp3::unc-54 3' UTR; lin-15(+)] III; lin-15AB(n765ts)* 5x outcrossed to MT8189
strain, strain background (*C. elegans*)	MT26375	this study		*lin-15AB(n765ts)*; *nEx3045 [C32F10.8p::GCaMP3; lin-15(+)]*
strain, strain background (*C. elegans*)	MT25631	this study		*lin-15(n765ts); nIs864 [glr-2$_{promoter}$::gfp::unc-54 3' UTR; lin-15(+)]*

bioRxiv preprint doi: https://doi.org/10.1101/2020.06.02.129825; this version posted June 9, 2021. The copyright holder for this preprint (which was not certified by peer review) is the author/funder, who has granted bioRxiv a license to display the preprint in perpetuity. It is made available under aCC-BY 4.0 International license.

				6x outcrossed
strain, strain background (*C. elegans*)	OK1020	Kozlova *et al.*, 2019		cuIs36 X
strain, strain background (*C. elegans*)	MT23370	this study		*nIs686 III; lite-1(ce314) gur-3(ok2245) lin-15(n765ts)*
strain, strain background (*C. elegans*)	VK1241	CGC		vkEx1241 [nhx-2p::mCherry::lgg-1 + myo-2p::GFP]
strain, strain background (*C. elegans*)	MT26333	CGC, this study		sIs11111[rCesC32F10.8::GFP + pCeh361] 8x outcrossed to N2
strain, strain background (*C. elegans*)	MT2249	Horvitz laboratory collection		*egl-47(n1082dm)*
strain, strain background (*C. elegans*)	RB850	CGC		*egl-47(ok677)*
strain, strain background (*C. elegans*)	MT21783	Bhatla and Horvitz, 2015		*gur-3(ok2245)*

bioRxiv preprint doi: https://doi.org/10.1101/2020.06.02.129825; this version posted June 9, 2021. The copyright holder for this preprint (which was not certified by peer review) is the author/funder, who has granted bioRxiv a license to display the preprint in perpetuity. It is made available under aCC-BY 4.0 International license.

strain, strain background (*C. elegans*)	RB845	CGC		*gur-4(ok672)*
strain, strain background (*C. elegans*)	FX06169	Dr. S. Mitani/NBRP		*gur-5(tm6169)*
strain, strain background (*C. elegans*)	KG1180	CGC		*lite-1(ce314)* 5x outcrossed
strain, strain background (*C. elegans*)	MT21793	Bhatla and Horvitz, 2015		*lite-1(ce314) gur-3(ok2245)*
strain, strain background (*C. elegans*)	DA1113	CGC		*eat-2(ad1113)* 2x outcrossed
strain, strain background (*C. elegans*)	MT25982	this study		*eat-2(ad1113); gur-3(ok2245)*
strain, strain background (*C. elegans*)	MT22899	this study		*eat-2(ad1113); lite-1(ce314)*
strain, strain background (*C. elegans*)	MT25983	this study		*eat-2(ad1113); lite-1(ce314) gur-3(ok2245)*
strain, strain background (*C. elegans*)	MT25999	this study		*eat-2(ad1113); lite-1(ce314) gur-3(ok2245); nIs687 [lite-1$_{promoter}$::gfp::lite-1; lin-15(+)]* *nIs687* was outcrossed 8x to MT22499

bioRxiv preprint doi: https://doi.org/10.1101/2020.06.02.129825; this version posted June 9, 2021. The copyright holder for this preprint (which was not certified by peer review) is the author/funder, who has granted bioRxiv a license to display the preprint in perpetuity. It is made available under aCC-BY 4.0 International license.

strain, strain background (*C. elegans*)	MT22499	this study		*lite-1(ce314) gur-3(ok2245) lin-15AB(n765ts)*
strain, strain background (*C. elegans*)	MT25809	this study		*lite-1(ce314) gur-3(ok2245) lin-15(n765ts); nEx2281 [lite-1$_{promoter}$::lite-1::gfp; lin-15(+)]*
strain, strain background (*C. elegans*)	MT25810	this study		*lite-1(ce314) gur-3(ok2245) lin-15(n765ts); nEx2157 [gur-3 gDNA; lin-15(+)]*
strain, strain background (*C. elegans*)	MT23415	this study		*nIs686 III; gur-3(ok2245) lin-15(n765ts)*
strain, strain background (*C. elegans*)	MT23417	this study		*nIs686 III; lite-1(ce314) lin-15(n765ts)*
strain, strain background (*C. elegans*)	MT25732	this study		*lin-15(n765ts); nIs864; nEx2905 [lury-1$_{promoter}$::ice::sl2::mcherry::unc-54 3' UTR; ttx-3$_{promoter}$::mcherry]*
strain, strain background (*C. elegans*)	MT25804	this study		*oxIs322 [myo-2$_{promoter}$::mcherry::h2b; myo-3$_{promoter}$::mcherry::h2b] II ; nIs310 [nlp-13$_{promoter}$::gfp] V; nEx2905*
strain, strain background (*C. elegans*)	MT25950	this study		*eat-2(ad1113); nIs865* (integrated transgene derived from *nEx2905 [lury-1$_{promoter}$::ice::sl2::mcherry::unc-54 3' UTR; ttx-3$_{promoter}$::mcherry]*)

bioRxiv preprint doi: https://doi.org/10.1101/2020.06.02.129825; this version posted June 9, 2021. The copyright holder for this preprint (which was not certified by peer review) is the author/funder, who has granted bioRxiv a license to display the preprint in perpetuity. It is made available under aCC-BY 4.0 International license.

strain, strain background (*C. elegans*)	MT25823	this study		*lin-15AB(n765ts); nEx2917*
strain, strain background (*C. elegans*)	MT23192	this study		*lin-15(n765ts); nIs678 [glr-2$_{promoter}$::gcamp6s::unc-54 3' UTR; lin-15(+)]* 5x outcrossed.
strain, strain background (*C. elegans*)	MT24110	this study		*lin-15(n765ts); nIs780 [gur-3$_{promoter}$::gfp; lin-15(+)]* 7x outcrossed to MT8189
strain, strain background (*C. elegans*)	MT23250	this study		*gur-3(ok2245) lin-15(n765ts); nIs678*
strain, strain background (*C. elegans*)	MT23230	this study		*lite-1(ce314) lin-15(n765ts); nIs678*
strain, strain background (*C. elegans*)	MT23369	this study		*lite-1(ce314) gur-3(ok2245) lin-15(n765ts); nIs678*
strain, strain background (*C. elegans*)	MT23343	this study		*unc-13(s69); lin-15(n765ts); nIs678*
strain, strain background (*C. elegans*)	MT23410	this study		*unc-31(u280); lin-15(n765ts); nIs678*
strain, strain background (*C. elegans*)	MT25468	this study		*lite-1(ce314) gur-3(ok2245) lin-15(n765ts); nEx2815 [lury-1$_{promoter}$::chr2::sl2::mcherry::unc-54 3' UTR]*

bioRxiv preprint doi: https://doi.org/10.1101/2020.06.02.129825; this version posted June 9, 2021. The copyright holder for this preprint (which was not certified by peer review) is the author/funder, who has granted bioRxiv a license to display the preprint in perpetuity. It is made available under aCC-BY 4.0 International license.

strain, strain background (*C. elegans*)	CB933	Horvitz laboratory collection		*unc-17(e245)*
strain, strain background (*C. elegans*)	PR1152	Horvitz laboratory collection		*cha-1(p1152)*
strain, strain background (*C. elegans*)	RM509	CGC		*ric-3(md158)*
strain, strain background (*C. elegans*)	CB156	Takayanagi-Kiya *et al.*, 2016		*unc-25(e156) dnj-17(ju1162)*
strain, strain background (*C. elegans*)	MT6308	CGC		*eat-4(ky5)*
strain, strain background (*C. elegans*)	CB1112	Horvitz laboratory collection		*cat-2(e1112)*
strain, strain background (*C. elegans*)	MT10661	Horvitz laboratory collection		*tdc-1(n3420)*
strain, strain background (*C. elegans*)	MT14984	Horvitz laboratory collection		*tph-1(n4622)*
strain, strain background (*C. elegans*)	MT15434	Horvitz laboratory collection		*tph-1(mg280)*
strain, strain background (*C. elegans*)	MT22280	Horvitz laboratory collection		*ser-4(ok512); mod-1(ok103); ser-1(ok345) ser-7(tm1325)*

bioRxiv preprint doi: https://doi.org/10.1101/2020.06.02.129825; this version posted June 9, 2021. The copyright holder for this preprint (which was not certified by peer review) is the author/funder, who has granted bioRxiv a license to display the preprint in perpetuity. It is made available under aCC-BY 4.0 International license.

strain, strain background (*C. elegans*)	MT23606	this study		*lite-1(ce314) gur-3(ok2245) lin-15AB(n765ts); nEx2144 [flp-15$_{promoter}$::mcherry::gur-3, lin-15(+)]*
strain, strain background (*C. elegans*)	MT23545	this study		*lite-1(ce314) gur-3(ok2245) lin-15AB(n765ts); nIs678; nEx2144*
strain, strain background (*C. elegans*)	MT26001	this study		*eat-2(ad1113); lite-1(ce314) gur-3(ok2245) nIs791 X* (integrated transgene derived from *[nEx2144: flp-15$_{promoter}$::mcherry::gur-3, lin-15(+)]*)
strain, strain background (*C. elegans*)	MT21421	Bhatla and Horvitz, 2015		*nIs569 [flp-15$_{promoter}$::csp-1b; ges-1$_{promoter}$::gfp]*
strain, strain background (*C. elegans*)	MT21791	Bhatla and Horvitz, 2015		*lite-1(ce314) nIs569*

Molecular biology

Transgenes were generated by standard cloning methods. DNA sequences used in the generation of transgenes were amplified with the primers indicated below.

bioRxiv preprint doi: https://doi.org/10.1101/2020.06.02.129825; this version posted June 9, 2021. The copyright holder for this preprint (which was not certified by peer review) is the author/funder, who has granted bioRxiv a license to display the preprint in perpetuity. It is made available under aCC-BY 4.0 International license.

Generated using the infusion cloning technique (Takara Bio, Mountain View, CA) and injected as plasmids:

nIs864 - pSS028 [glr-2$_{promoter}$::gfp::unc-54 3' UTR]

nEx2905 and nIs865 - pSS042 [lury-1$_{promoter}$::ice::sl2::mcherry::unc-54 3' UTR]

nEx2815 - pSS034 [lury-1$_{promoter}$::chr2::sl2::mcherry::unc-54 3' UTR]

glr-2$_{promoter}$: TTGGGACAAATGTGGAAACGA,

TTCGCTTTTTACAGAGTTAACTCTGC

lury-1$_{promoter}$: TTCATTAAGTAATCCGTTTAGGGCAAAT,

GATTGGATTTTCTGGAATAATCGGGT

ice: ATGGCCGACAAGGTCCTGA,

TTAATGTCCTGGGAAGAGGTAGAAACATC

Generated and injected as PCR product:

nIs686 - pcNB1 [gpa-16$_{promoter}$::gcamp3::unc-54 3' UTR]

nEx2157 – pcNB20 [gur-3$_{promoter}$::gur-3 gDNA::gur-3 3' UTR]

nIs678 - [glr-2$_{promoter}$::gcamp6s::unc-54 3' UTR]

bioRxiv preprint doi: https://doi.org/10.1101/2020.06.02.129825; this version posted June 9, 2021. The copyright holder for this preprint (which was not certified by peer review) is the author/funder, who has granted bioRxiv a license to display the preprint in perpetuity. It is made available under aCC-BY 4.0 International license.

gpa-16$_{promoter}$: ACCAACCTGAACAGCGAATC,

AAAGGGAATTTTATGTGAATAATATCG

gur-3$_{promoter}$*::gur-3 gDNA::gur-3 3' UTR:* GCCTGATGGAACACACTTCCAAC

GTTTACCCCGTCTCTATTTCCGCTTTG

gcamp6s: ATGGGTTCTCATCATCATCATCATC,

GCCCGTACGGCCGACTAGTAGG

Grinder Pumping Assay

Previously, we used a xenon bulb (Till Photonics Polychrome V, 150 W; Thermo Fischer Scientific, Waltham, MA) to deliver 365 nm UV light through an inverted microscope (Axiovert S100; Zeiss, Oberkochen, Germany) to individual worms on an agar pad (Bhatla and Horvitz, 2015). Because of the low throughput of this approach, we designed a device to deliver 365 nm UV light to standard Petri dishes used for culturing worms and used this apparatus to assay behavioral responses to 365 nm UV light as described previously for 436 nm violet light (Bhatla and Horvitz, 2015). The apparatus consists of a UV-light-emitting LED (M365F1; Thorlabs, Newton, NJ) coupled by a fiber-optic cable to a collimating lens. The LED system delivers 365 nm UV light in a 3-4 mm spot at a power of ~1.5mW/mm^2 to young (1-day post-L4) hermaphrodite adults moving

bioRxiv preprint doi: https://doi.org/10.1101/2020.06.02.129825; this version posted June 9, 2021. The copyright holder for this preprint (which was not certified by peer review) is the author/funder, who has granted bioRxiv a license to display the preprint in perpetuity. It is made available under aCC-BY 4.0 International license.

freely on a Petri dish, producing a burst pumping response indistinguishable from that obtained previously (Bhatla and Horvitz, 2015). Custom Matlab software was used to control the LED, and the contraction rate of the grinder before, during, and after application of light was observed by eye via a dissecting microscope and manually recorded via this software (Bhatla and Horvitz, 2015). The data in Figure 1B, Figure 5I, Figure 3—figure supplement 1A-1L, Figure 4—figure supplement 1B, 1D, 1M-1V), and Figure 4—figure supplement 2A-2P') were collected using this method.

Genotypes were not typically scored by a researcher blinded to the conditions, but in many cases we performed both real-time scoring and automated video recording of identical genotypes and always observed similar burst pumping behavior in both cases. Specifically, Figure 1B is reproduced by Figure 1D and 1E, Figure 3—figure supplement 1C, 1F, and 1G is reproduced by Figure 3A-3G, and Figure 4—figure supplement 1B is reproduced by Figure 4—figure supplement 1G. All behavioral data were visualized as described in (Bhatla and Horvitz, 2015; Bhatla *et al.*, 2015). All behavioral assays and imaging experiments were performed in the same location, at which temperature averaged 19°C, with a standard deviation of 1.2°C.

Pharyngeal transport assay

bioRxiv preprint doi: https://doi.org/10.1101/2020.06.02.129825; this version posted June 9, 2021. The copyright holder for this preprint (which was not certified by peer review) is the author/funder, who has granted bioRxiv a license to display the preprint in perpetuity. It is made available under aCC-BY 4.0 International license.

Pharyngeal transport assays were performed as described previously (Bhatla *et al.*, 2015). To visualize the direction of particle motion in the pharynx during each pump, worms were fed a 50% dilution of a 2.5% weight by volume (4.55 x 10^{10} particles per mL) solution of 1 µm diameter polystyrene beads (Polysciences, Inc. Warrington, PA, Catalog number 07310-15) in M9 buffer. Young (1-day post-L4) hermaphrodite adults were placed with bacteria on an NGM agar pad on a coverslip and observed with a 20x objective on an inverted microscope (Axiovert S100; Zeiss). Videos were recorded at 1000 frames per sec using a high-speed video camera (Fastcam Mini; Photron, Tokyo, Japan). 365 nm UV light (0.88-1.5 mW/mm^2) was presented to the worm for 10 sec (Till Photonics Polychrome V, 150 W xenon bulb; Thermo Fischer Scientific). Unlike the burst pumping assay described above, which illuminates the entire body of the worm, this method selectively illuminates the animal's head. Hydrogen peroxide was administered as described previously (Bhatla and Horvitz, 2015). Videos were viewed and manually annotated, using custom Matlab software, for specific behavioral events: ingestion (beads being retained in the procorpus after procorpus relaxation), spitting (beads being pushed out of the procorpus), and pumping (movement of the grinder). In some cases, the worm moved temporarily out of the focal plane of the microscope or field-of-view of the camera. These unscorable frames were annotated as "missing" and

bioRxiv preprint doi: https://doi.org/10.1101/2020.06.02.129825; this version posted June 9, 2021. The copyright holder for this preprint (which was not certified by peer review) is the author/funder, who has granted bioRxiv a license to display the preprint in perpetuity. It is made available under aCC-BY 4.0 International license.

excluded from further analysis. We were unable to resolve the flaps of the metastomal filter directly, and the position of these flaps was inferred based on whether beads passed freely through or accumulated in the buccal cavity during feeding or spitting, and the fraction of feeding and spitting pumps with the filter open or closed was calculated for the period before and during illumination. Animals with fewer than five scorable pumps in a given 10 sec interval were censored from these analyses. Videos were not scored with experimenters blinded to genotype and/or condition.

Muscle motion visualization assay

To visualize the timing of pharyngeal muscle motions during each pump, young (1-day post-L4) hermaphrodite adults were placed with bacteria on an NGM agar pad underneath a coverslip and observed with a 20x objective on an inverted microscope (Axiovert S100; Zeiss). Videos were recorded at 86 frames per sec using an EMCCD camera (iXon^{+}; Andor, Belfast, United Kingdom). 365 nm UV light was presented to the worm for 10 sec (Till Photonics Polychrome V, 150 W xenon bulb; Thermo Fischer Scientific). Slow-moving *unc-29(e1072)* animals were filmed to facilitate video capture.

bioRxiv preprint doi: https://doi.org/10.1101/2020.06.02.129825; this version posted June 9, 2021. The copyright holder for this preprint (which was not certified by peer review) is the author/funder, who has granted bioRxiv a license to display the preprint in perpetuity. It is made available under aCC-BY 4.0 International license.

Videos were viewed and manually annotated based on whether the anterior tip of the pharynx closed or remained open at the end of each pump.

Laser ablations

We used a pulsed nitrogen laser (MicroPoint; Andor) coupled to a compound microscope (Axioplan; Zeiss) to conduct laser microsurgery of individual pharyngeal neurons, as previously described (Fang-Yen *et al.*, 2012). Briefly, worms were immobilized using 10 mM sodium azide and mounted for viewing through a 100x oil objective. Ablations were performed on hermaphrodite larvae of stages 1 or 2 (L1 or L2), with cell nuclei identified by either Nomarski differential interference contrast optics or cell-specific GFP reporters. Specifically, M1 was identified by Nomarski optics or by the M1-expressed GFP reporter *nIs864*, which drives expression of GFP in M1 via the *glr-2* promoter (Brockie *et al.*, 2001), while pm1 was identified by GFP reporter *nIs507*, which drives expression of GFP in pm1 via the *inx-4* promoter (Altun *et al.*, 2009). The pm2 muscles, the I2 and I4 neurons, and, in some experiments, the M1 neuron were identified by Nomarski optics. Ablations were confirmed the following day by appearance under Nomarski optics and/or by the loss of cell-specific fluorescence. On

bioRxiv preprint doi: https://doi.org/10.1101/2020.06.02.129825; this version posted June 9, 2021. The copyright holder for this preprint (which was not certified by peer review) is the author/funder, who has granted bioRxiv a license to display the preprint in perpetuity. It is made available under aCC-BY 4.0 International license.

day 3 or 4, adults were assayed for their response to light. Mock-ablated animals were mounted alongside ablation animals and received identical treatments (i.e., observation of nuclear morphology and/or GFP expression) at each step. Animals were allocated into mock and ablation groups randomly.

Calcium imaging

Calcium imaging was performed as described previously (Bhatla and Horvitz, 2015). Calcium changes in pharyngeal muscle were monitored using GCaMP3 (Tian *et al.*, 2009) expressed from one of three transgenes: *nIs686* (this study), driven by the *gpa-16* promoter (Jansen *et al.*, 1999); *cuIs36* (Kozlova *et al.*, 2019), driven by the *myo-2* promoter (Okkema and Fire, 1994; Okkema *et al.*, 1993); or *nEx3045* (this study), driven by the *C32F10.8* promoter (McKay *et al.*, 2003; Hunt-Newbury *et al.*, 2007; this study). Calcium changes in M1 were monitored using GCaMP6s (Chen *et al.*, 2013) expressed in M1 using the transgene *nIs678* driven by the *glr-2* promoter (Brockie *et al.*, 2001). The free-moving spitting behavior of *nIs686* and *nIs678* animals was indistinguishable from that of wild-type animals (Figure 2—figure supplement 1H and Figure 4—figure supplement 1W).

bioRxiv preprint doi: https://doi.org/10.1101/2020.06.02.129825; this version posted June 9, 2021. The copyright holder for this preprint (which was not certified by peer review) is the author/funder, who has granted bioRxiv a license to display the preprint in perpetuity. It is made available under aCC-BY 4.0 International license.

As described by Kim *et al.*, 2013a, adult hermaphrodite worms were immobilized on 10% agarose pads under a coverslip using the friction produced by 0.10 µm diameter polystyrene beads (Polysciences, Inc. Catalog number 00876) and imaged using an inverted microscope (Axiovert S100; Zeiss) with a 40x air objective. To stimulate animals with UV light and image GCaMP fluorescence simultaneously, light was flickered between 365 nm UV and 485 nm light at a rate of 2 Hz. Monochromatic 365 nm light, 365 nm/485 nm flickered light, and monochromatic 485 nm light all stimulated immobilized animals to pump, with 365 nm monochromatic and 365 nm/485 nm flickered light evoking pumps more potently than 485 nm light by some strains (Figure 2—figure supplement 1C and 1D). While the response of *nIs686*-bearing animals was indistinguishable from that of the wild type, the response of *nEx3045*-bearing animals was significantly weaker, and *cuIs36*-bearing animals did not pump at all during illumination. This reduced responsivity of some muscle GCaMP3-expressing strains could be a consequence of GCaMP-mediated intracellular calcium-buffering (e.g., as noted by Singh *et al.*, 2018) or another abnormality induced by transgene overexpression. To determine whether the light-induced pumps of immobilized animals are spits we illuminated worms immobilized with droplets of mineral oil in their anterior pharynges and filmed the direction in which droplets were drive by pharyngeal pumps.

bioRxiv preprint doi: https://doi.org/10.1101/2020.06.02.129825; this version posted June 9, 2021. The copyright holder for this preprint (which was not certified by peer review) is the author/funder, who has granted bioRxiv a license to display the preprint in perpetuity. It is made available under aCC-BY 4.0 International license.

Videos were recorded using an EMCCD camera (iXon^{+}; Andor) at 2 frames per sec and an exposure time of 250 msec, with the exception of videos of animals expressing the *myo-2p::GFP* transgene *vkEx1241*, which were collected with an exposure time of 15 msec, or of animals expressing the *gpa-16p::gcamp3* transgene *nIs686* induced to pump with serotonin, which were collected at 4 frames per second with an exposure time of 250 msec. Videos were analyzed using custom Matlab software as described previously (Bhatla and Horvitz, 2015; Bhatla *et al.*, 2015). The immobilized pumping assay described in Figure 2—figure supplement 1C and 1D was performed under the same conditions described above for calcium imaging. Animals that were imaged pumping in response to serotonin were prepared for calcium imaging as described above, with the exception that the M9 solution used to make the agarose imaging pads was supplemented with serotonin hydrochloride (Sigma) to a final concentration of 10 mM.

Confocal microscopy

Expression patterns of reporter transgenes *nIs686 (gpa-16p::GCaMP3), cuIs36 (myo-2p::GCaMP3), sIs11111 (C32F10.8p::GFP),* and *nEx3045 (C32F10.8p::GCaMP3)* were

bioRxiv preprint doi: https://doi.org/10.1101/2020.06.02.129825; this version posted June 9, 2021. The copyright holder for this preprint (which was not certified by peer review) is the author/funder, who has granted bioRxiv a license to display the preprint in perpetuity. It is made available under aCC-BY 4.0 International license.

determined using a 63x objective lens (Zeiss) on an LSM 800 confocal microscope system (Zeiss). To identify individual *nEx3045* transgene-positive cells responding to light, we first recorded videos of light-induced changes in GCaMP fluorescence as described above, preselecting animals with sparse transgene expression patterns in the anterior pharynx for imaging. We then anesthetized each animal using 50 mM sodium azide and recorded its individual *C32F10.8p::GCaMP3* expression patterns by collecting 20 confocal micrographs evenly spaced across the pharynx. We then used the "ortho" function of the Zen imaging software (Zeiss) to assemble these micrographs into a 3D reconstruction of GCaMP3 expression. Cells in calcium imaging videos were identified based on their dimensions, unique morphological features (i.e., the pm3s are each characterized by the presence of a branch of the pharyngeal nerve cord, which is visible as a deep, GCaMP-negative groove that runs anterior-to-posterior along the outside surface of each pm3, while the mc1s are characterized by distinctive finger-like projections into the pm3s and by and a sickle-shaped posterior projection into the anterior bulb), and their position relative to other transgene-expressing cells in Z-stack-derived 3D reconstructions of transgenic pharynges.

Genetic ablation

bioRxiv preprint doi: https://doi.org/10.1101/2020.06.02.129825; this version posted June 9, 2021. The copyright holder for this preprint (which was not certified by peer review) is the author/funder, who has granted bioRxiv a license to display the preprint in perpetuity. It is made available under aCC-BY 4.0 International license.

M1 was ablated genetically by overexpressing the mammalian caspase ICE (Cerretti *et al.*, 1992; Thornberry *et al.*, 1992; Zheng *et al.*, 1999) fused to an *sl2::mcherry* sequence in M1 driven by the *lury-1* promoter (Ohno *et al.*, 2017). For all animals assayed, genetic ablation of M1 was confirmed beforehand using an M1-specific GFP marker *(nIs864)*, which drives expression of GFP in M1 via the *glr-2* promoter (Brockie *et al.*, 2001). The *nEx2905* genetic ablation transgene also killed the M2 neurons in approximately 50% of animals assayed (Figure 4—figure supplement 1A), as confirmed using an M2-specific GFP marker (*nIs310*) (Luo and Horvitz, 2017). The *sl2::mcherry* sequence used drove varying degrees of mCherry expression in pharyngeal muscle, and we found that the brightness of this mCherry expression correlated with the rate of M2-killing, such that selecting animals with dim pharyngeal mCherry expression reduced the rate of M2-killing to 1-2% (Figure 4—figure supplement 1C). Animals assayed in Figure 4D and 4E were not selected in this way. We did not determine the rate of M1 or M2 killing in *nIs865* animals.

Neuronal silencing via histamine-gated chloride channels

bioRxiv preprint doi: https://doi.org/10.1101/2020.06.02.129825; this version posted June 9, 2021. The copyright holder for this preprint (which was not certified by peer review) is the author/funder, who has granted bioRxiv a license to display the preprint in perpetuity. It is made available under aCC-BY 4.0 International license.

Animals expressing the *Drosophila melanogaster* HisCl1 histamine-gated chloride channel (Pokala *et al.*, 2014) in M1 under the control of the *glr-2* promoter (Brockie *et al.*, 2001) from the transgene *nEx2917* (*glr-2p::hiscl1::sl2::mcherry*) were transferred to plates containing 10 mM histamine dihydrochloride (Sigma) and assayed over a 3-hour interval starting 1 hour after exposure to histamine. As controls, transgene-negative animals were tested in the presence of histamine and transgene-positive animals were tested in the absence of histamine. Array-positive animals were selected based on HisCl1::mCherry expression in M1, visualized using a stereofluorescent dissecting microscope (SMZ18, Nikon, Tokyo, Japan). To control for variations in the duration of histamine exposure, array-positive and array-negative animals were tested in alternation.

Optogenetic depolarization

Optogenetic manipulations were performed as described previously (Bhatla *et al.*, 2015). Cultivation plates were seeded with 300 µL of OP50 *E. coli* mixed with 0.5 µL of 100 mM all-*trans* retinal (ATR+) (Sigma) or ethanol alone (ATR-) and stored in the dark. Transgenic hermaphrodite worms carrying the channelrhodopsin 2 (*chr2*) coding

bioRxiv preprint doi: https://doi.org/10.1101/2020.06.02.129825; this version posted June 9, 2021. The copyright holder for this preprint (which was not certified by peer review) is the author/funder, who has granted bioRxiv a license to display the preprint in perpetuity. It is made available under aCC-BY 4.0 International license.

sequence (Nagel *et al.*, 2003; Boyden *et al.*, 2005) fused to a *sl2::mcherry* sequence were cultivated on these plates in the dark from egg to adulthood. For behavioral assays, one-day-old animals were analyzed as described above ('Pharyngeal Transport Assay'), except that 470 nm light was used in the place of 365 nm UV light. *nEx2815 [lury-1$_{promoter}$::chr2::sl2::mcherry::unc-54 3' UTR]* was expressed in both M1 and the M2s driven by the *lury-1* promoter (Ohno *et al.*, 2017). To avoid confounding optogenetic activation of the M2s, we assayed only mosaic animals pre-selected for expression of mCherry in M1 but not the M2s. Animals were allocated into ATR- and ATR+ groups randomly.

Behavioral Statistics

For all measurements, each animal was scored once. Biological replicates were performed using separate populations of animals on different days and consisted of 20 animals unless indicated otherwise. Statistics for significance of differences between fractions in metastomal filter analyses were calculated as follows. Fractions were log-transformed, and any fractions with a numerator of zero were approximated to 0.1 prior to transformation. Similar results were obtained by approximating numerators of zero

bioRxiv preprint doi: https://doi.org/10.1101/2020.06.02.129825; this version posted June 9, 2021. The copyright holder for this preprint (which was not certified by peer review) is the author/funder, who has granted bioRxiv a license to display the preprint in perpetuity. It is made available under aCC-BY 4.0 International license.

with 0.01. Log-transformed datasets were assessed for significance with an unpaired t-test when a single pair of conditions was compared or unpaired ordinary one-way ANOVA analysis when multiple conditions were compared. These analyses assumed that log-transformed data followed a normal distribution with similar standard deviations. Statistics for significance between average spitting rates were calculated as follows. For each animal, the total number of spits observed during stimulation with light was divided by the number of scorable frames in the light administration phase for that animal to give the average pumping rate during light administration. Significance of differences between groups was assessed by unpaired, ordinary one-way ANOVA analysis, with the assumption that the data followed a Gaussian distribution with similar standard deviations. In the cases in which data did not follow a Gaussian distribution, significance was assessed using the Kruskal-Wallis test, followed by Dunn's multiple comparison test. Pumping inhibition was calculated by dividing the average pumping rate during light stimulation ($10 < t < 20$) by the average pumping rate in the feeding phase ($0 < t < 10$). All statistics were calculated using Prism (GraphPad Software, San Diego, CA).

bioRxiv preprint doi: https://doi.org/10.1101/2020.06.02.129825; this version posted June 9, 2021. The copyright holder for this preprint (which was not certified by peer review) is the author/funder, who has granted bioRxiv a license to display the preprint in perpetuity. It is made available under aCC-BY 4.0 International license.

References

Albertson, D.G., and Thomson, J.N. (1976). The pharynx of *Caenorhabditis elegans*. Philosophical Transactions of the Royal Society of London. B, Biological Sciences *275*, 299–325.

Altun, Z.F., Chen, B., Wang, Z.W., and Hall, D.H. (2009). High resolution map of *Caenorhabditis elegans* gap junction proteins. Developmental Dynamics *238*, 1936–1950.

Arenas, O.M., Zaharieva, E.E., Para, A., Vásquez-Doorman, C., Petersen, C.P., and Gallio, M. (2017). Activation of planarian TRPA1 by reactive oxygen species reveals a conserved mechanism for animal nociception. Nat Neurosci *20*, 1686–1693.

Avery, L. (1993). Motor neuron M3 controls pharyngeal muscle relaxation timing in *Caenorhabditis elegans*. Journal of Experimental Biology *175*, 283–297.

Avery, L., and Horvitz, H.R. (1987). A cell that dies during wild-type *C. elegans* development can function as a neuron in a *ced-3* mutant. Cell *51*, 1071–1078.

Avery, L., and Horvitz, H.R. (1989). Pharyngeal pumping continues after laser killing of the pharyngeal nervous system of *C. elegans*. Neuron *3*, 473–485.

Avery, L., and You, Y. (2012). *C. elegans* feeding. WormBook, ed. The *C. elegans* Research Community, WormBook, doi/10.1895/wormbook.1.150.1, http://www.wormbook.org.

Berwin, B., Floor, E., and Martin, T.F.J. (1998). CAPS (mammalian UNC-31) protein localizes to membranes involved in dense-core vesicle exocytosis. Neuron *21*, 137–145.

Bhatla, N., and Horvitz, H.R. (2015). Light and hydrogen peroxide inhibit *C. elegans* feeding through gustatory receptor orthologs and pharyngeal neurons. Neuron *85*, 804–818.

Bhatla, N., Droste, R., Sando, S.R., Huang, A., and Horvitz, H.R. (2015). Distinct neural circuits control rhythm inhibition and spitting by the myogenic pharynx of *C. elegans*. Current Biology *25*, 2075–2089.

Birkholz, T.R., and Beane, W.S. (2017). The planarian TRPA1 homolog mediates extraocular behavioral responses to near-ultraviolet light. Journal of Experimental Biology *220*, 2616–2625.

Boyden, E.S., Zhang, F., Bamberg, E., Nagel, G., and Deisseroth, K. (2005). Millisecond-timescale, genetically targeted optical control of neural activity. Nat Neurosci *8*, 1263–1268.

Briggman, K.L., and Kristan, W.B. (2008). Multifunctional pattern-generating circuits. Annual Review of Neuroscience *31*, 271–294.

Brockie, P.J., Madsen, D.M., Zheng, Y., Mellem, J., and Maricq, A.V. (2001). Differential expression of glutamate receptor subunits in the nervous system of *Caenorhabditis elegans* and their regulation by the homeodomain protein UNC-42. J. Neurosci. *21*, 1510–1522.

Cerretti, D.P., Kozlosky, C.J., Mosley, B., Nelson, N., Ness, K.V., Greenstreet, T.A., March, C.J., Kronheim, Druck, T., Cannizzaro, L.A., *et al.* (1992). Molecular cloning of the interleukin-1 beta converting enzyme. Science *256*, 97–100.

bioRxiv preprint doi: https://doi.org/10.1101/2020.06.02.129825; this version posted June 9, 2021. The copyright holder for this preprint (which was not certified by peer review) is the author/funder, who has granted bioRxiv a license to display the preprint in perpetuity. It is made available under aCC-BY 4.0 International license.

Chen, T., Wardill, T.J., Sun, Y., Pulver, S.R., Renninger, S.L., Baohan, A., Schreiter, E.R., Kerr, R.A., Orger, M.B., Jayaraman, V., *et al.* (2013). Ultrasensitive fluorescent proteins for imaging neuronal activity. Nature *499*, 295–300.

Cheng, H., Lederer, W., and Cannell, M. (1993). Calcium sparks: elementary events underlying excitation-contraction coupling in heart muscle. Science *262*, 740–744.

Cook, S.J., Crouse, C.M., Yemini, E., Hall, D.H., Emmons, S.W., and Hobert, O. (2020). The connectome of the *Caenorhabditis elegans* pharynx. Journal of Comparative Neurology *528*, 2767–2784.

Dent, J.A., Smith, M.M., Vassilatis, D.K., and Avery, L. (2000). The genetics of ivermectin resistance in *Caenorhabditis elegans*. PNAS *97*, 2674–2679.

Du, E.J., Ahn, T.J., Wen, X., Seo, D.-W., Na, D.L., Kwon, J.Y., Choi, M., Kim, H., Cho, H., and Kang, K. (2016). Nucleophile sensitivity of *Drosophila* TRPA1 underlies light-induced feeding deterrence. ELife *5*, e18425.

Edwards, S.L., Charlie, N.K., Milfort, M.C., Brown, B.S., Gravlin, C.N., Knecht, J.E., and Miller, K.G. (2008). A novel molecular solution for ultraviolet light detection in *Caenorhabditis elegans*. PLOS Biology *6*, e198.

Fang-Yen, C., Avery, L., and Samuel, A.D.T. (2009). Two size-selective mechanisms specifically trap bacteria-sized food particles in *Caenorhabditis elegans*. PNAS *106*, 20093–20096.

Fang-Yen, C., Gabel, C.V., Samuel, A.D.T., Bargmann, C.I., and Avery, L. (2012). Laser microsurgery in *Caenorhabditis elegans*. In Methods in Cell Biology, (Elsevier), pp. 177–206.

Flavell, S.W., Pokala, N., Macosko, E.Z., Albrecht, D.R., Larsch, J., and Bargmann, C.I. (2013). Serotonin and the neuropeptide PDF initiate and extend opposing behavioral states in *C. elegans*. Cell *154*, 1023–1035.

Franks, C.J., Murray, C., Ogden, D., O'Connor, V., and Holden-Dye, L. (2009). A comparison of electrically evoked and channel rhodopsin-evoked postsynaptic potentials in the pharyngeal system of *Caenorhabditis elegans*. Invert Neurosci *9*, 43–56.

Guntur, A.R., Gu, P., Takle, K., Chen, J., Xiang, Y., and Yang, C. (2015). *Drosophila* TRPA1 isoforms detect UV light via photochemical production of H_2O_2. Proc Natl Acad Sci USA *112*, E5753–E5761.

Guntur, A.R., Gou, B., Gu, P., He, R., Stern, U., Xiang, Y., and Yang, C. (2017). H_2O_2-sensitive isoforms of *Drosophila melanogaster* TRPA1 act in bitter-sensing gustatory neurons to promote avoidance of UV during egg-laying. Genetics *205*, 749–759.

Halevi, S., McKay, J., Palfreyman, M., Yassin, L., Eshel, M., Jorgensen, E., and Treinin, M. (2002). The *C. elegans ric-3* gene is required for maturation of nicotinic acetylcholine receptors. The EMBO Journal *21*, 1012–1020.

Hill, K., and Schaefer, M. (2009). Ultraviolet light and photosensitising agents activate TRPA1 via generation of oxidative stress. Cell Calcium *45*, 155–164.

bioRxiv preprint doi: https://doi.org/10.1101/2020.06.02.129825; this version posted June 9, 2021. The copyright holder for this preprint (which was not certified by peer review) is the author/funder, who has granted bioRxiv a license to display the preprint in perpetuity. It is made available under aCC-BY 4.0 International license.

Hunt-Newbury, R., Viveiros, R., Johnsen, R., Mah, A., Anastas, D., Fang, L., Halfnight, E., Lee, D., Lin, J., Lorch, A., *et al.* (2007). High-throughput in vivo analysis of gene expression in Caenorhabditis elegans. PLoS Biol *5*, e237.

Jansen, G., Thijssen, K.L., Werner, P., van der Horst, M., Hazendonk, E., and Plasterk, R.H.A. (1999). The complete family of genes encoding G proteins of *Caenorhabditis elegans*. Nature Genetics *21*, 414.

Kerr, R., Lev-Ram, V., Baird, G., Vincent, P., Tsien, R.Y., and Schafer, W.R. (2000). Optical imaging of calcium transients in neurons and pharyngeal muscle of *C. elegans*. Neuron *26*, 583–594.

Kim, M.J., and Johnson, W.A. (2014). ROS-mediated activation of *Drosophila* larval nociceptor neurons by UVC irradiation. BMC Neurosci *15*, 14.

Kim, E., Sun, L., Gabel, C.V., and Fang-Yen, C. (2013a). Long-term imaging of *Caenorhabditis elegans* using nanoparticle-mediated immobilization. PLoS ONE *8*, e53419.

Kim, M.J., Ainsley, J.A., Carder, J.W., and Johnson, W.A. (2013b). Hyperoxia-triggered aversion behavior in *Drosophila* foraging larvae is mediated by sensory detection of hydrogen peroxide. Journal of Neurogenetics *27*, 151–162.

Kohn, R.E., Duerr, J.S., McManus, J.R., Duke, A., Rakow, T.L., Maruyama, H., Moulder, G., Maruyama, I.N., Barstead, R.J., and Rand, J.B. (2000). Expression of Multiple UNC-13 Proteins in the *Caenorhabditis elegans* Nervous System. Mol Biol Cell *11*, 3441–3452.

Kozlova, A.A., Lotfi, M., and Okkema, P.G. (2019). Crosstalk with the GAR-3 Receptor Contributes to Feeding Defects in *Caenorhabditis elegans eat-2* Mutants. Genetics *212*, 231–243.

Kuo, I.Y., and Ehrlich, B.E. (2015). Signaling in muscle contraction. Cold Spring Harb Perspect Biol *7*, :a006023.

Li, Z., Li, Y., Yi, Y., Huang, W., Yang, S., Niu, W., Zhang, L., Xu, Z., Qu, A., Wu, Z., *et al.* (2012). Dissecting a central flip-flop circuit that integrates contradictory sensory cues in *C. elegans* feeding regulation. Nature Communications *3*, 1–8.

Liu, J., Ward, A., Gao, J., Dong, Y., Nishio, N., Inada, H., Kang, L., Yu, Y., Ma, D., Xu, T., *et al.* (2010). *C. elegans* phototransduction requires a G protein–dependent cGMP pathway and a taste receptor homolog. Nature Neuroscience *13*, 715–722.

Luo, S., and Horvitz, H.R. (2017). The CDK8 complex and proneural proteins together drive neurogenesis from a mesodermal lineage. Current Biology *27*, 661–672.

Marder, E., and Calabrese, R.L. (1996). Principles of rhythmic motor pattern generation. Physiological Reviews *76*, 687–717.

Maruyama, I.N., and Brenner, S. (1991). A phorbol ester/diacylglycerol-binding protein encoded by the *unc-13* gene of *Caenorhabditis elegans*. PNAS *88*, 5729–5733.

McKay, S.J., Johnsen, R., Khattra, J., Asano, J., Baillie, D.L., Chan, S., Dube, N., Fang, L., Goszczynski, B., Ha, E., *et al.* (2003). Gene Expression Profiling of Cells, Tissues, and Developmental Stages of the Nematode *C. elegans*. Cold Spring Harb Symp Quant Biol *68*, 159–170.

bioRxiv preprint doi: https://doi.org/10.1101/2020.06.02.129825; this version posted June 9, 2021. The copyright holder for this preprint (which was not certified by peer review) is the author/funder, who has granted bioRxiv a license to display the preprint in perpetuity. It is made available under aCC-BY 4.0 International license.

Miedel, M.T., Graf, N.J., Stephen, K.E., Long, O.S., Pak, S.C., Perlmutter, D.H., Silverman, G.A., and Luke, C.J. (2012). A Pro-Cathepsin L Mutant Is a Luminal Substrate for Endoplasmic-Reticulum-Associated Degradation in *C. elegans*. PLOS ONE *7*, e40145.

Nagel, G., Szellas, T., Huhn, W., Kateriya, S., Adeishvili, N., Berthold, P., Ollig, D., Hegemann, P., and Bamberg, E. (2003). Channelrhodopsin-2, a directly light-gated cation-selective membrane channel. PNAS *100*, 13940–13945.

Navedo, M.F., Amberg, G.C., Votaw, V.S., and Santana, L.F. (2005). Constitutively active L-type Ca^{2+} channels. Proceedings of the National Academy of Sciences *102*, 11112–11117.

Nelson, M.T., Cheng, H., Rubart, M., Santana, L.F., Bonev, A.D., Knot, H.J., and Lederer, W.J. (1995). Relaxation of arterial smooth muscle by calcium sparks. Science *270*, 633–637.

Nieves-Cintrón, M., Amberg, G.C., Navedo, M.F., Molkentin, J.D., and Santana, L.F. (2008). The control of Ca^{2+} influx and NFATc3 signaling in arterial smooth muscle during hypertension. PNAS *105*, 15623–15628.

Ohno, H., Yoshida, M., Sato, T., Kato, J., Miyazato, M., Kojima, M., Ida, T., and Iino, Y. (2017). Luqin-like RYamide peptides regulate food-evoked responses in *C. elegans*. ELife *6*, e28877.

Okkema, P.G., and Fire, A. (1994). The *Caenorhabditis elegans* NK-2 class homeoprotein CEH-22 is involved in combinatorial activation of gene expression in pharyngeal muscle. Development *120*, 2175–2186.

Okkema, P.G., Harrison, S.W., Plunger, V., Aryana, A., and Fire, A. (1993). Sequence Requirements for Myosin Gene Expression and Regulation in *Caenorhabditis Elegans*. Genetics *135*, 385–404.

O'Sullivan, A., Lindsay, T., Prudnikova, A., Erdi, B., Dickinson, M., and von Philipsborn, A.C. (2018). Multifunctional wing motor control of song and flight. Current Biology *28*, 2705-2717.e4.

Pokala, N., Liu, Q., Gordus, A., and Bargmann, C.I. (2014). Inducible and titratable silencing of Caenorhabditis elegans neurons in vivo with histamine-gated chloride channels. PNAS *111*, 2770–2775.

Raizen, D.M., Lee, R.Y., and Avery, L. (1995). Interacting genes required for pharyngeal excitation by motor neuron MC in *Caenorhabditis elegans*. Genetics *141*, 1365–1382.

Rhoades, J.L., Nelson, J.C., Nwabudike, I., Yu, S.K., McLachlan, I.G., Madan, G.K., Abebe, E., Powers, J.R., Colón-Ramos, D.A., and Flavell, S.W. (2019). ASICs mediate food responses in an enteric serotonergic neuron that controls foraging behaviors. Cell *176*, 85-97.e14.

Richmond, J.E., Davis, W.S., and Jorgensen, E.M. (1999). UNC-13 is required for synaptic vesicle fusion in *C. elegans*. Nat Neurosci *2*, 959–964.

Richmond, J.E., Weimer, R.M., and Jorgensen, E.M. (2001). An open form of syntaxin bypasses the requirement for UNC-13 in vesicle priming. Nature *412*, 338–341.

Sabrin, K.M., Wei, Y., Heuvel, M.P. van den, and Dovrolis, C. (2020). The hourglass organization of the *Caenorhabditis elegans* connectome. PLOS Computational Biology *16*, e1007526.

bioRxiv preprint doi: https://doi.org/10.1101/2020.06.02.129825; this version posted June 9, 2021. The copyright holder for this preprint (which was not certified by peer review) is the author/funder, who has granted bioRxiv a license to display the preprint in perpetuity. It is made available under aCC-BY 4.0 International license.

Sawin, E.R., Ranganathan, R., and Horvitz, H.R. (2000). *C. elegans* locomotory rate is modulated by the environment through a dopaminergic pathway and by experience through a serotonergic pathway. Neuron *26*, 619–631.

Shimozono, S., Fukano, T., Kimura, K.D., Mori, I., Kirino, Y., and Miyawaki, A. (2004). Slow Ca^{2+} dynamics in pharyngeal muscles in *Caenorhabditis elegans* during fast pumping. EMBO Rep. *5*, 521–526.

Singh, M., Lujan, B., and Renden, R. (2018). Presynaptic GCaMP expression decreases vesicle release probability at the calyx of Held. Synapse *72*.

Speese, S., Petrie, M., Schuske, K., Ailion, M., Ann, K., Iwasaki, K., Jorgensen, E.M., and Martin, T.F.J. (2007). UNC-31 (CAPS) is required for dense-core vesicle but not synaptic vesicle exocytosis in *Caenorhabditis elegans*. J. Neurosci. *27*, 6150–6162.

Stinchcomb, D.T., Shaw, J.E., Carr, S.H., and Hirsh, D. (1985). Extrachromosomal DNA transformation of *Caenorhabditis elegans*. Mol. Cell. Biol. *5*, 3484–3496.

Taylor, S.R., Santpere, G., Reilly, M., Glenwinkel, L., Poff, A., McWhirter, R., Xu, C., Weinreb, A., Basavaraju, M., Cook, S.J., *et al.* (2019). Expression profiling of the mature *C. elegans* nervous system by single-cell RNA-Sequencing. BioRxiv https://doi.org/10.1101/737577.

The *C. elegans* Deletion Mutant Consortium (2012). Large-scale screening for targeted knockouts in the *Caenorhabditis elegans* genome. G3: Genes, Genomes, Genetics *2*, 1415–1425.

Thornberry, N.A., Bull, H.G., Calaycay, J.R., Chapman, K.T., Howard, A.D., Kostura, M.J., Miller, D.K., Molineaux, S.M., Weidner, J.R., Aunins, J., *et al.* (1992). A novel heterodimeric cysteine protease is required for interleukin-1β processing in monocytes. Nature *356*, 768.

Tian, L., Hires, S.A., Mao, T., Huber, D., Chiappe, M.E., Chalasani, S.H., Petreanu, L., Akerboom, J., McKinney, S.A., Schreiter, E.R., *et al.* (2009). Imaging neural activity in worms, flies and mice with improved GCaMP calcium indicators. Nature Methods *6*, 875–881.

Trojanowski, N.F., Padovan-Merhar, O., Raizen, D.M., and Fang-Yen, C. (2014). Neural and genetic degeneracy underlies *Caenorhabditis elegans* feeding behavior. Journal of Neurophysiology *112*, 951–961.

Yamazawa, T., and Iino, M. (2002). Simultaneous imaging of Ca^{2+} signals in interstitial cells of Cajal and longitudinal smooth muscle cells during rhythmic activity in mouse ileum. The Journal of Physiology *538*, 823–835.

Zheng, Y., Brockie, P.J., Mellem, J.E., Madsen, D.M., and Maricq, A.V. (1999). Neuronal control of locomotion in *C. elegans* is modified by a dominant mutation in the GLR-1 ionotropic glutamate receptor. Neuron *24*, 347–361.

bioRxiv preprint doi: https://doi.org/10.1101/2020.06.02.129825; this version posted June 9, 2021. The copyright holder for this preprint (which was not certified by peer review) is the author/funder, who has granted bioRxiv a license to display the preprint in perpetuity. It is made available under aCC-BY 4.0 International license.

Summary of figures and supplemental material

Main figures:

Figure 1

Figure 2

Figure 3

Figure 4

Figure 5

Figure 6

Figure 7

Supplemental material:

Figure 1—figure supplement 1

Figure 2—figure supplement 1

Figure 3—figure supplement 1

Figure 4—figure supplement 1

Figure 4—figure supplement 2

Figure 6—figure supplement 1

Video 1: Feeding pumps in polystyrene bead feeding assay.

Video 2: Spitting pumps in polystyrene bead feeding assay.

Video 3: Feeding pumps in muscle motion visualization assay.

bioRxiv preprint doi: https://doi.org/10.1101/2020.06.02.129825; this version posted June 9, 2021. The copyright holder for this preprint (which was not certified by peer review) is the author/funder, who has granted bioRxiv a license to display the preprint in perpetuity. It is made available under aCC-BY 4.0 International license.

Video 4: Spitting pumps in muscle motion visualization assay.

Video 5: "Gulping" pumps in polystyrene bead feeding assay.

Video 6: pm2-ablated animals are defective in opening the metastomal filter during spitting behavior in polystyrene bead feeding assay.

Video 7: a subset of pm1-ablated animals spit less efficiently.

Video 8: a subset of pm1-ablated animals exhibit normal spitting behavior.

Video 9: pm1/pm2 double-ablated animals can spit.

Video 10: Light induces immobilized animals to spit.

Video 11: Pharyngeal muscle calcium response to light (*gpa-16p::gcamp3* transgene).

Video 12: Exogenous serotonin does not induce localized calcium increases.

Video 13: Pharyngeal muscle calcium response to light (*myo-2p::gcamp3* transgene).

Video 14: Pharyngeal muscle calcium response to light (*C32F10.8p::gcamp3* transgene).

Video 15: The pharyngeal neuron M1 is activated by light.

bioRxiv preprint doi: https://doi.org/10.1101/2020.06.02.129825; this version posted June 9, 2021. The copyright holder for this preprint (which was not certified by peer review) is the author/funder, who has granted bioRxiv a license to display the preprint in perpetuity. It is made available under aCC-BY 4.0 International license.

Figure 1. Worms Spit as a Consequence of the Sustained Contraction of Anterior Pharyngeal Muscles

(A) Anatomy of the *C. elegans* pharynx; a, anterior; d, dorsal.

(B) Grinder pumping response to 365 nm UV light (from Bhatla and Horvitz [2015]). Left, adult wild-type *C. elegans* head showing one pump of the grinder; center, raster plot of individual animals, each grinder contraction shown by a tick; right, backward moving average of the pumping rate of the same animals. Labels indicate the “acute inhibition,” “burst,” and “recovery” phases of the response. Phases previously described by Bhatla and Horvitz, 2015. Scale bar, 20 μm.

(C) Representative images of worms feeding and spitting in the polystyrene bead feeding assay. Pumps were scored as “feeding” if they resulted in the retention of particles in the anterior pharynx (arrows), while pumps were scored as “spitting” if they released beads from the procorpus into the environment or if beads ingested during a procorpus contraction were not retained. In feeding pumps, the metastomal filter was typically partially closed, such that food accumulated in the buccal cavity (arrowheads and inset). Spitting pumps involved the opening of the metastomal filter such that the buccal cavity did not fill.

bioRxiv preprint doi: https://doi.org/10.1101/2020.06.02.129825; this version posted June 9, 2021. The copyright holder for this preprint (which was not certified by peer review) is the author/funder, who has granted bioRxiv a license to display the preprint in perpetuity. It is made available under aCC-BY 4.0 International license.

(D) Raster plot of representative results from polystyrene bead feeding assay. Animals carried the transgene *nIs678 (M1$_{promoter}$::gcamp6s)*. "*M1$_{promoter}$*" refers to the *glr-2* promoter.

(E) Quantification of average grinder pumping and spitting rates of animals shown in (D).

(F) Representative images of the pumping cycles of feeding (left column) and spitting worms (right column). When open, the lumen of the pharynx (arrowheads) is visible as a white line. The food-trapping pharyngeal valve (left arrowhead) is located at the anterior end of the lumen. In the absence of UV light (left column), the lumen and pharyngeal valve open (yellow arrowheads) and close (white arrowheads) nearly synchronously, enabling the trapping and eventual ingestion of food (Fang-yen *et al.*, 2009). By contrast, in the presence of UV (right column) light the opening of the lumen and the pharyngeal valve become uncoupled. While the lumen continues to open and close, the muscle region at the site of the pharyngeal valve undergoes sustained contraction and thus opens the valve such that the conclusion of a pump ejects material from the pharynx. Animals were *unc-29(e1072)* mutants to facilitate video capture.

bioRxiv preprint doi: https://doi.org/10.1101/2020.06.02.129825; this version posted June 9, 2021. The copyright holder for this preprint (which was not certified by peer review) is the author/funder, who has granted bioRxiv a license to display the preprint in perpetuity. It is made available under aCC-BY 4.0 International license.

(G) Quantification of frequencies at which the metastomal filter was open in feeding and spitting pumps in (D). Center bar, mean; error bars, standard deviation (SD). ****, $p < 0.0001$; t test.

(H) Diagrammatic summary of feeding and spitting behavior.

Shading around traces indicates standard error of the mean (SEM). See also **Figure supplement 1**.

bioRxiv preprint doi: https://doi.org/10.1101/2020.06.02.129825; this version posted June 9, 2021. The copyright holder for this preprint (which was not certified by peer review) is the author/funder, who has granted bioRxiv a license to display the preprint in perpetuity. It is made available under aCC-BY 4.0 International license.

Figure 2. Subcellularly Localized Muscle Contractions and Calcium Increases Open the Pharyngeal Valve to Produce Spitting

(A) Anatomy of the anterior pharynx showing pharyngeal muscles pm1, pm2, and pm3. Double-headed arrows indicate orientation of muscle fibers.

(B-E) Mock-ablated (n = 9 animals), pm1-ablated (n = 5), pm2-ablated (n = 8), and pm1/pm2 double-ablated animals (n = 4) spit in response to light. All animals carried transgene *nIs507 (pm1$_{promoter}$::gfp)* to mark pm1. *"pm1$_{promoter}$"* refers to the *inx-4* promoter.

(F) Laser ablation of the pm2 pharyngeal muscles partially suppresses the light-induced opening of the metastomal filter. Center bar, mean; error bars, SD. ***, $p < 0.001$; t test. $n \geq 5$ animals.

(G) Diagram of the eight classes of pharyngeal muscle (pm1-8; borders indicated by thin solid black lines; lumen indicated with thick solid black lines). Dashed boxes indicate regions analyzed for GCaMP3 fluorescence changes.

(H) Representative images from video of pharyngeal muscle GCaMP3 calcium imaging. Light induces subcellularly localized increases in pharyngeal muscle GCaMP fluorescence at the anterior end of the pharynx. Yellow arrowhead

bioRxiv preprint doi: https://doi.org/10.1101/2020.06.02.129825; this version posted June 9, 2021. The copyright holder for this preprint (which was not certified by peer review) is the author/funder, who has granted bioRxiv a license to display the preprint in perpetuity. It is made available under aCC-BY 4.0 International license.

indicates spatially restricted calcium increases. Images false-colored based on the intensity of fluorescence changes. See also Video 11.

(I) Pharyngeal muscle GCaMP responses of individual animals to light. Each row represents a different animal; $\Delta F/F_0$ over time is indicated according to the heatmap at left. Light induces subcellularly localized increases in pharyngeal muscle GCaMP fluorescence at the anterior end of the pharynx. Animals carried transgene *nIs686 (gpa-16p::GCaMP3)*, which expresses GCaMP in pharyngeal muscle under the *gpa-16* promoter. Each line indicates an independent trial from a different animal. Regions analyzed are indicated in (G). n = 20 animals.

(J) Average GCaMP response of animals shown in (I).

(K) GCaMP responses to light of pm3 muscles in individual animals. Light induces subcellularly localized increases in pm3 GCaMP fluorescence at the anterior end of pm3. Animals carried transgene *cuIs36 (myo-2p::GCaMP3)*, which expresses GCaMP in pm3 under the *myo-2* promoter. Each line represents an independent trial of a different animal. Regions analyzed are indicated in (G). n = 20 animals.

(L) Average GCaMP response of animals shown in (K)

bioRxiv preprint doi: https://doi.org/10.1101/2020.06.02.129825; this version posted June 9, 2021. The copyright holder for this preprint (which was not certified by peer review) is the author/funder, who has granted bioRxiv a license to display the preprint in perpetuity. It is made available under aCC-BY 4.0 International license.

(M) GCaMP responses to light of pm3 muscle cells in individual mosaic animals. Light induces subcellularly localized increases in pm3 GCaMP fluorescence at the anterior end of pm3. Animals carried transgene *nEx3045 (C32F10.8p::GCaMP3)*, which expresses GCaMP in pm3 under the *C32F10.8* promoter. Each line represents an independent trial of a different animal. Regions analyzed are indicated in (G). n = 10 animals.

(N) Average GCaMP response of animals shown in (M)

Shading around traces indicates SEM.. See also **Figure supplement 1** and **Figure supplement 2**.

bioRxiv preprint doi: https://doi.org/10.1101/2020.06.02.129825; this version posted June 9, 2021. The copyright holder for this preprint (which was not certified by peer review) is the author/funder, who has granted bioRxiv a license to display the preprint in perpetuity. It is made available under aCC-BY 4.0 International license.

Figure 3. Pharyngeally-Expressed Gustatory Receptor Orthologs *lite-1* and *gur-3* Play Major and Minor Roles, Respectively, in the Light-Induced Spitting Reflex

(A-D) Light-induced spitting is reduced in *gur-3* and *lite-1* single mutants and eliminated in *lite-1 gur-3* double mutants. n = 10 animals except $n_{gur\text{-}3}$ = 9.

(E-F) Expression of wild-type *lite-1 (*transgene *nEx2281; lite-1*$_{promoter}$*::lite-1::gfp)* or *gur-3* (transgene *nEx2157*; *gur-3*$_{promoter}$*::gur-3 gDNA*) respectively restores wild-type or partial spitting to *lite-1 gur-3* double mutants. n = 10 animals.

(G) Quantification of average spitting rate during light exposure of animals from (H-M). ****, approximate adjusted p value < 0.0001; ***, adjusted p value < 0.0005, **, adjusted p value < 0.005; n.s., not significant; ordinary one-way ANOVA.

(H) Quantification of the frequencies at which the metastomal filter was open in feeding and spitting pumps in (H-M). ****, approximate adjusted p value < 0.0001; ***, adjusted p value < 0.0005, *, adjusted p value < 0.05; n.s., not significant; ordinary one-way ANOVA.

bioRxiv preprint doi: https://doi.org/10.1101/2020.06.02.129825; this version posted June 9, 2021. The copyright holder for this preprint (which was not certified by peer review) is the author/funder, who has granted bioRxiv a license to display the preprint in perpetuity. It is made available under aCC-BY 4.0 International license.

(I) Pharyngeal muscle GCaMP responses of individual animals to light. Each row represents a different animal; $\Delta F/F_0$ over time is indicated according to the heatmap at left. n ≥ 20 animals. Control data duplicated from Figure 2I-2J.

(J-L) Light-induced pharyngeal muscle calcium increases depend on *lite-1* (which accounts for 99% of the response) and *gur-3* (which makes a small contribution to the initial activation of pharyngeal muscle; black arrows). n ≥ 20 animals. Control data duplicated from Figure 2I-2J.

(M) Quantification of peak GCaMP $\Delta F/F_0$ from (Q-T). *lite-1*, but not *gur-3*, is required for the amplitude of the pharyngeal muscle response to light. ****, approximate adjusted p value < 0.0001; n.s., not significant; Kruskal-Wallis test, followed by Dunn's multiple comparison test.

(N) Quantification of acute ($F_{t = 0.5\ sec}/F_0$) GCaMP response from (Q-T). *gur-3*, but not *lite-1*, is required for the acute GCaMP response of pharyngeal muscle to light. ****, approximate adjusted p value < 0.0001; **, adjusted p value < 0.001; *, adjusted p value < 0.05; n.s., not significant; Kruskal-Wallis test, followed by Dunn's multiple comparison test.

Shading around traces indicates SEM. All *gur-3* alleles are null allele *gur-3*(*ok2245)* and all *lite-1* alleles are null allele *lite-1*(*ce314)*. Center bar, mean;

bioRxiv preprint doi: https://doi.org/10.1101/2020.06.02.129825; this version posted June 9, 2021. The copyright holder for this preprint (which was not certified by peer review) is the author/funder, who has granted bioRxiv a license to display the preprint in perpetuity. It is made available under aCC-BY 4.0 International license.

error bars, SD. ****, approximate adjusted p value < 0.0001; ***, adjusted p value < 0.0005, **, adjusted p value < 0.005; *, adjusted p value < 0.05; n.s., not significant; ordinary one-way ANOVA. See also **Figure supplement 1**.

bioRxiv preprint doi: https://doi.org/10.1101/2020.06.02.129825; this version posted June 9, 2021. The copyright holder for this preprint (which was not certified by peer review) is the author/funder, who has granted bioRxiv a license to display the preprint in perpetuity. It is made available under aCC-BY 4.0 International license.

Figure 4. The Pharyngeal Neuron M1 Controls the Spitting Reflex

(A) The anatomy of M1 (red) suggests that it controls spitting directly, as it is the only neuron to make neuromuscular junctions (bolded blue segment) with the region of pharyngeal muscle that undergoes sustained contraction during spitting.

(B-C) M1 laser-ablated, but not mock-ablated, animals are completely defective in light-induced spitting and burst pumping. Animals carried GFP reporter transgene *nIs864 ($M1_{promoter}$::gfp)* to mark M1. *"$M1_{promoter}$"* refers to the *glr-2* promoter. n ≥ 12 animals.

(D-E) M1 genetically-ablated animals, but not transgene-negative sibling controls, are completely defective in light-induced spitting and burst pumping. Ablated animals carried genetic-ablation transgene *nEx2905* (*$M1_{promoter}$::ice::sl2::mcherry*) and all animals carried GFP reporter transgene *nIs864.* "*$M1_{promoter}$*" refers to the *lury-1* promoter. n = 10 animals.

(F) Pharyngeal muscle GCaMP responses of individual animals to light. Each row represents a different animal; $\Delta F/F_0$ over time is indicated according to the heatmap at left. n ≥ 11 animals.

bioRxiv preprint doi: https://doi.org/10.1101/2020.06.02.129825; this version posted June 9, 2021. The copyright holder for this preprint (which was not certified by peer review) is the author/funder, who has granted bioRxiv a license to display the preprint in perpetuity. It is made available under aCC-BY 4.0 International license.

(G) Average response of animals from (F). Spatially restricted calcium signals depend on M1. “Anterior tip” region analyzed is indicated in Figure 2G. Animals carried pharyngeal muscle GCaMP3 transgene *nIs686 (gpa-16p::GCaMP3)*.

(H-J) Histamine-exposed animals expressing the inhibitory histamine-gated chloride channel HisCl1 in M1 (n = 8) but neither of histamine-exposed animals lacking HisCl1 expression in M1 (n = 4) or non-histamine-exposed animals expressing HisCl1 in M1 (n = 6) exhibited significantly delayed spitting in response to light.

(K) Comparison of the light-induced spitting behavior of animals from (I-J).

(L) Quantification of H-J. Histamine-exposed animals expressing HisCl1 in M1 exhibit significantly greater spitting latencies than control animals. ****, adjusted p value < 0.0001; n.s., not significant; ordinary one-way ANOVA.

(M) Representative example of light-induced GCaMP6s fluorescence increase in M1. Animal carried transgene *nIs678 (M1$_{promoter}$::gcamp6s)*. “*M1$_{promoter}$*” refers to the *glr-2* promoter. The unchanging signal common to both images was caused by GCaMP6s fluorescence in additional *glr-2*-expressing neurons in the nerve ring. See also Video 15.

(N) M1 somatic GCaMP responses of individual animals to light; n = 20.

bioRxiv preprint doi: https://doi.org/10.1101/2020.06.02.129825; this version posted June 9, 2021. The copyright holder for this preprint (which was not certified by peer review) is the author/funder, who has granted bioRxiv a license to display the preprint in perpetuity. It is made available under aCC-BY 4.0 International license.

(O) Average response of animals shown in (N).

(P) M1 somatic GCaMP responses of individual control, *gur-3*, *lite-1*, and *lite-1 gur-3* mutant animals to light. n = 2 biological replicates (40 animals total).

(Q-S) Light-induced calcium increases in the M1 neuron depend on *lite-1* (which accounts for 99% M1's response) and *gur-3 (*which makes a small but consistent contribution to M1's initial activation; black arrows). n = 2 biological replicates (40 animals total).

(T) Quantification of peak GCaMP $\Delta F/F_0$ from (P-S). *lite-1*, but not *gur-3*, is required for the amplitude of the M1 GCaMP response to light. ****, approximate adjusted p value < 0.0001; n.s., not significant; Kruskal-Wallis test, followed by Dunn's multiple comparison test.

(U) Quantification of acute ($F_{t = 0.5\ sec}/F_0$) GCaMP response from (P-S). *gur-3*, but not *lite-1*, is required for the acute M1 GCaMP response to light. ****, approximate adjusted p value < 0.0001; n.s., not significant; Kruskal-Wallis test, followed by Dunn's multiple comparison test.

(V-W) A subset (~25%) of *lite-1 gur-3* animals expressing an M1-specific ChR2 transgene *nEx2815 (M1$_{promoter}$::chr2::sl2::mcherry)* grown in the presence, but not

bioRxiv preprint doi: https://doi.org/10.1101/2020.06.02.129825; this version posted June 9, 2021. The copyright holder for this preprint (which was not certified by peer review) is the author/funder, who has granted bioRxiv a license to display the preprint in perpetuity. It is made available under aCC-BY 4.0 International license.

the absence, of ATR spit in response to 470 nm light. "*M1*$_{promoter}$" refers to the *lury-1* promoter. n ≥ 10 animals.

Shading around traces indicates SEM. All *gur-3* alleles are null allele *gur-3*(*ok2245),* and all *lite-1* alleles are null allele *lite-1*(*ce314)*. See also **Figure supplement 1** and **Figure supplement 2**.

bioRxiv preprint doi: https://doi.org/10.1101/2020.06.02.129825; this version posted June 9, 2021. The copyright holder for this preprint (which was not certified by peer review) is the author/funder, who has granted bioRxiv a license to display the preprint in perpetuity. It is made available under aCC-BY 4.0 International license.

Figure 5. The *gur-3*-Expressing I2 Neurons Can Activate M1 to Produce an Attenuated Form of Spitting

(A-B) I2-specific expression of *gur-3* restores light-induced spitting to *lite-1 gur-3* mutants. n = 5 animals.

(C) Quantification of the frequencies at which the metastomal filter was open in feeding and spitting pumps in (A) and (B). Center bar, mean; error bars, SEM; ****, $p < 0.0001$; t test. n = 5 animals.

(D) I2-specific expression of *gur-3* restores the light-induced M1 calcium response of *lite-1 gur-3* mutants. M1 somatic GCaMP responses of individual animals to light. Each row is a different animal; $\Delta F/F_0$ over time is indicated according to the heatmap at left. n ≥ 26 animals.

(E) Average of (D).

(F-G) Laser ablation of M1 suppresses the I2-specific *gur-3* rescue of *lite-1 gur-3* spitting defects. n = 11 animals.

(H) Quantification of the frequencies at which the metastomal filter was open in feeding and spitting pumps in (F) and (G). Center bar, mean; error bars, SEM; ****, $p < 0.0001$; t test. n ≥ 8 animals.

bioRxiv preprint doi: https://doi.org/10.1101/2020.06.02.129825; this version posted June 9, 2021. The copyright holder for this preprint (which was not certified by peer review) is the author/funder, who has granted bioRxiv a license to display the preprint in perpetuity. It is made available under aCC-BY 4.0 International license.

(I) I2-specific expression of *gur-3* via transgene *nIs791* (*I2$_{promoter}$::mcherry::gur-3(+))* does not rescue the burst pumping defect of *eat-2; lite-1 gur-3* animals in the grinder pumping assay. n = 20 animals.

(J) Comparison of grinder pumping rates in (F) and (G). While mock-ablated animals from (F) do not inhibit pumping in response to light, M1-ablated animals from (G) exhibit robust light-induced inhibition, indicating that the I2s' promotion of pumping via M1 outweighs their inhibition of pumping.

(K) Comparison of feeding pumping rates from (F) and (G).

(L) Model for the effects of the I2 neurons on M1 and pumping. The I2 neurons reduce overall feeding by two mechanisms: direct inhibition of feeding pumps and M1-dependent promotion of spitting pumps.

Shading around traces indicates SEM. Unless indicated otherwise, "I2-specific expression of *gur-3"* refers to transgene *nEx2144* (*I2$_{promoter}$::mcherry::gur-3(+))*. "Genetic ablation of the I2 neurons" refers to transgene *nIs569 (I2$_{promoter}$::csp-1b)* (Bhatla and Horvitz, 2015). "*I2$_{promoter}$*" refers to the *flp-15* promoter.

bioRxiv preprint doi: https://doi.org/10.1101/2020.06.02.129825; this version posted June 9, 2021. The copyright holder for this preprint (which was not certified by peer review) is the author/funder, who has granted bioRxiv a license to display the preprint in perpetuity. It is made available under aCC-BY 4.0 International license.

Figure 6. The I4 Neuron Functions with the I2 Neurons to Promote Spitting and Inhibit Feeding

(A) Genetic ablation of the I2 neurons in a wild-type background does not eliminate light-induced spitting. n = 5 animals.

(B) Genetic ablation of the I2 neurons of *lite-1(ce314)* mutants does not eliminate light-induced spitting. n = 6 animals.

(C) Diagram indicating the cellular morphology of M1 and the *gur-3*-expressing I2 and I4 pharyngeal neurons. The I2 neurons are bilaterally symmetric; only one I2 neuron is depicted.

(D) Mock-ablated *lite-1* animals inhibit pumping and spit in response to light. n = 8 animals.

(E) I2-ablated *lite-1* animals spit in response to light but do not inhibit pumping. n = 8 animals.

(F) I4-ablated *lite-1* animals inhibit pumping and spit in response to light. n = 10 animals.

(G) I2/I4 double-ablated *lite-1* animals exhibit delayed spitting and do not inhibit pumping in response to light. n = 8 animals.

bioRxiv preprint doi: https://doi.org/10.1101/2020.06.02.129825; this version posted June 9, 2021. The copyright holder for this preprint (which was not certified by peer review) is the author/funder, who has granted bioRxiv a license to display the preprint in perpetuity. It is made available under aCC-BY 4.0 International license.

(H) Quantification of average spitting rate during light exposure of animals from (C-D). **, adjusted p value < 0.005; n.s., not significant; ordinary one-way ANOVA.

(I) Quantification of pumping inhibition during light exposure of animals from (D-G). ****, approximate adjusted p value < 0.0001; **, adjusted p value < 0.005; n.s., not significant; ordinary one-way ANOVA.

(J) Mock-ablated *lite-1* animals inhibit pumping and spit in response to light. n = 5 animals.

(K-M) M1-ablated (n = 6 animals), M1/I2-ablated (n = 6), and M1/I4-ablated (n = 7) *lite-1* animals inhibit pumping, but do not spit, in response to light.

(N) M1/I2/I4 triple-ablated *lite-1* animals neither inhibit pumping nor spit in response to light. n = 4 animals.

(O) Quantification of pumping inhibition in (J-N). Ablation of the I2 neurons eliminates light-induced pumping inhibition by M1/I4-ablated animals. **, adjusted p value < 0.005; *, adjusted p value < 0.05; n.s., not significant; ordinary one-way ANOVA.

Shading around traces indicates SEM. All animals were *lite-1*(ce314) null mutants and carried transgene *nIs678 ($M1_{promoter}$::gcamp6s)*. "$M1_{promoter}$" refers to

bioRxiv preprint doi: https://doi.org/10.1101/2020.06.02.129825; this version posted June 9, 2021. The copyright holder for this preprint (which was not certified by peer review) is the author/funder, who has granted bioRxiv a license to display the preprint in perpetuity. It is made available under aCC-BY 4.0 International license.

the *glr-2* promoter. Center bar, mean; error bars, SD. See also **Figure supplement 1**.

bioRxiv preprint doi: https://doi.org/10.1101/2020.06.02.129825; this version posted June 9, 2021. The copyright holder for this preprint (which was not certified by peer review) is the author/funder, who has granted bioRxiv a license to display the preprint in perpetuity. It is made available under aCC-BY 4.0 International license.

Figure 7. Models of Spitting Behavior and Neural Circuitry

(A) Model for feeding and spitting. During feeding, the M1 neuron is inactive. Thus, the metastomal filter is partially closed, restricting particle influx, and the pharyngeal valve closes at the end of each pump, trapping food. During spitting induced by light or reactive oxygen species (ROS), M1 is active, thus inducing spitting of ingested material by opening the pharyngeal valve and facilitating rinsing of the pharynx by opening the metastomal filter.

(B) Model for neural circuitry controlling light- and ROS-induced spitting. Light or ROS stimulate the M1, I2, and I4 neurons via LITE-1 and GUR-3. The I2 and I4 neurons excite M1, which is situated in the “waist” of an “hourglass” circuit motif. In turn, M1 makes diverging outputs to multiple pharyngeal muscle classes, each driving distinct aspects of the spitting reflex: the pm1 and pm2 muscles open the metastomal filter, a subcellular compartment of the pm3 muscles opens the pharyngeal valve, and the remainder of pm3 pumps. The M1 and I2 neurons each also inhibit pumping.

bioRxiv preprint doi: https://doi.org/10.1101/2020.06.02.129825; this version posted June 9, 2021. The copyright holder for this preprint (which was not certified by peer review) is the author/funder, who has granted bioRxiv a license to display the preprint in perpetuity. It is made available under aCC-BY 4.0 International license.

Figure 1—figure supplement 1.

(A) The odor of 9M hydrogen peroxide induces spitting. Animals are *unc-29(e1072)* mutants to facilitate video capture. n = 4 animals.

(B) Raster plot showing occurrence of “closed” (black) and “open” (green) pumps in pharyngeal muscle motion visualization assay. n = 7 animals.

(C) Moving averages of animals from (B), indicating that the burst pumping phase consists almost completely of “open” pumps.

Shading around traces indicates SEM.

(D) Comparison of bead intake in typical feeding (filter part-closed) and gulping (filter open) pumps. Each grouping represents a separate animal and each circle represents a single pump. Gulping pumps capture more particles than typical feeding pumps. n = 11 animals.

bioRxiv preprint doi: https://doi.org/10.1101/2020.06.02.129825; this version posted June 9, 2021. The copyright holder for this preprint (which was not certified by peer review) is the author/funder, who has granted bioRxiv a license to display the preprint in perpetuity. It is made available under aCC-BY 4.0 International license.

Figure 2—figure supplement 1.

(A-B) pm1-ablated animals lack the metastomal filter and thus ingest more material into the procorpus than mock-ablated controls do. Images were obtained from the first frame of the videos used to make Figure 2B and 2C. Each panel shows a different animal. Dark material in the pharyngeal lumen is a mixture of *E. coli* and 1 µm polystyrene beads. In mock-ablated animals, accumulation is visible in the pharyngeal isthmus but is minimal in the procorpus of most animals. pm1-ablated animals accumulate markedly more material in the procorpus. We also noticed qualitatively that pm1-ablated animals often spit material less efficiently than control animals, but this difference could stem from the differences in the average amount of ingested material in the pharynx in each condition. All animals carry transgene *nIs507 ($pm1_{promoter}$::gfp).* "$pm1_{promoter}$" refers to the *inx-4* promoter.

(C) Raster plots of the pumping response of immobilized animals to calcium imaging protocol (365/485 nm light flickered at 2 Hz) derived from analysis of behavioral videos. Each row represents an individual animals and each tick represents a contraction of the grinder. n ≥ 16 animals.

(D) Quantification of pumping by immobilized worms induced by 365 nm, 365/485 nm 2 Hz flickered (i.e., pharyngeal muscle/M1 calcium imaging protocol stimulus), or 485 nm

bioRxiv preprint doi: https://doi.org/10.1101/2020.06.02.129825; this version posted June 9, 2021. The copyright holder for this preprint (which was not certified by peer review) is the author/funder, who has granted bioRxiv a license to display the preprint in perpetuity. It is made available under aCC-BY 4.0 International license.

light. All light-induced pumping depends on M1. Animals carrying the *nEx2045 (C32F10.8p::gcamp3)* transgene exhibited reduced light-induced pumping, and animals carrying the *cuIs36 (myo-2p::gcamp3)* transgene were completely defective in light-induced pumping. Center bar, mean; error bars, SD. ****, approximate adjusted p value < 0.0001; ***, adjusted p value < 0.001; *, adjusted p value < 0.05; n.s., not significant; Kruskal-Wallis test, followed by Dunn's multiple comparison test. n ≥ 15 animals.

(E) Animals induced to pump using 10 mM serotonin do not exhibit sustained anteriorly localized calcium signals; GCaMP signal increases synchronously in the anterior tip and procorpus regions. Animals were *lite-1 gur-3* double mutants carrying the *gpa-16p::gcamp3* transgene *nIs686*. Fluorescence changes during pumping were recorded from three separate animals. See also Video 12.

(F) No anteriorly localized fluorescence increase was detected in animals expressing GFP in pm3. Animals carried transgene *vkEx1241 (myo-2p::GFP)*, which expresses GFP in pm3 under the *myo-2* promoter. n = 20 animals.

(G) Pharyngeal muscle GCaMP responses to light of individual mosaic animals selected for bright transgene expression in the anterior pharynx. Each row represents a different animal; $\Delta F/F_0$ over time is indicated according to the heatmap at left. Light induces subcellularly localized increases in pharyngeal muscle GCaMP fluorescence at the

bioRxiv preprint doi: https://doi.org/10.1101/2020.06.02.129825; this version posted June 9, 2021. The copyright holder for this preprint (which was not certified by peer review) is the author/funder, who has granted bioRxiv a license to display the preprint in perpetuity. It is made available under aCC-BY 4.0 International license.

anterior end of the pharynx. Animals carried transgene *nEx3045 (C32F10.8p::GCaMP3)*, which expresses GCaMP in the pm3 pharyngeal muscles and mc1 marginal cells under the *C32F10.8* promoter. Each line indicates an independent trial from a different animal. Regions analyzed are indicated in Figure 2G. n = 10 animals. Average GCaMP response of animals shown to right of individual traces. (H) The light-induced spitting behavior of animals carrying the transgene *nIs686 (pharyngeal muscle*$_{promoter\ -\ gpa\text{-}16p}$*::gcamp3)* resembles that of wild-type animals. n = 3 animals.

bioRxiv preprint doi: https://doi.org/10.1101/2020.06.02.129825; this version posted June 9, 2021. The copyright holder for this preprint (which was not certified by peer review) is the author/funder, who has granted bioRxiv a license to display the preprint in perpetuity. It is made available under aCC-BY 4.0 International license.

Figure 2—figure supplement 2.

(A) Transgene *nIs686 (gpa-16p::gcamp3)* drives GCaMP expression in pharyngeal muscles pm2 and pm3 and in the mc1 marginal cells (not shown). Occasional dim expression was observed in pm1 (not shown).

(B) Transgene *cuIs36 (myo-2p::gcamp3)* drives GCaMP expression in the pm3 pharyngeal muscles but not pm1, pm2, or the mc1 marginal cells (not shown).

(C) Transgene *sIs11111 (C32F10.8p::gfp)* drives GFP expression in the pm3 pharyngeal muscles and the mc1 marginal cells (not shown) but not pm1 or pm2.

(D) Transgene *nEx3045 (C32F10.8p::gcamp3)* drives GCaMP expression in the pm3 pharyngeal muscles and the mc1 marginal cells (not shown) but not pm1 or pm2.

bioRxiv preprint doi: https://doi.org/10.1101/2020.06.02.129825; this version posted June 9, 2021. The copyright holder for this preprint (which was not certified by peer review) is the author/funder, who has granted bioRxiv a license to display the preprint in perpetuity. It is made available under aCC-BY 4.0 International license.

Figure 3—figure supplement 1.

(A) *egl-47/gur-1(n1082dm)* mutants were normal in burst pumping. n = 20 animals.

(B) *egl-47/gur-1(ok677)* mutants were normal in burst pumping. n = 20 animals.

(C) *gur-3* is not required for light-induced burst pumping. n = 3 biological replicates (60 animals total).

(D) *gur-4(ok672)* mutants were normal in burst pumping. n = 20 animals.

(E) *gur-5(tm6169)* mutants were normal in burst pumping. n = 20 animals.

(F-G) The contribution of *lite-1* to burst pumping cannot be evaluated directly because *lite-1* mutants are partially defective in pumping inhibition. $n_{lite\text{-}1}$ = 2 biological replicates (40 animals total); $n_{lite\text{-}1\ gur\text{-}3}$ = 20 animals.

(H-J) Burst pumping of *eat-2(ad1113)* mutants depends on *lite-1* but not *gur-3*. n = 3 biological replicates (60 animals total).

(K) *lite-1* rescuing transgene *nIs687* (*lite-1*$_{promoter}$*::gfp::lite-1)* rescues the burst pumping defect of *eat-2; lite-1 gur-3* mutants. n = 3 biological replicates (60 animals total).

(L) Quantification of burst pumping from (D-G). ****, approximate adjusted p value < 0.0001; ***, adjusted p value < 0.0005, *, adjusted p value < 0.05; n.s., not significant; ordinary one-way ANOVA.

bioRxiv preprint doi: https://doi.org/10.1101/2020.06.02.129825; this version posted June 9, 2021. The copyright holder for this preprint (which was not certified by peer review) is the author/funder, who has granted bioRxiv a license to display the preprint in perpetuity. It is made available under aCC-BY 4.0 International license.

(M-N) Integrated *gur-3* transcriptional reporter transgene *nIs780 (gur-3*$_{promoter}$*::gfp)* is expressed in the MI and M1 pharyngeal neurons and an unidentified head neuron (not shown), in addition to being expressed in the I2, I4, and AVD neurons as previously reported by Bhatla and Horvitz (2015).

Shading around traces indicates SEM.

bioRxiv preprint doi: https://doi.org/10.1101/2020.06.02.129825; this version posted June 9, 2021. The copyright holder for this preprint (which was not certified by peer review) is the author/funder, who has granted bioRxiv a license to display the preprint in perpetuity. It is made available under aCC-BY 4.0 International license.

Figure 4—figure supplement 1.

(A) Overexpression of the mammalian caspase ICE in M1 via the transgene *nEx2905* (*M1*$_{promoter\ –\ lury\text{-}1}$*::ice::sl2::mCherry)* kills M1 with high efficiency and the M2 pharyngeal neurons with moderate efficiency. The presence of M1 and the M2s was determined by the expression of transgenes *nIs864 (M1*$_{promoter\ –\ glr\text{-}2}$*::gfp)* and *nIs310 (nlp-13*$_{promoter}$*::gfp)*, respectively.

(B) M1 genetic-ablation transgene eliminates burst pumping in the grinder pumping assay. Ablation animals carried transgene *nEx2905 (M1*$_{promoter\ -\ lury\text{-}1}$*::ice::sl2::mcherry);* all animals carried *nIs864 (M1*$_{promoter\ –\ glr\text{-}2}$*::gfp).* n = 40 animals.

(C) Screening animals based on the brightness of pharyngeal mCherry expression allows the selection of animals lacking the M1 neuron but not the M2 neurons. When pharyngeal muscle mCherry expression is high, animals are more likely to lack the M2s. Animals with dim pharyngeal muscle mCherry expression very rarely lack M2s; thus dim mCherry expression can be used to enrich for animals lacking only M1. Center bar, mean; error bars, SEM. n = 3 biological replicates (more than 65 animals total).

(D) Genetic ablation of M1 eliminates burst pumping in *eat-2* mutants. Ablation animals carried transgene *nIs865* (*M1*$_{promoter\ –\ lury\text{-}1}$*::ice::sl2::mCherry).* n = 3 biological replicates (60 animals total).

bioRxiv preprint doi: https://doi.org/10.1101/2020.06.02.129825; this version posted June 9, 2021. The copyright holder for this preprint (which was not certified by peer review) is the author/funder, who has granted bioRxiv a license to display the preprint in perpetuity. It is made available under aCC-BY 4.0 International license.

(E) Comparison of grinder pumping rates of mock and M1 laser-ablated animals from Figure 4B and 4C. In addition to eliminating burst pumping and spitting, M1 ablation enhances the rate of pumping recovery after illumination. n ≥ 12 animals.

(F) Laser-ablated animals from Figure 4B exhibit abnormal “uncoupled” pumps, during which the grinder pumps while the procorpus does not. n ≥ 12 animals.

(G) Comparison of grinder pumping rates of control and M1 genetic-ablated animals from Figure 4D and 4E. In addition to eliminating burst pumping and spitting, M1 ablation enhances the rate of pumping recovery after illumination. n = 10 animals.

(H) M1 genetic-ablation animals from Figure 4E exhibit abnormal “uncoupled” pumps, during which the grinder pumps while the procorpus does not. n = 10 animals.

(I) Light-induced calcium increases in M1 are reduced but still significant in *unc-13(s69)* mutants. n = 2 biological replicates (greater than 41 animals total).

(J) Quantification of M1’s calcium response to light in *unc-13(s69)* mutants in (M). Error bars, SEM; *, $p < 0.05$; t test.

(K) Light-induced calcium increases in M1 are reduced but still significant in *unc-31(u280)* mutants. n = 20 animals.

(L) Quantification of M1’s calcium response to light in *unc-31(u280)* mutants in (O). Error bars, SEM; **, $p < 0.01$; t test.

bioRxiv preprint doi: https://doi.org/10.1101/2020.06.02.129825; this version posted June 9, 2021. The copyright holder for this preprint (which was not certified by peer review) is the author/funder, who has granted bioRxiv a license to display the preprint in perpetuity. It is made available under aCC-BY 4.0 International license.

(M) *unc-17(e245)* vesicular acetylcholine transporter mutants defective in vesicular acetylcholine transport were severely defective in both feeding and burst pumping. n = 3 biological replicates (60 animals total).

(N) *cha-1(p1152)* choline acetyltransferase mutants defective in acetylcholine synthesis were severely defective in both feeding and burst pumping. n = 20 animals.

(O) *ric-3(md158)* mutants defective in nicotinic acetylcholine receptor maturation were severely defective in both feeding and burst pumping. n = 20 animals.

(P) *unc-25(e156)* glutamate decarboxylase mutants defective in GABA synthesis were normal in burst pumping. n = 20 animals.

(Q) *eat-4(ky5)* vesicular glutamate transporter mutants defective in vesicular glutamate transport were defective in acute inhibition (Bhatla and Horvitz, 2015) but normal in burst pumping. n = 20 animals.

(R) *cat-2(e1113)* tyrosine hydroxylase mutants defective in dopamine synthesis were normal in burst pumping. n = 20 animals.

(S) *tdc-1(n3420)* tyrosine decarboxylase mutants defective in tyramine and octopamine synthesis were normal in burst pumping. n = 20 animals.

bioRxiv preprint doi: https://doi.org/10.1101/2020.06.02.129825; this version posted June 9, 2021. The copyright holder for this preprint (which was not certified by peer review) is the author/funder, who has granted bioRxiv a license to display the preprint in perpetuity. It is made available under aCC-BY 4.0 International license.

(T) *tph-1(n4622)* tryptophan hydroxylase mutants defective in serotonin synthesis were mildly defective in both feeding and burst pumping. n = 3 biological replicates (60 animals total).

(U) *tph-1(mg280)* tryptophan hydroxylase mutants defective in serotonin synthesis were mildly defective in both feeding and burst pumping. n = 3 biological replicates (60 animals total).

(V) *ser-4(ok512); mod-1(ok103); ser-1(ok345) ser-7(tm1325)* quadruple serotonin receptor mutants were defective in feeding but normal in burst pumping. n = 20 animals.

(W) The light-induced spitting behavior of animals carrying the transgene *nIs678* *(M1$_{promoter\ -\ glr\text{-}2p}$::gcamp6s)* resembles that of wild-type animals. n = 3 animals. Shading around traces indicates SEM. "*M1$_{promoter\ –\ lury\text{-}1}$*" refers to the *lury-1* promoter and "*M1$_{promoter\ –\ glr\text{-}2}$*" refers to the *glr-2* promoter. (1E-H and 1W) are derived from videos of bead feeding assays, (1I-1L) are derived from calcium imaging videos, and all other behavior plots were grinder pumping assays scored in real time.

bioRxiv preprint doi: https://doi.org/10.1101/2020.06.02.129825; this version posted June 9, 2021. The copyright holder for this preprint (which was not certified by peer review) is the author/funder, who has granted bioRxiv a license to display the preprint in perpetuity. It is made available under aCC-BY 4.0 International license.

Figure 4—figure supplement 2: Burst pumping responses of acetylcholine receptor mutants to UV light.

(A) *lev-1/acr-1(e211)* nicotinic acetylcholine receptor mutants were normal in burst pumping. n = 20 animals.

(B) *acr-2(n2595 n2420)* nicotinic acetylcholine receptor mutants were normal in burst pumping. n = 20 animals.

(C) *acr-3(ok2049)* nicotinic acetylcholine receptor mutants were normal in burst pumping. n = 20 animals.

(D) *deg-3(u662); des-2/acr-4(u695)* nicotinic acetylcholine receptor mutants were normal in burst pumping. n = 20 animals.

(E) *acr-5(ok180)* nicotinic acetylcholine receptor mutants were normal in burst pumping. n = 20 animals.

(F) *acr-6(tm3723)* nicotinic acetylcholine receptor mutants were subtly defective in burst pumping. n = 3 biological replicates (60 animals total).

(G) *acr-7(tm863)* nicotinic acetylcholine receptor mutants were modestly defective in burst pumping. n = 3 biological replicates (60 animals total).

(H) *acr-8(ok1240)* nicotinic acetylcholine receptor mutants were normal in burst pumping. n = 3 biological replicates (60 animals total).

bioRxiv preprint doi: https://doi.org/10.1101/2020.06.02.129825; this version posted June 9, 2021. The copyright holder for this preprint (which was not certified by peer review) is the author/funder, who has granted bioRxiv a license to display the preprint in perpetuity. It is made available under aCC-BY 4.0 International license.

(I) *acr-10(tm2515)* nicotinic acetylcholine receptor mutants were normal in burst pumping. n = 20 animals.

(J) *acr-11(gk827759)* nicotinic acetylcholine receptor mutants were normal in burst pumping. n = 20 animals.

(K) *acr-12(ok367)* nicotinic acetylcholine receptor mutants were normal in burst pumping. n = 20 animals.

(L) *lev-8/acr-13(x15)* nicotinic acetylcholine receptor mutants were normal in burst pumping. n = 20 animals.

(M) *acr-14(tm5819)* nicotinic acetylcholine receptor mutants were normal in burst pumping. n = 20 animals.

(N) *acr-15(ok1214)* nicotinic acetylcholine receptor mutants were normal in burst pumping. n = 20 animals.

(O) *acr-16(ok789)* nicotinic acetylcholine receptor mutants were normal in burst pumping. n = 20 animals.

(P) *acr-17(gk804825)* nicotinic acetylcholine receptor mutants were defective in both feeding and burst pumping. n = 2 biological replicates (40 animals total).

(Q) *acr-17(gk661490)* nicotinic acetylcholine receptor mutants were normal in burst pumping. n = 20 animals.

bioRxiv preprint doi: https://doi.org/10.1101/2020.06.02.129825; this version posted June 9, 2021. The copyright holder for this preprint (which was not certified by peer review) is the author/funder, who has granted bioRxiv a license to display the preprint in perpetuity. It is made available under aCC-BY 4.0 International license.

(R) *acr-18(gk324494)* nicotinic acetylcholine receptor mutants were defective in feeding but normal in burst pumping. n = 20 animals.

(S) *acr-19(ok967)* nicotinic acetylcholine receptor mutants were normal in burst pumping. n = 20 animals.

(T) *acr-20(gk161737)* nicotinic acetylcholine receptor mutants were normal in burst pumping. n = 20 animals.

(U) *acr-21(ok1314)* nicotinic acetylcholine receptor mutants were normal in burst pumping. n = 20 animals.

(V) *acr-23(gk231233)* nicotinic acetylcholine receptor mutants were subtly defective in feeding and defective in burst pumping. n = 3 biological replicates (60 animals total).

(W) *acr-23(ox429)* nicotinic acetylcholine receptor mutants were subtly defective in burst pumping. n = 3 biological replicates (60 animals total).

(X) *acr-23(ok2804)* nicotinic acetylcholine receptor mutants were normal in burst pumping. n = 20 animals.

(Y) *acr-24(gk387895)* nicotinic acetylcholine receptor mutants were defective in both feeding and burst pumping. n = 2 biological replicates (40 animals total).

(Z) *acr-24(gk557791)* nicotinic acetylcholine receptor mutants were defective in burst pumping. n = 3 biological replicates (60 animals total).

bioRxiv preprint doi: https://doi.org/10.1101/2020.06.02.129825; this version posted June 9, 2021. The copyright holder for this preprint (which was not certified by peer review) is the author/funder, who has granted bioRxiv a license to display the preprint in perpetuity. It is made available under aCC-BY 4.0 International license.

(A') *deg-3(u773)* nicotinic acetylcholine receptor mutants were normal in burst pumping. n = 20 animals.

(B') *unc-29(e1072)* nicotinic acetylcholine receptor mutants were normal in burst pumping. n = 3 biological replicates (60 animals total).

(C') *unc-38(e264)* nicotinic acetylcholine receptor mutants were normal in burst pumping. n = 20 animals.

(D') *lev-7/unc-63(x13)* nicotinic acetylcholine receptor mutants were normal in burst pumping. n = 20 animals.

(E') *acc-1(tm3268)* acetylcholine-gated chloride channel mutants were normal in burst pumping. n = 20 animals.

(F') *acc-2(gk501637)* acetylcholine-gated chloride channel mutants were normal in burst pumping. n = 20 animals.

(G') *acc-2(ok2216)* acetylcholine-gated chloride channel mutants were defective in feeding and burst pumping. n = 3 biological replicates (60 animals total).

(H') *acc-2(tm3219)* acetylcholine-gated chloride channel mutants were normal in burst pumping. n = 20 animals.

(I') *acc-3(tm3174)* acetylcholine-gated chloride channel mutants were normal in burst pumping. n = 20 animals.

bioRxiv preprint doi: https://doi.org/10.1101/2020.06.02.129825; this version posted June 9, 2021. The copyright holder for this preprint (which was not certified by peer review) is the author/funder, who has granted bioRxiv a license to display the preprint in perpetuity. It is made available under aCC-BY 4.0 International license.

(J') *acc-4(ok2371)* acetylcholine-gated chloride channel mutants were normal in burst pumping. n = 20 animals.

(K') *lgc-40(tm3377)* acetylcholine-gated chloride channel mutants were normal in burst pumping. n = 20 animals.

(L') *pbo-5(gk963058)* nicotinic acetylcholine receptor family mutants were normal in burst pumping. n = 20 animals.

(M') *pbo-6(ok1564)* nicotinic acetylcholine receptor family mutants were normal in burst pumping. n = 20 animals.

(N') *gar-1(ok755)* muscarinic acetylcholine receptor mutants were subtly defective in burst pumping. n = 3 biological replicates (60 animals total).

(O') *gar-2(ok520)* muscarinic acetylcholine receptor mutants were normal in burst pumping. n = 20 animals.

(P') *gar-3(gk337)* muscarinic acetylcholine receptor mutants were normal in burst pumping. n = 20 animals.

bioRxiv preprint doi: https://doi.org/10.1101/2020.06.02.129825; this version posted June 9, 2021. The copyright holder for this preprint (which was not certified by peer review) is the author/funder, who has granted bioRxiv a license to display the preprint in perpetuity. It is made available under aCC-BY 4.0 International license.

Figure 6—figure supplement 1

(A) M1 somatic GCaMP responses to light of individual mock-, I2-, I4-, and I2/I4-ablated animals. Each row represents a different animal; $\Delta F/F_0$ over time is indicated according to the heatmap at left. I2- and I4-ablated *lite-1* animals exhibit small M1 calcium responses; I2/I4 double-ablated animals do not have detectable M1 calcium responses. Animals carried transgene *nIs686 (gpa-16p::gcamp3)*. n ≥ 8 animals.

(B) Average GCaMP responses of animals shown in (A).

(C) Quantification of (A). Center bar, mean; error bars, SD. n.s., not significant; ordinary one-way ANOVA.

(D) Quantification of the frequencies at which the metastomal filter was open in feeding and spitting pumps in (B-E). Center bar, mean; error bars, SD. n.s., not significant; ordinary one-way ANOVA. n ≥ 4 animals.

bioRxiv preprint doi: https://doi.org/10.1101/2020.06.02.129825; this version posted June 9, 2021. The copyright holder for this preprint (which was not certified by peer review) is the author/funder, who has granted bioRxiv a license to display the preprint in perpetuity. It is made available under aCC-BY 4.0 International license.

Video 1: Feeding pumps in polystyrene bead feeding assay.

High frame rate video of *C. elegans* feeding in polystyrene bead feeding assay. The small, dark particles are polystyrene beads. During typical feeding pumps, beads accumulate in the buccal cavity. Beads filter gradually from the buccal cavity into the pharyngeal lumen, where they are trapped by the closure of the pharyngeal valve at the front of the pharynx upon the conclusion of each pump. Video was recorded at 1,000 frames per second. Playback is at 3% of original speed.

Video 2: Spitting pumps in polystyrene bead feeding assay.

High frame rate video of *C. elegans* spitting in response to light in polystyrene bead feeding assay. During spitting pumps, beads no longer accumulate in the buccal cavity, but instead freely enter the pharyngeal lumen. At the end of the pump, all material ingested during the pump is expelled. Video was recorded at 1,000 frames per second. Playback is at 3% of original speed.

Video 3: Feeding pumps in muscle motion visualization assay.

Video of *C. elegans* feeding beneath a coverslip. The pharyngeal lumen is visible as a white space when it is opened by the contraction of pharyngeal muscle. In feeding, the

bioRxiv preprint doi: https://doi.org/10.1101/2020.06.02.129825; this version posted June 9, 2021. The copyright holder for this preprint (which was not certified by peer review) is the author/funder, who has granted bioRxiv a license to display the preprint in perpetuity. It is made available under aCC-BY 4.0 International license.

musculature of the anterior pharynx relaxes at the end of each pump, closing the pharyngeal valve and thereby trapping ingested material. Video was recorded at 86 frames per second. Playback is at 50% of original speed.

Video 4: Spitting pumps in muscle motion visualization assay.

Video of *C. elegans* beneath a coverslip spitting in response to light. In contrast to feeding pumps, spitting pumps are characterized by the sustained contraction of the anterior musculature of the pharynx, which remains contracted open as the rest of the pharynx continues to contract and relax. Video was recorded at 86 frames per second. Playback is at 50% of original speed.

Video 5: "Gulping" pumps in polystyrene bead feeding assay.

High frame rate video of *C. elegans* "gulping" in polystyrene bead feeding assay. As in spitting pumps, beads pass freely through the buccal cavity and into the pharyngeal lumen. As in feeding pumps, this material is subsequently trapped and retained by the pharyngeal valve, resulting in ingestion. Video was recorded at 1,000 frames per second. Playback is at 3% of original speed.

bioRxiv preprint doi: https://doi.org/10.1101/2020.06.02.129825; this version posted June 9, 2021. The copyright holder for this preprint (which was not certified by peer review) is the author/funder, who has granted bioRxiv a license to display the preprint in perpetuity. It is made available under aCC-BY 4.0 International license.

Video 6: pm2-ablated animals are defective in opening the metastomal filter during spitting behavior in polystyrene bead feeding assay. High frame rate video of pm2-ablated *C. elegans* spitting in response to light in polystyrene bead feeding assay. In contrast to typical spitting pumps, beads accumulate in the buccal cavity, indicating that the metastomal filter is partially closed. At the end of the pump, ingested material is still expelled, indicating that the pharyngeal valve is open. Video was recorded at 1,000 frames per second. Playback is at 3% of original speed.

Video 7: a subset of pm1-ablated animals spit less efficiently. High frame rate video of pm1-ablated *C. elegans* spitting in response to light in polystyrene bead feeding assay. At the end of the pump, ingested material is expelled, indicating that the pharyngeal valve is open, but material already held in procorpus is ejected less efficiently in comparison to mock-ablated animals. Video was recorded at 1,000 frames per second. Playback is at 3% of original speed.

Video 8: a subset of pm1-ablated animals exhibit normal spitting behavior. High frame rate video of pm1-ablated *C. elegans* spitting in response to light in polystyrene

bioRxiv preprint doi: https://doi.org/10.1101/2020.06.02.129825; this version posted June 9, 2021. The copyright holder for this preprint (which was not certified by peer review) is the author/funder, who has granted bioRxiv a license to display the preprint in perpetuity. It is made available under aCC-BY 4.0 International license.

bead feeding assay. Spitting behavior is comparable to that of mock-ablated animals. Video was recorded at 1,000 frames per second. Playback is at 3% of original speed.

Video 9: pm1/pm2 double-ablated animals can hold open the pharyngeal valve and spit. High frame rate video of pm1/pm2 double-ablated *C. elegans* spitting in response to light in polystyrene bead feeding assay. At the end of the pump, the material ingested during the pump is spat out, indicating that the pharyngeal valve is open and that animals lacking both pm1 and the pm2s can spit. Video was recorded at 1,000 frames per second. Playback is at 3% of original speed.

Video 10: Light induces immobilized animals to spit.
Video of immobilized *C. elegans* spitting in response to 2 Hz flickered 365/485 nm light (i.e., the same as delivered to animals during calcium imaging). Animal was selected based on its ingestion of mineral oil into the anterior pharynx. Oil is visible as dark liquid that is ejected from the anterior pharynx over the course of several pumps. Video was recorded at 50 frames per second. Playback is at 100% of original speed.

bioRxiv preprint doi: https://doi.org/10.1101/2020.06.02.129825; this version posted June 9, 2021. The copyright holder for this preprint (which was not certified by peer review) is the author/funder, who has granted bioRxiv a license to display the preprint in perpetuity. It is made available under aCC-BY 4.0 International license.

Video 11: Pharyngeal muscle calcium response to light (*gpa-16p::gcamp3* transgene).

The pharyngeal muscle calcium response to light, as reported by fluorescence of GCaMP3 transgene *nIs686* (*gpa-16p::gcamp3*), which is expressed in the pm2 and pm3 pharyngeal muscles, the mc1 marginal cells, and occasionally/dimly in the pm1 pharyngeal muscle. Pumps result in fluorescence increases across the entirety of the anterior pharynx. Before and between pumps, localized and sustained calcium increases occur at the anterior tip of the pharynx. Video was recorded at 15 frames per second and false-colored based on the intensity of fluorescence changes (blue, low intensity; red, high intensity). Playback is at 100% of original speed.

Video 12: Sustained, anteriorly localized calcium signals do not occur when animals are induced to pump using serotonin. Animals carrying the muscle-GCaMP transgene *nIs686 (gpa-16p::gcamp3)* were immobilized in the presence of 10 mM serotonin and filmed at the onset of pumping. Video was recorded at 4 frames per second and false-colored based on the intensity of fluorescence changes (blue, low intensity; red, high intensity). Playback is at 100% of original speed.

bioRxiv preprint doi: https://doi.org/10.1101/2020.06.02.129825; this version posted June 9, 2021. The copyright holder for this preprint (which was not certified by peer review) is the author/funder, who has granted bioRxiv a license to display the preprint in perpetuity. It is made available under aCC-BY 4.0 International license.

Video 13: Pharyngeal muscle calcium response to light (*myo-2p::gcamp3* transgene).

The pharyngeal muscle calcium response to light as reported by fluorescence of GCaMP3 transgene *culs36* (*myo-2p::gcamp3*), which is expressed specifically in the pm3s. Localized and sustained calcium increases occur at the anterior tip of the pharynx. Video was recorded at 2 frames per second and false-colored based on the intensity of fluorescence changes (blue, low intensity; red, high intensity). Playback is at 100% of original speed.

Video 14: Pharyngeal muscle calcium response to light (*C32F10.8p::gcamp3* transgene).

The pharyngeal muscle calcium response to light, as reported by fluorescence of GCaMP3 transgene *nEx3045* (*C32F10.8p::gcamp3*), which is expressed specifically in the pm3 pharyngeal muscles and mc1 marginal cells. Localized and sustained calcium increases occur at the anterior tip of the pharynx. Video was recorded at 2 frames per second and false-colored based on the intensity of fluorescence changes (blue, low intensity; red, high intensity). Playback is at 100% of original speed.

bioRxiv preprint doi: https://doi.org/10.1101/2020.06.02.129825; this version posted June 9, 2021. The copyright holder for this preprint (which was not certified by peer review) is the author/funder, who has granted bioRxiv a license to display the preprint in perpetuity. It is made available under aCC-BY 4.0 International license.

Video 15: The pharyngeal neuron M1 is activated by light.

The pharyngeal neuron M1 is acutely activated by light, as reported by GCaMP6s fluorescence. Video was recorded at 2 frames per second and false-colored based on the intensity of fluorescence changes (blue, low intensity; red, high intensity). Playback is at 100% of original speed.

bioRxiv preprint doi: https://doi.org/10.1101/2020.06.02.129825; this version posted June 9, 2021. The copyright holder for this preprint (which was not certified by peer review) is the author/funder, who has granted bioRxiv a license to display the preprint in perpetuity. It is made available under aCC-BY 4.0 International license.

Figure 1

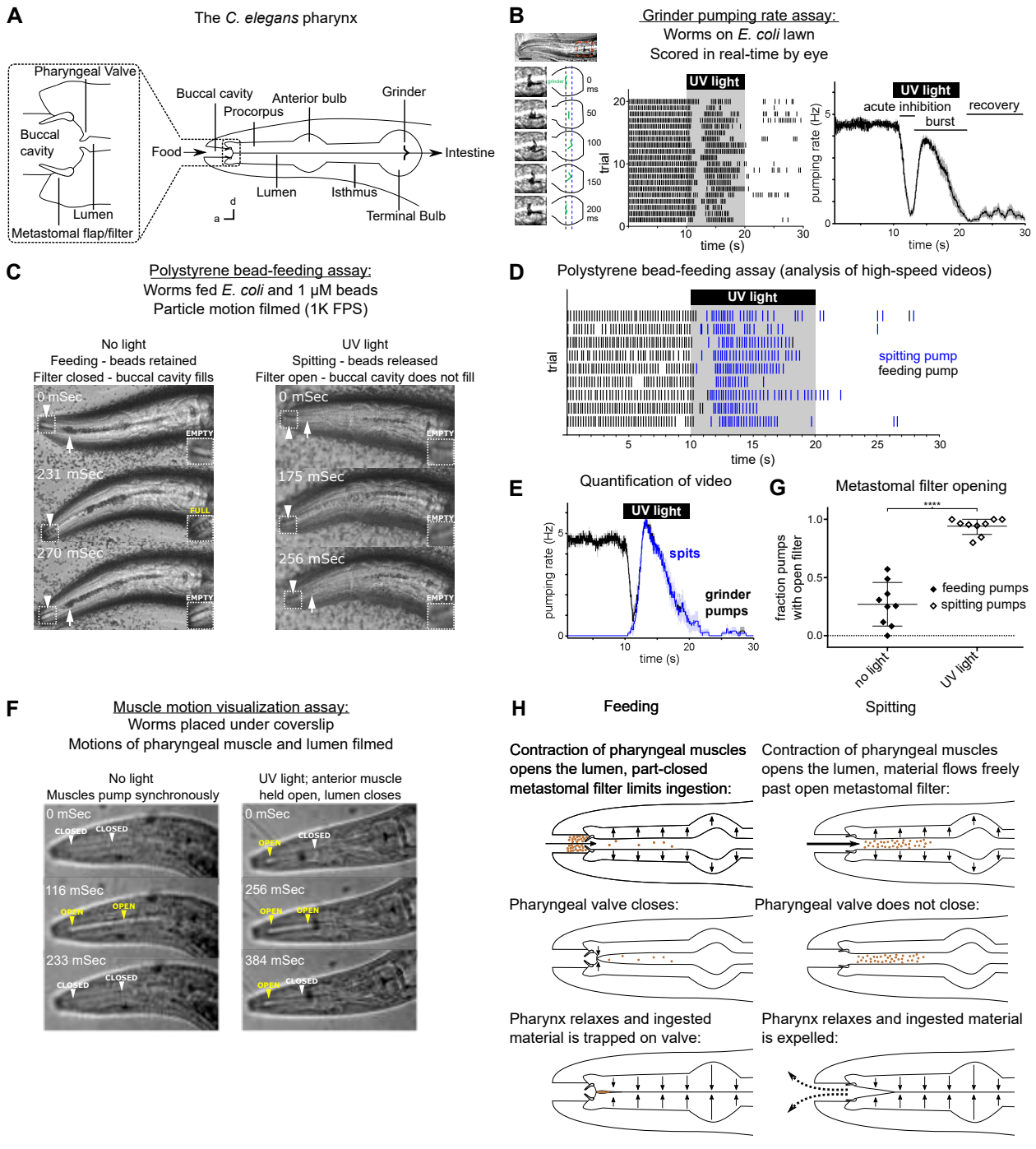

bioRxiv preprint doi: https://doi.org/10.1101/2020.06.02.129825; this version posted June 9, 2021. The copyright holder for this preprint (which was not certified by peer review) is the author/funder, who has granted bioRxiv a license to display the preprint in perpetuity. It is made available under aCC-BY 4.0 International license.

Figure 2

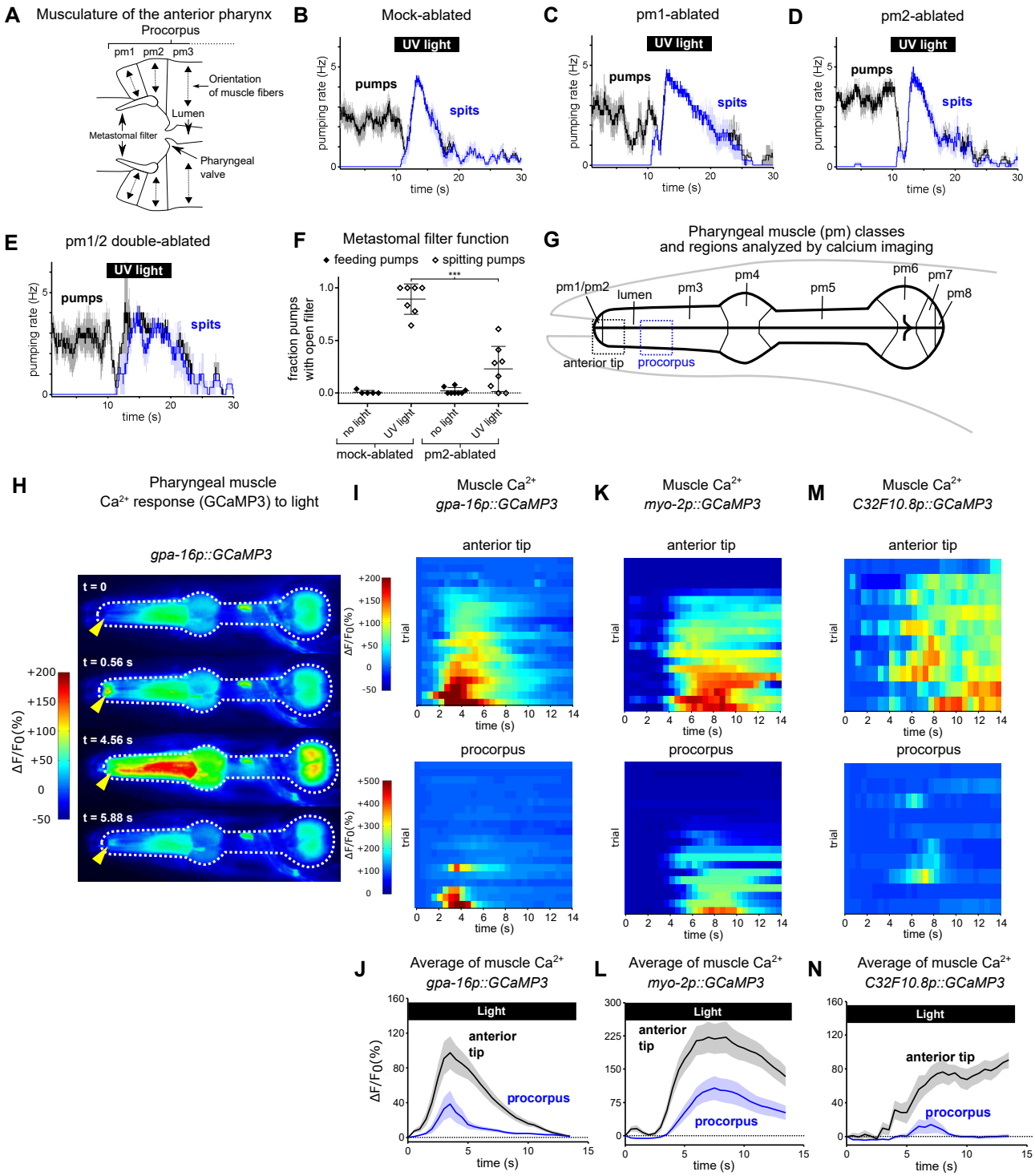

bioRxiv preprint doi: https://doi.org/10.1101/2020.06.02.129825; this version posted June 9, 2021. The copyright holder for this preprint (which was not certified by peer review) is the author/funder, who has granted bioRxiv a license to display the preprint in perpetuity. It is made available under aCC-BY 4.0 International license.

Figure 3

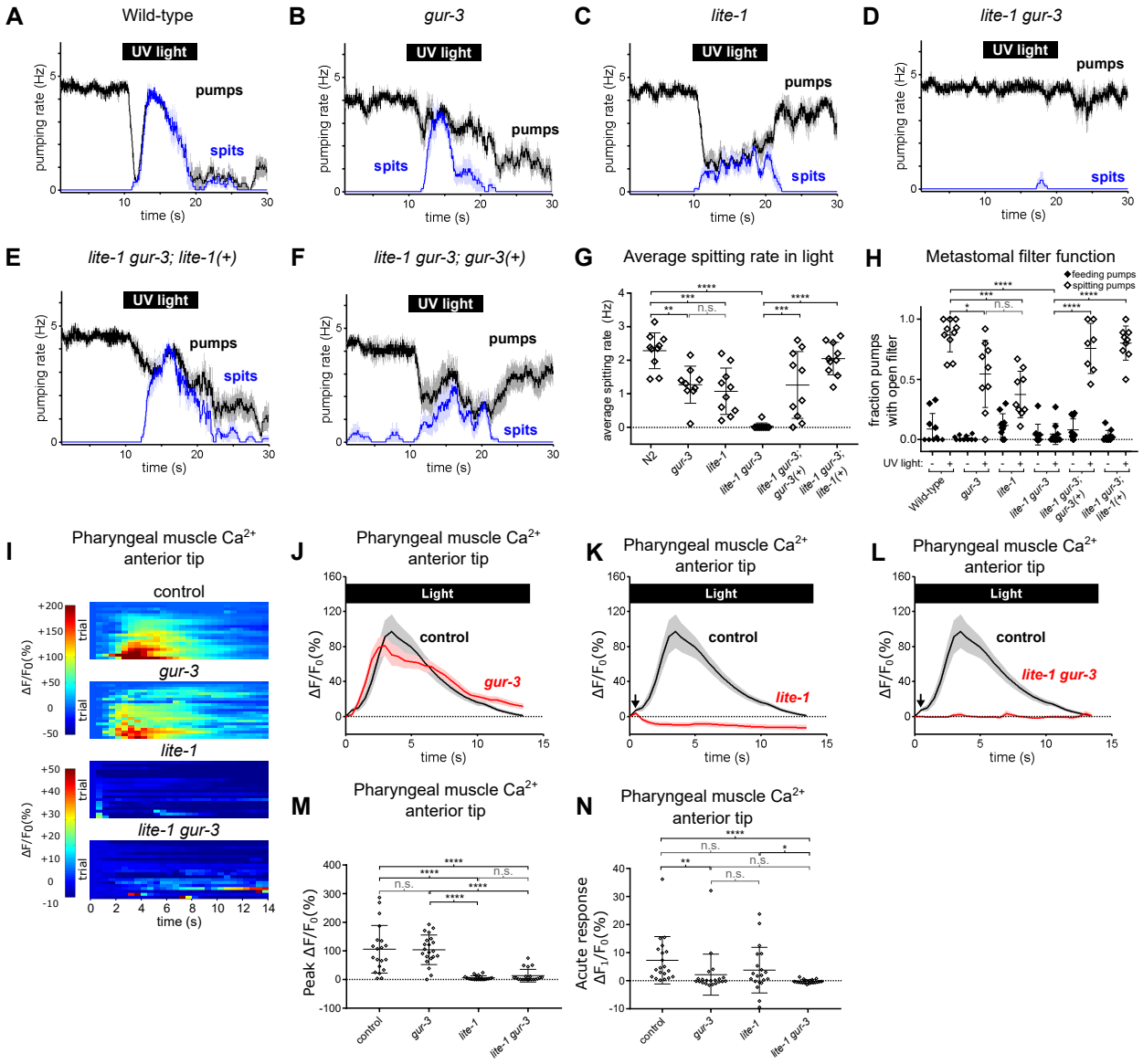

bioRxiv preprint doi: https://doi.org/10.1101/2020.06.02.129825; this version posted June 9, 2021. The copyright holder for this preprint (which was not certified by peer review) is the author/funder, who has granted bioRxiv a license to display the preprint in perpetuity. It is made available under aCC-BY 4.0 International license.

Figure 4

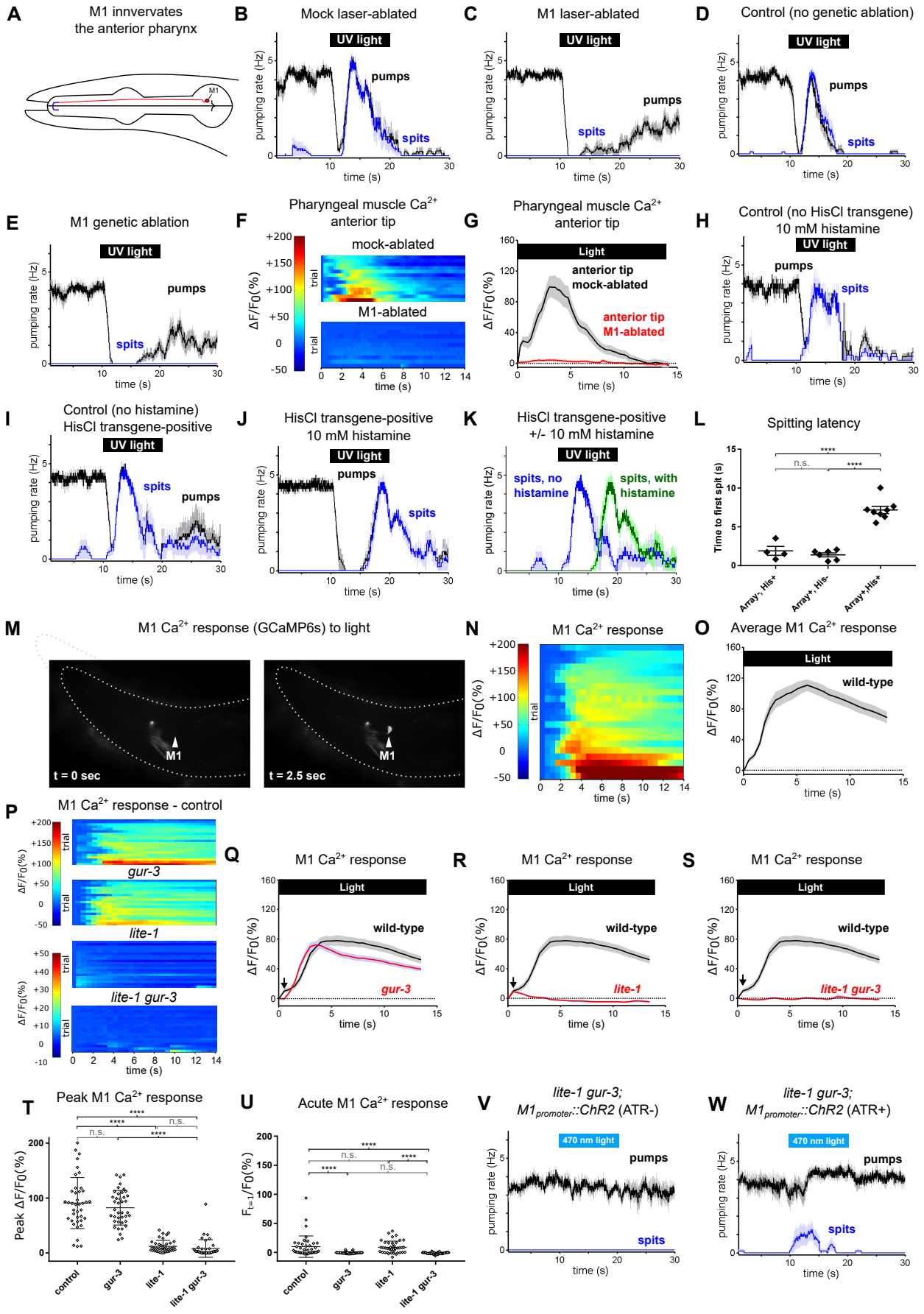

bioRxiv preprint doi: https://doi.org/10.1101/2020.06.02.129825; this version posted June 9, 2021. The copyright holder for this preprint (which was not certified by peer review) is the author/funder, who has granted bioRxiv a license to display the preprint in perpetuity. It is made available under aCC-BY 4.0 International license.

Figure 5

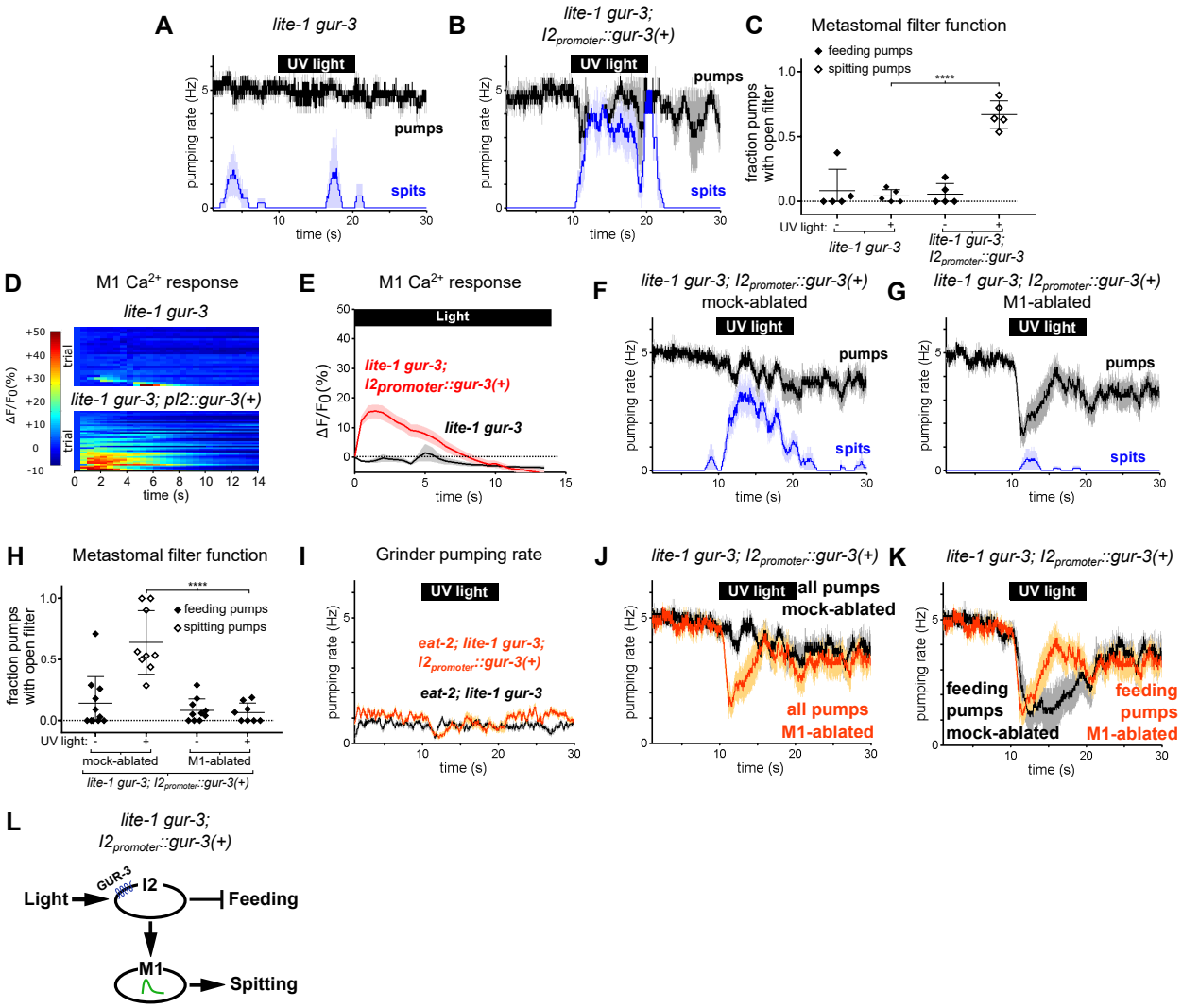

bioRxiv preprint doi: https://doi.org/10.1101/2020.06.02.129825; this version posted June 9, 2021. The copyright holder for this preprint (which was not certified by peer review) is the author/funder, who has granted bioRxiv a license to display the preprint in perpetuity. It is made available under aCC-BY 4.0 International license.

Figure 6

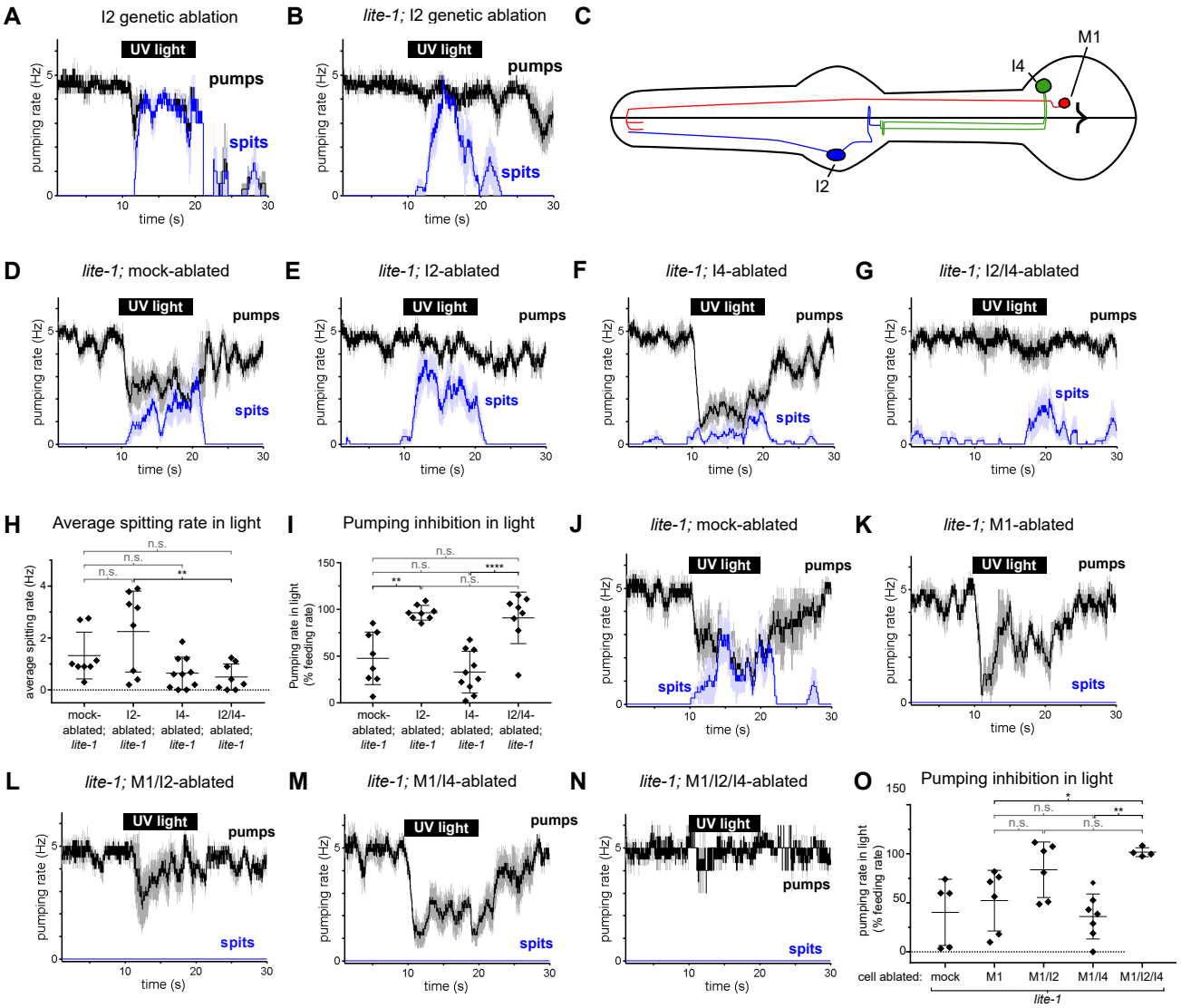

bioRxiv preprint doi: https://doi.org/10.1101/2020.06.02.129825; this version posted June 9, 2021. The copyright holder for this preprint (which was not certified by peer review) is the author/funder, who has granted bioRxiv a license to display the preprint in perpetuity. It is made available under aCC-BY 4.0 International license.

Figure 7

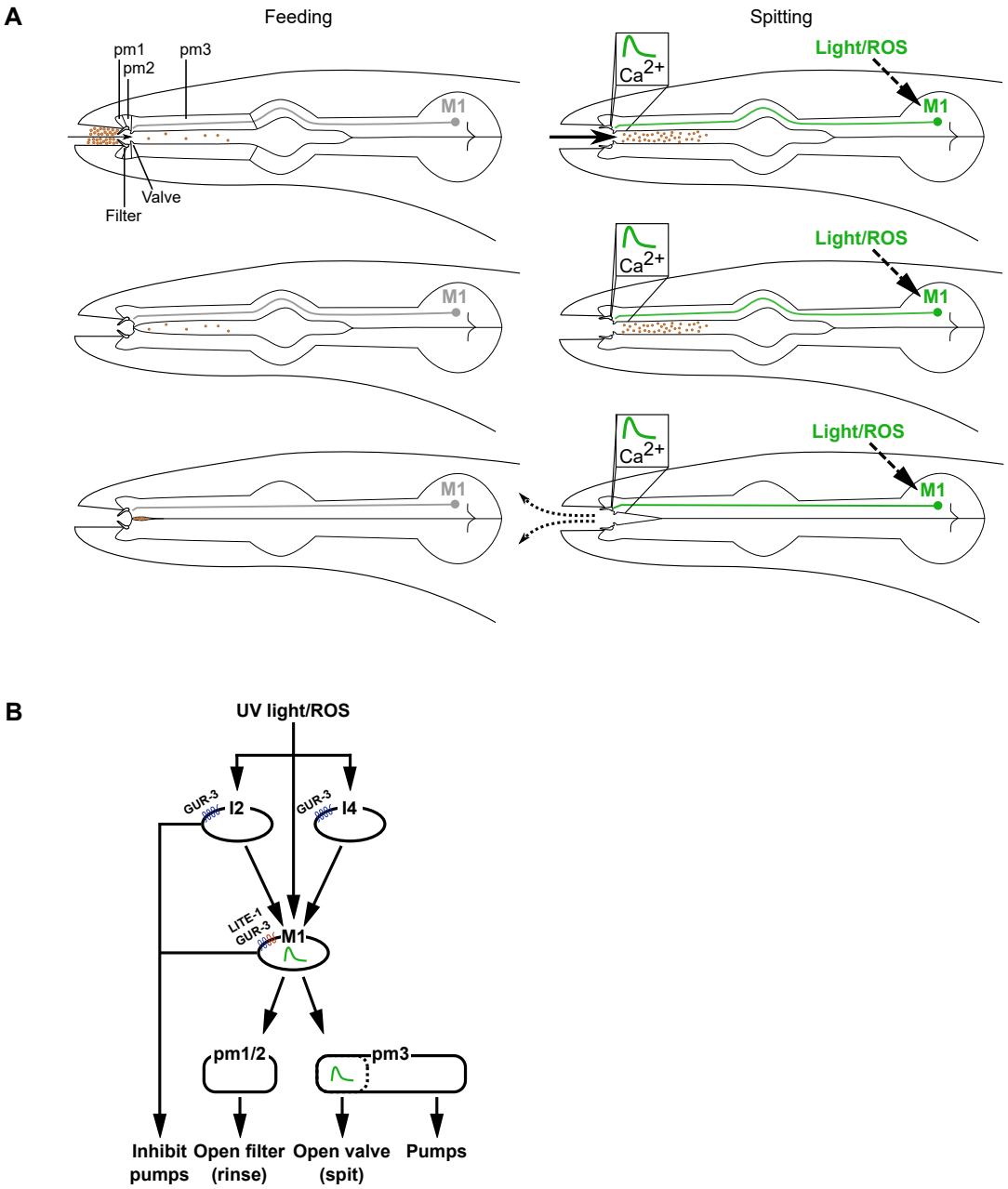

bioRxiv preprint doi: https://doi.org/10.1101/2020.06.02.129825; this version posted June 9, 2021. The copyright holder for this preprint (which was not certified by peer review) is the author/funder, who has granted bioRxiv a license to display the preprint in perpetuity. It is made available under aCC-BY 4.0 International license.

Figure 1—figure supplement 1

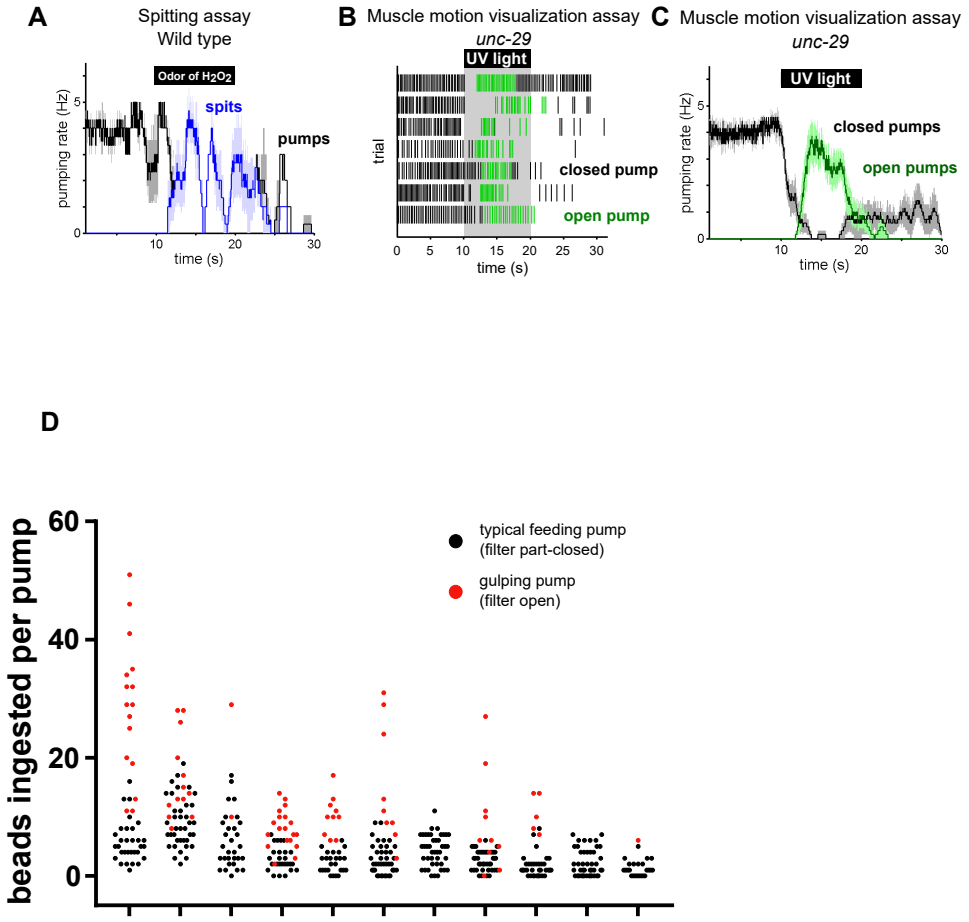

bioRxiv preprint doi: https://doi.org/10.1101/2020.06.02.129825; this version posted June 9, 2021. The copyright holder for this preprint (which was not certified by peer review) is the author/funder, who has granted bioRxiv a license to display the preprint in perpetuity. It is made available under aCC-BY 4.0 International license.

Figure 2—figure supplement 1

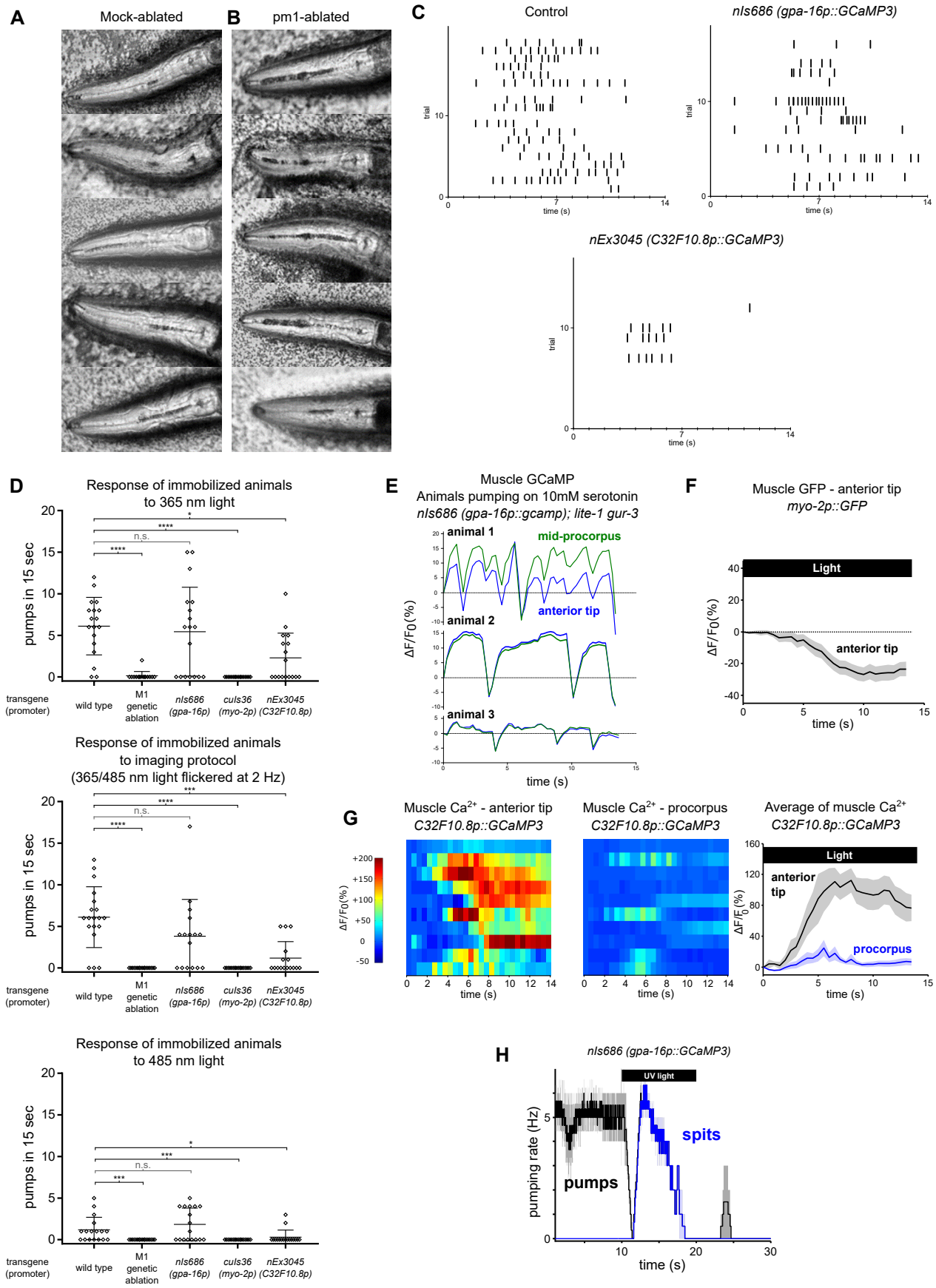

bioRxiv preprint doi: https://doi.org/10.1101/2020.06.02.129825; this version posted June 9, 2021. The copyright holder for this preprint (which was not certified by peer review) is the author/funder, who has granted bioRxiv a license to display the preprint in perpetuity. It is made available under aCC-BY 4.0 International license.

Figure 2—figure supplement 2

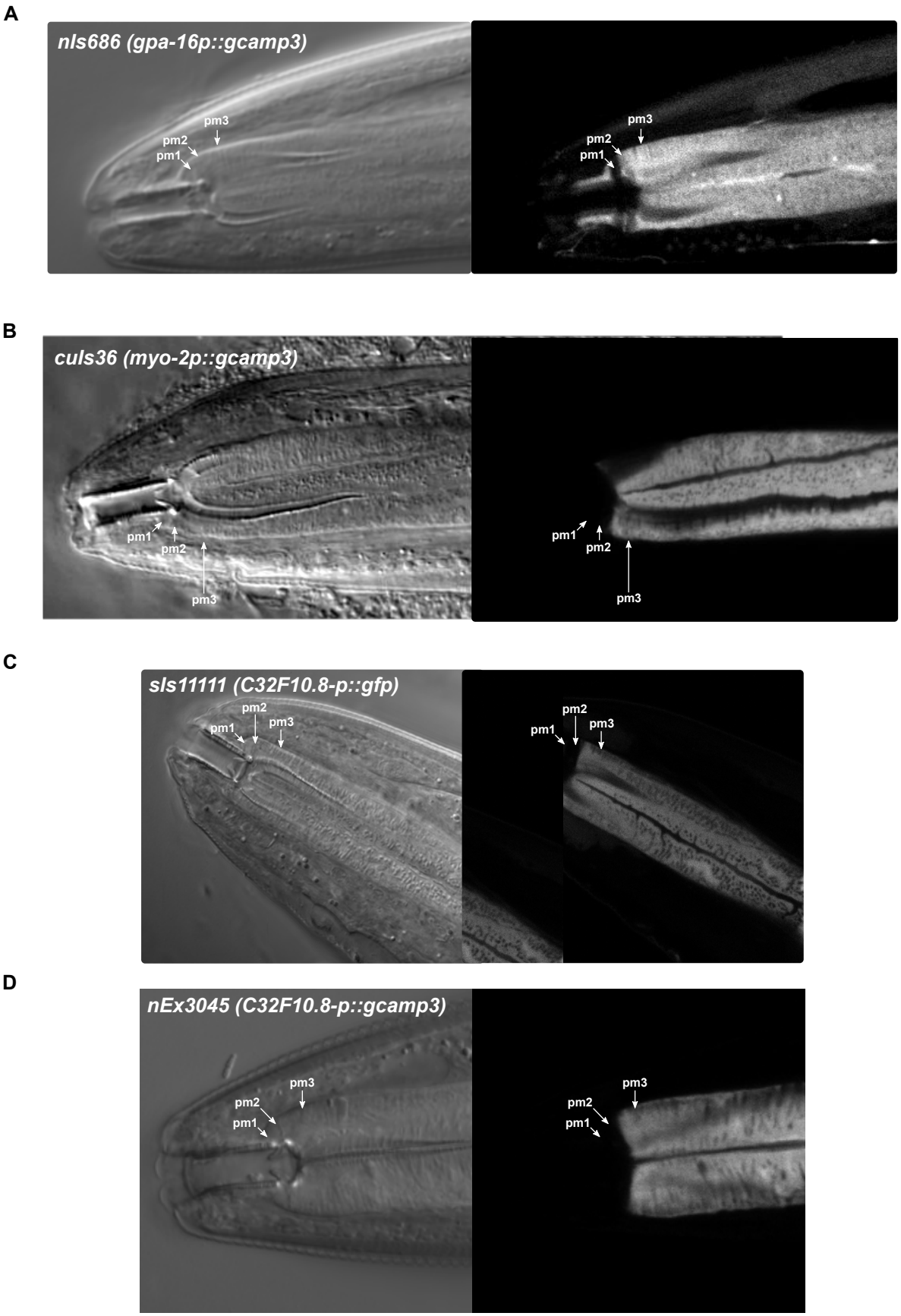

bioRxiv preprint doi: https://doi.org/10.1101/2020.06.02.129825; this version posted June 9, 2021. The copyright holder for this preprint (which was not certified by peer review) is the author/funder, who has granted bioRxiv a license to display the preprint in perpetuity. It is made available under aCC-BY 4.0 International license.

Figure 3—figure supplement 1

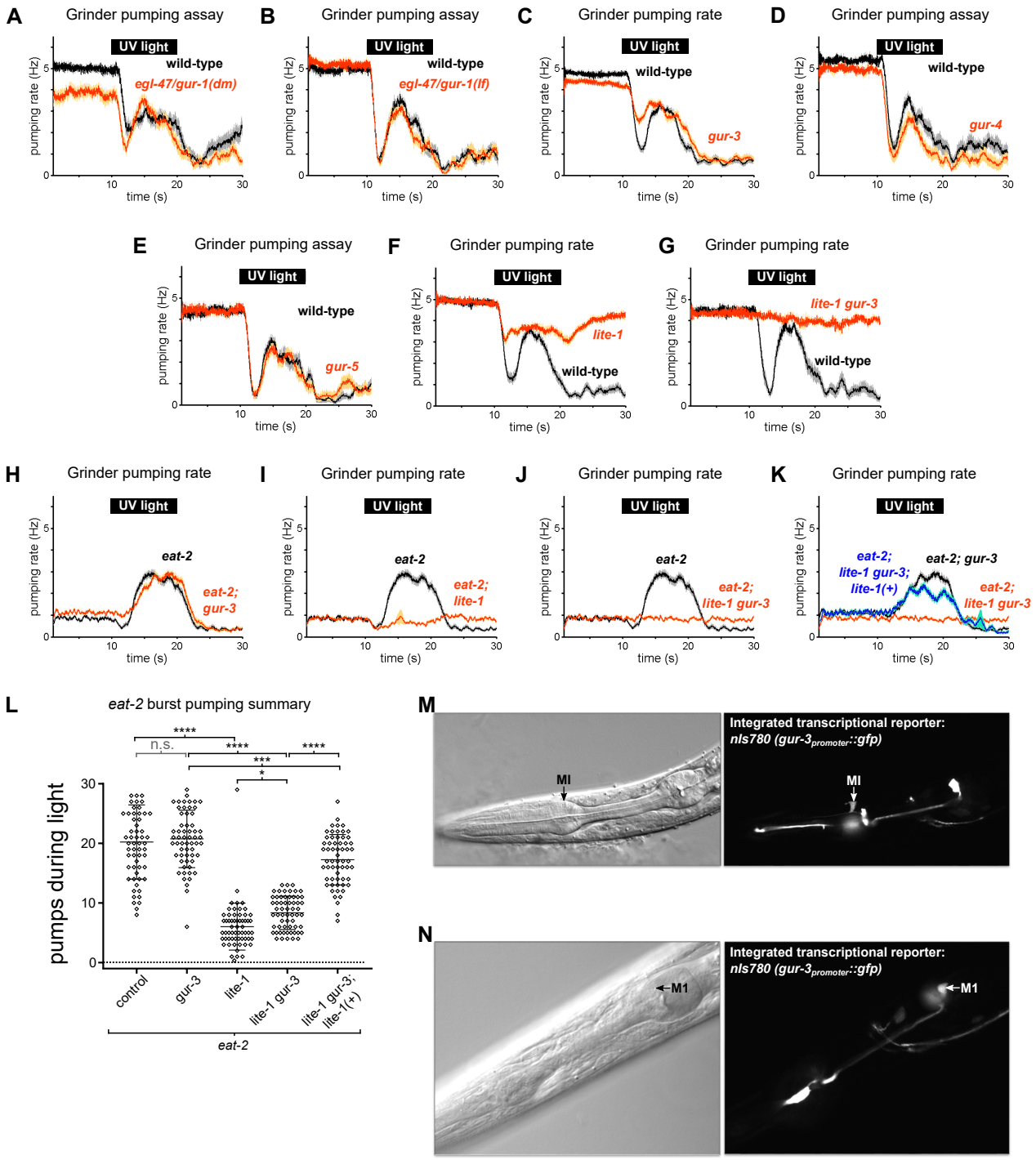

bioRxiv preprint doi: https://doi.org/10.1101/2020.06.02.129825; this version posted June 9, 2021. The copyright holder for this preprint (which was not certified by peer review) is the author/funder, who has granted bioRxiv a license to display the preprint in perpetuity. It is made available under aCC-BY 4.0 International license.

Figure 4—figure supplement 1

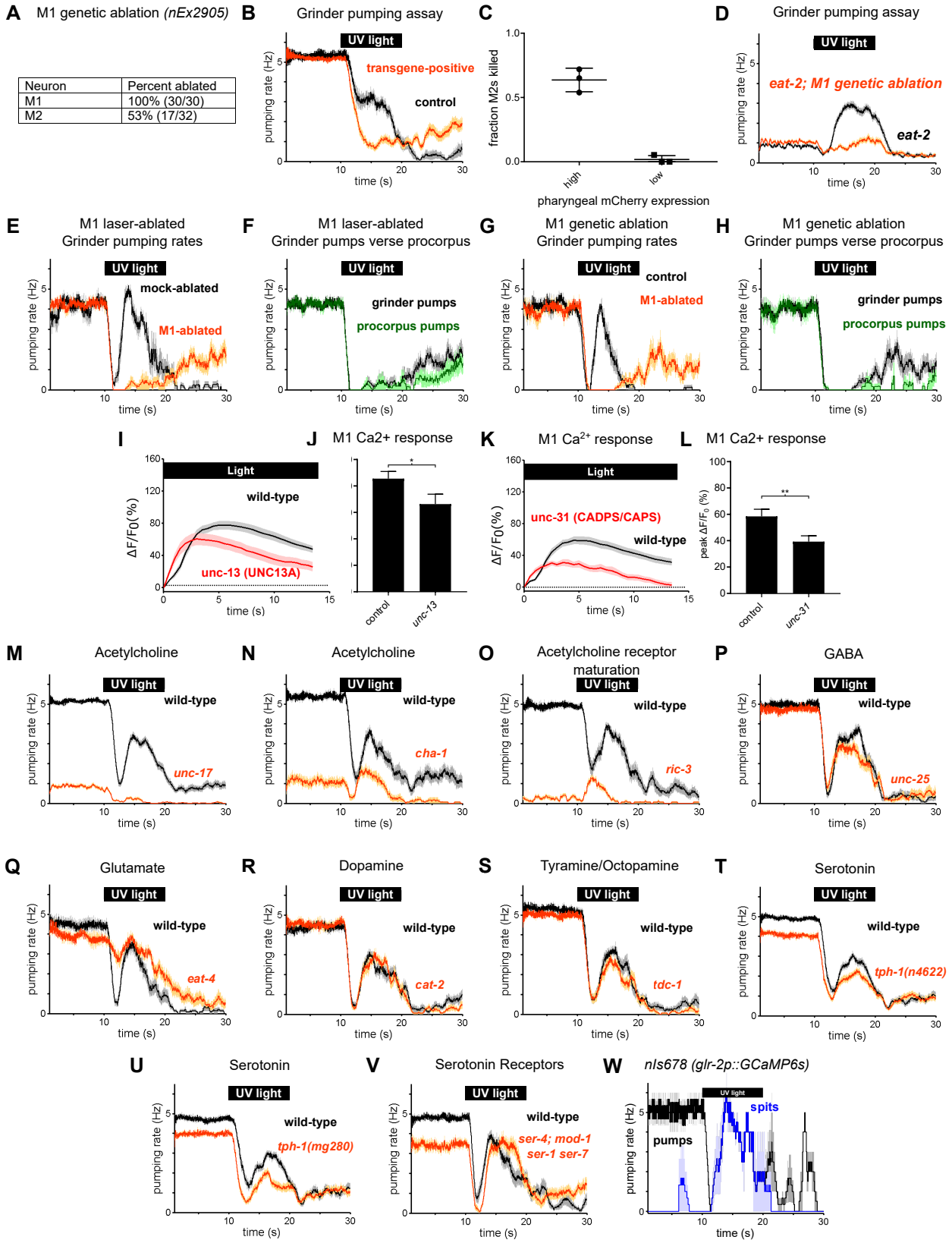

bioRxiv preprint doi: https://doi.org/10.1101/2020.06.02.129825; this version posted June 9, 2021. The copyright holder for this preprint (which was not certified by peer review) is the author/funder, who has granted bioRxiv a license to display the preprint in perpetuity. It is made available under aCC-BY 4.0 International license.

Figure 4—figure supplement 2, p. 1

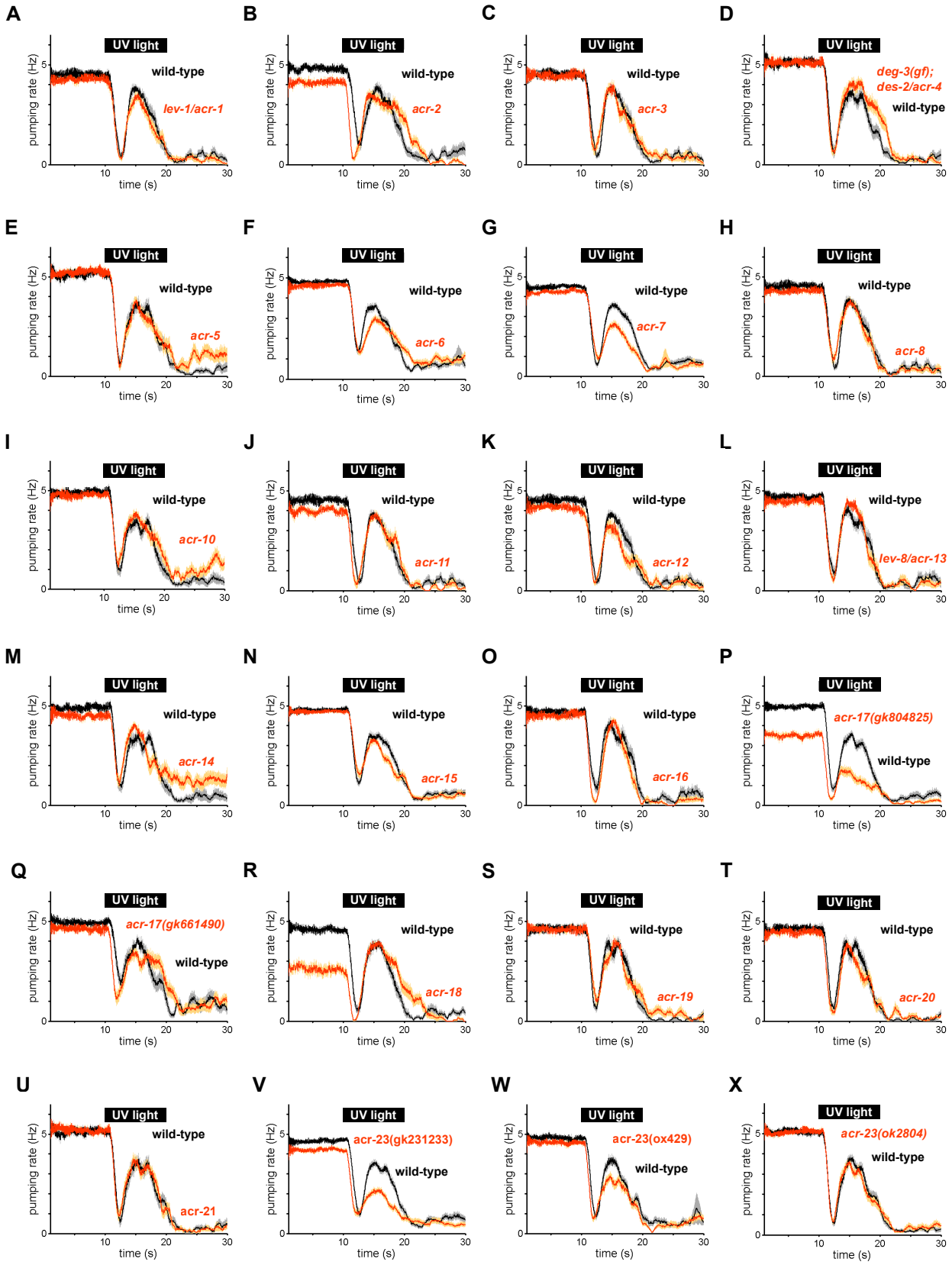

bioRxiv preprint doi: https://doi.org/10.1101/2020.06.02.129825; this version posted June 9, 2021. The copyright holder for this preprint (which was not certified by peer review) is the author/funder, who has granted bioRxiv a license to display the preprint in perpetuity. It is made available under aCC-BY 4.0 International license.

Figure 4—figure supplement 2, p. 2

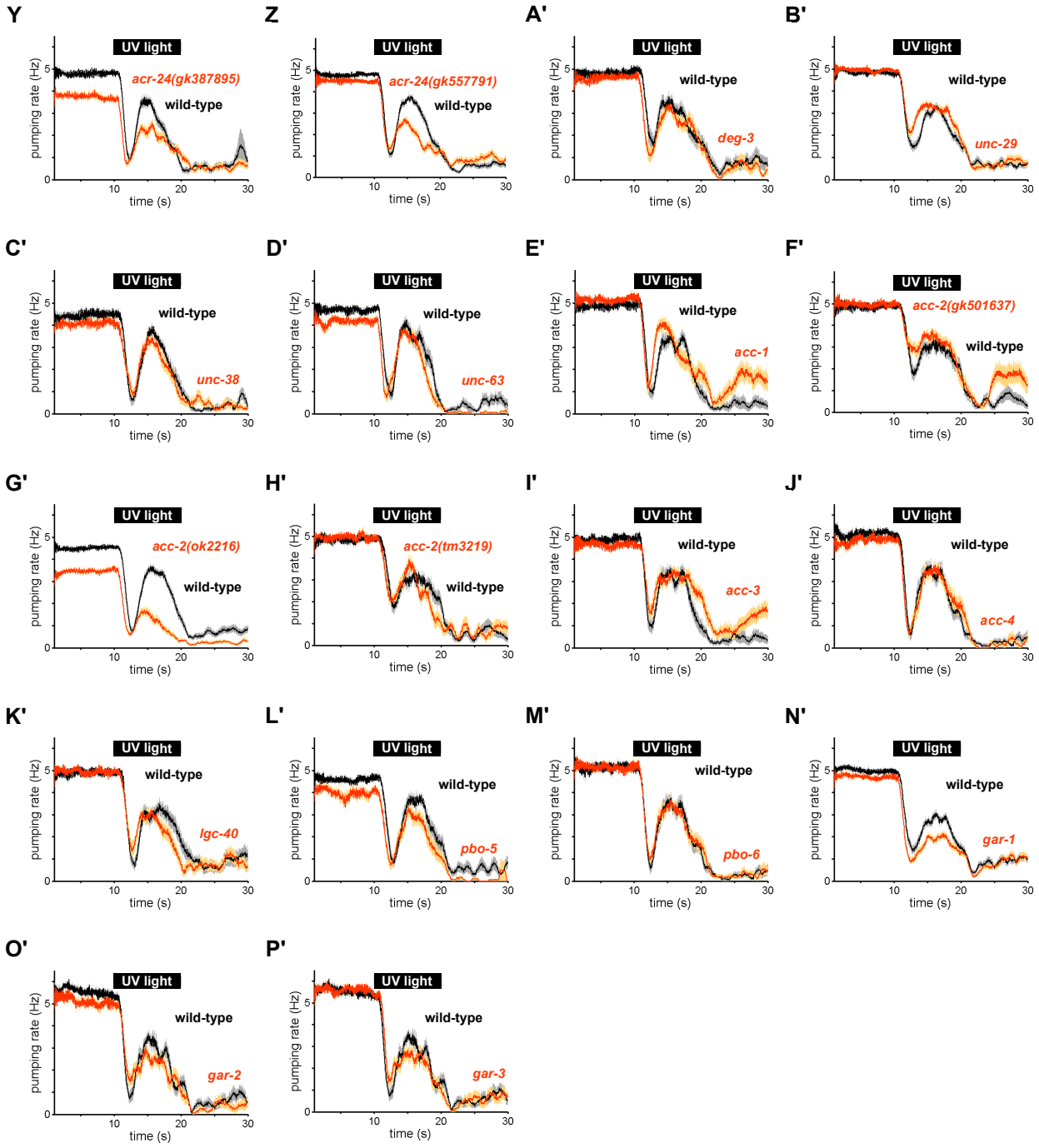

bioRxiv preprint doi: https://doi.org/10.1101/2020.06.02.129825; this version posted June 9, 2021. The copyright holder for this preprint (which was not certified by peer review) is the author/funder, who has granted bioRxiv a license to display the preprint in perpetuity. It is made available under aCC-BY 4.0 International license.
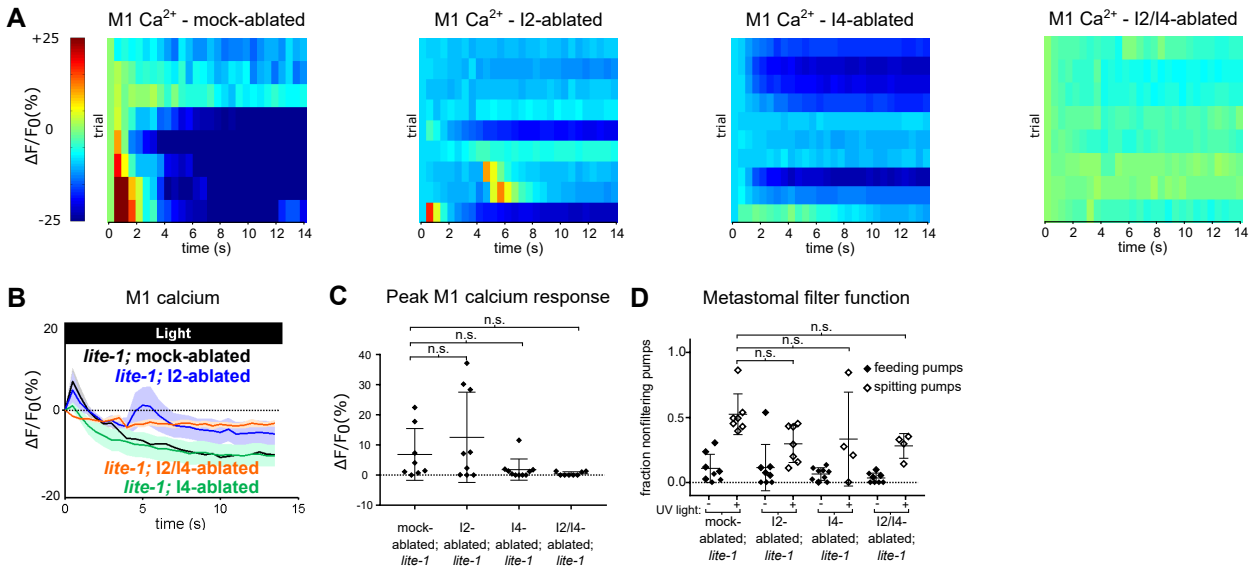
Figure 6—figure supplement 1